The transcription factor Zfx is required for tumorigenesis caused by Hedgehog pathway activation

Colin J. Palmer

Submitted in partial fulfillment of the
requirements for the degree of
Doctor of Philosophy
under the Executive Committee
of the Graduate School of Arts and Sciences

COLUMBIA UNIVERSITY

2013

ABSTRACT

The transcription factor Zfx is required for tumorigenesis caused by Hedgehog pathway activation

Colin J. Palmer

The Hedgehog (Hh) signaling pathway regulates normal development and cell proliferation across the metazoa. Upon its aberrant activation, mammalian Hh signaling can also cause tumor formation. Hh-induced tumors can arise from different tissues and can be locally invasive but rarely metastatic or highly aggressive, as is the case with basal cell carcinoma (BCC) of the skin and the cerebellar tumor medulloblastoma (MB), respectively. Little is known about common cell-intrinsic factors that control the development of such diverse Hh-dependent tumors. The zinc-finger transcription factor Zfx is required for the self-renewal of several stem cell types in both mouse and human, but its role in malignant transformation remains controversial. We found that Zfx is variably required for the development of two distinct Hh-dependent tumors *in vivo*. Co-deletion of *Zfx* prevented BCC formation initiated by Hh pathway overactivation in the skin following deletion of the inhibitory receptor *Ptch1.* Co-deletion of *Zfx* also

delayed development of Hh-dependent MB caused by *Ptch1* deletion *in vivo*. In contrast, Zfx was dispensable for the development of the PTEN-dependent brain tumor glioblastoma, showing that a requirement for Zfx is not generalizable across all cancers. We used genome-wide expression and chromatin binding analysis in a human MB cell line to identify direct, evolutionarily conserved targets of Zfx. These targets included the Hh signal transducer *Smoothened* (*Smo*). Smo expression data from Zfx-deficient BCC and MB cells *in vivo* and *in vitro* suggest that Zfx may directly regulate Hh pathway activation in some cancers. We identified two additional conserved downstream targets of Zfx, *Dis3L* and *Ube2j1*, which were required for optimal growth of human MB cells *in vitro*. These results identify Zfx as a common cell-intrinsic regulator of diverse Hh-induced tumors. Further investigation of the requirement for Zfx and its conserved downstream target genes, such as *Dis3L* and *Ube2j1*, in *in vivo* models of Hh-dependent BCC and MB could lead to the identification of novel targetable molecules for therapies directed against these malignancies.

Table of Contents

List of Figures

Acknowledgments

There are many people to whom I owe great thanks, and without whom the thesis document you are about to read would surely not exist. I owe thanks first to my mentor, Boris Reizis, for accepting me into his laboratory, for challenging me to better myself as a student and as a scientist, for providing me with exemplary mentorship throughout my time at Columbia University, and for serving as a role model to be emulated as I move forward as a postdoc. I would also like to thank all the members of the Reizis laboratory, past and present, for all their help and advice over the years and for making the laboratory such a wonderful place to work and pursue a graduate degree. In particular, I thank Jose Galan, Stuart Weisberg, and Manny Esquilin, off of whose previous work on Zfx, mice strains, and lentiviral constructs I built my thesis research on Zfx and its role in regulating Smo expression and the progression of Hh-dependent cancers.

I also would like to acknowledge the members of my thesis committee, Lloyd Greene, Ken Olive, and David Owens, for the thoughtful questions, experimental suggestions, and helpful insights they proffered in many committee meetings over the past several years. Thank you as well to Peter Canoll, for agreeing to participate as the outside committee member and reader for my thesis defense.

I would like to acknowledge my graduate program at Columbia, the Integrated Program in Cellular, Molecular, and Biomedical Studies- - in particular, the program directors, Ron Liem and Lorraine Symington, and the program coordinator, Zaia Sivo. Thank you for getting me through to the end. I thank Chris Henderson, Hynek Wichterle, and Angela Christiano for helpful discussions. My thanks to Fiona Doetsch, Sankar Ghosh, Thomas Ludwig, and Brandon Wainwright for mice, equipment, and reagents used in the experiments I will detail below. I thank also our collaborators Peter Canoll, Gist Croft, Liang Lei, and David Owens, whose work and aid led to the data soon to be presented from GBM models, *in vitro* MN generation, and BCC pathology scoring. I would also like to gratefully thank the Skin Phenotyping Core Facility of the NIH Skin Diseases Research Center at CUMC, as well as the HICCC Histology Service, for all of their help with histological processing and analysis of skin and cerebellar samples. Without their aid in embedding, sectioning, and staining my many, many skin and cerebellar tissue samples over the past 4 years, the thesis you are about to read most certainly could not have come into being.

To all of you, and to any I have omitted in haste or forgetfulness, all of my thanks. I am most deeply obliged to you all.

For my parents, who were my first teachers and who always encouraged me through all the schools, study, and years that led to here

GENERAL INTRODUCTION

Tissue stem cells, developmental signaling pathways, and cancer

A hallmark of cancer is the aberrant acquisition, continuation, or reactivation of a self-renewal program more properly restricted in a mature organism only to tissue-regenerating adult stem cells. It is perhaps not surprising, then, that the cell-of-origin for a growing number of cancers is thought to reside in stem-and-progenitor compartments [1]. In the hematopoietic system, chronic myelogenous leukemia (CML) driven by BCR-Abl is thought to initiate from hematopoietic stem cells (HSC) exclusively [1], and models of acute myeloid leukemias (AML) suggest that they too originate in stem cells or early uncommitted progenitors [1-3]. Examples also abound in solid tumors. Intestinal adenomas have been suggested to arise from the various $Lgr5^+$, $prominin^+$, and $Bmi1^+$ cells identified as intestinal stem cells in intestinal crypts [4-6]. In the skin, the cell-of-origin for the common tumor basal cell carcinoma (BCC) is thought to dwell in the stem/progenitor compartment of the hair follicle, the hair follicle bulge [7, 8], or in a pool of resident progenitor cells in the interfollicular epidermis [9]. In the brain, mouse models have demonstrated that different subtypes of the cerebellar tumor medulloblastoma (MB) originate in proliferating precursor cells on the surface of the developing cerebellum [10, 11] or in the dorsal brainstem [12].

A common etiology among cancers is the aberrant activation of one of the handful of evolutionarily conserved, intercellular signaling pathways critical for normal embryonic development - - such as the Wnt pathway, the Notch pathway, and the Hedgehog (Hh) pathway, to name a few examples. Frequently, the

pathway whose activation causes the cancer will have also played a vital role in the normal development of the cell-type or tissue from which the cancer derives. For example, Wnt signaling is required for intestinal crypt stem cell self-renewal and long-term maintenance of crypts in the intestine, and mutations in Wnt pathway components APC and β-catenin have long been causally linked with intestinal cancer [13]. In the case of T-cell acute lymphoblastic leukemia (T-ALL), over half of T-ALL cases stem from activating mutations in the NOTCH1 receptor [14, 15], and Notch1 is also critical for early T-cell development in the thymus [16, 17]. Nor is the Hh pathway exempt from this rule. Functional Hh signaling is essential for hair follicle morphogenesis in developing murine skin [18, 19], and hyperactivation of the Hh pathway is necessary and sufficient for development of the follicle-derived tumor BCC in mouse models [20-22]. Hh pathway activity is also necessary for expansion of proliferating granule neuron precursors (GNP) and for full growth and normal foliation in the developing cerebellum [23, 24], and induction of uncontrolled Hh pathway hyperactivation in those self-same GNP generates the cerebellar tumor MB [10, 11].

The Hedgehog (Hh) signaling pathway

The Hh signaling pathway is an intercellular signaling pathway conserved across the metazoa and crucially important for a whole host of developmental processes, as well as for maintenance of tissues in adult organisms [25, 26]. The pathway is named for the single ligand *hedgehog* in the fruit fly *Drosophila*

melanogaster, which was first identified in a screen for segment polarity genes in the *Drosophila* embryo [27]. In contrast, the Hh pathway has three diffusible extracellular ligands in mammals - - Sonic hedgehog (Shh), Desert hedgehog (Dhh), and Indian hedgehog (Ihh) - - of which Shh is the most widely expressed and consequently has the larger number of developmental processes that depend upon it [26]. The core components of the mammalian Hh pathway downstream of the Hh ligand are diagrammed below in Figure 1.

Hh protein is initially translated as a 45 kDa peptide, but it undergoes an autoproteolytic cleavage event that processes it into its truncated extracellular ligand form, with the N-terminal fragment of cleaved Hh (HH-N) bearing the signaling functionality [25, 28]. HH-N is also subjected to post-translational lipid modifications, including palmitoylation at its N-terminus [29, 30] and addition of a cholesterol moiety at its C-terminus [25, 31, 32]. Lipid-modified HH-N is secreted into the extracellular milieu by the membrane protein Dispatched [33-35], where its cholesterol-modification is thought to be crucial for the long-range dispersal of Hh ligand [25, 36] that allows for formation of the gradients of Hh signal integral in Hh-dependent developmental processes.

Graded Hh signal is received by the receptor and 12-pass transmembrane protein, Patched (Patched1, or Ptch1, in mammals). In vertebrates, Hh ligand binds to two large extracellular domains of Ptch1 [25, 37] with the assistance of transmembrane co-receptors CDO and Brother of CDO (BOC) [38]. Somewhat unusually, the Hh receptor Ptch1 is an inhibitory receptor. In the absence of any

extracellular Hh ligand, Ptch1 functions by inhibiting a downstream signal transducer of the Hh pathway. Binding of Hh ligand then inhibits the inhibitory receptor Ptch1, freeing the downstream pathway for activation.

Downstream of Patched, the single, non-redundant signal transducer of the Hh signaling pathway is Smoothened (Smo). *Smo* encodes a 7-pass transmembrane protein that is a member of the G-protein coupled receptor protein family, although it does not appear to function as a receptor or interact with G-proteins [25, 39]. Knockouts of *Smo* have confirmed that *Smo* is essentially required in both invertebrates and in vertebrates for Hh pathway activity [40-44]. The precise molecular mechanisms governing upstream Ptch1 inhibition of Smo, as well as the effect of Smo on downstream GLI-type transcriptional effectors of the Hh pathway, remain mysterious and incompletely understood. However, it is clear that, in the absence of signal from extracellular Hh ligand, Ptch1 catalytically inhibits Smo (without direct protein-protein interaction) [45]. Upon Hh ligand binding and inhibition of Ptch1, Smo is freed from upstream inhibition. Notably, in cases where Ptch1 is inactivated by mutation, Smo is permanently released from upstream inhibition, in ligand-independent fashion. In vertebrates, once Ptch1 is inhibited, Smo is subsequently translocated to a primitive organelle, the primary cilium, where its accumulation is essential for downstream Hh pathway activation [25, 46, 47]. Induction of the Hh pathway *via* graded Hh signal also activates Smo by leading to phosphorylation of and dimerization of the cytoplasmic tails of Smo [48].

Inhibition of Ptch1 by Hh ligand binding and translocation of Smo to the primary cilium lead to activation of GLI proteins, the transcriptional effectors of the Hh pathway.[25] In mammalian systems, in the absence of Hh ligand and while Smo remains inhibited by Ptch1, the GLI-type transcription factors Gli2 and Gli3 are proteolytically processed into truncated transcriptional repressor forms, with Gli2 and Gli3 acting as weak and strong transcriptional repressors, respectively [25, 49]. Association of Gli2 and Gli3 into complexes with suppressor of Fused (SUFU) directs the GLI proteins towards processing by the proteasome [50]. In contrast, when Ptch1 binds Hh ligand, inhibition of Smo is lifted, allowing for Smo migration to primary cilia. SUFU-Gli complexes also translocate to the primary cilium where Smo activation leads to their dissociation [51, 52], and Gli2 and Gli3 are therefore retained in their full-length forms as strong and weak transcriptional activators, respectively, driving expression of Hh pathway target genes [25].

Downstream targets of Gli-mediated Hh pathway transcriptional activation include genes favoring proliferation and cell cycle progression like *Mycn* and *Ccnd1* and *Ccnd2* [53, 54]. Other known targets include core Hh pathway components. This includes the inhibitory receptor *Ptch1*, which is upregulated after pathway activation and attenuates Hh signal gradient by sequestering additional Hh extracellular ligand [25]. Another Hh pathway component that is also a downstream transcriptional target is the GLI-type transcription factor, Gli1, which differs from homologs Gli2 and Gli3 in that it only functions as a transcriptional activator [25, 55]. Gli1 thus represents both a positive feedback

mechanism during and also an excellent readout (*via* measuring of its expression) for Hh pathway activation.

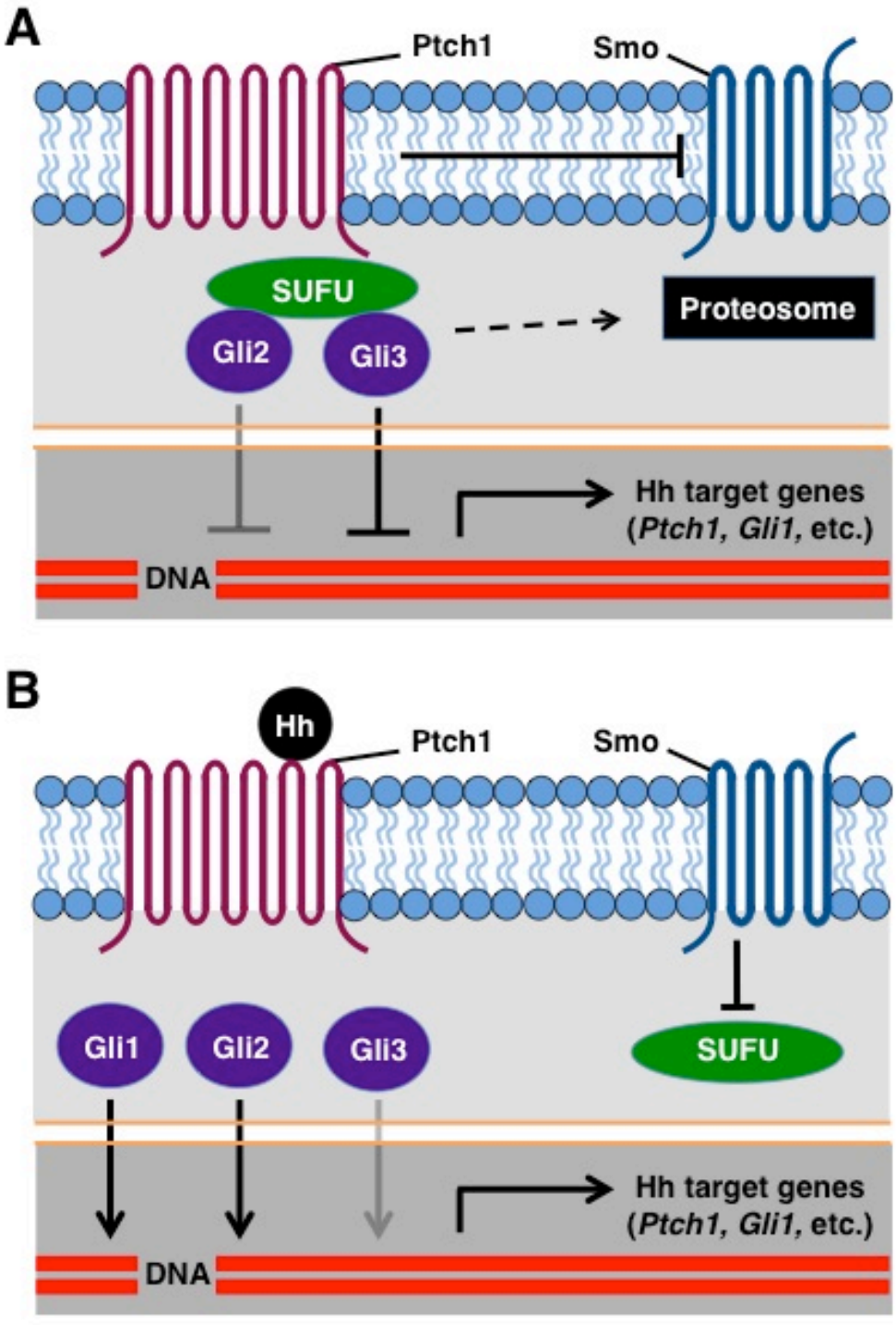

Figure 1. Core components of the mammalian Hh signaling pathway

Shown are diagrams depicting the core components of the mammalian Hh signaling pathway and their interactions in the absence (A) and presence (B) of extracellular Hh ligand signal.

Diagrams are adapted from Figure 1 of Ng and Curran (2011) [7].

(A) In the absence of Hh ligand, the inhibitory receptor Ptch1 inhibits Smo, allowing downstream SUFU-assisted proteolytic truncation of GLI-type transcription factors Gli2 and Gli3 into weak and strong transcriptional repressor forms, respectively.

(B) After detection of Hh ligand by Ptch1, Ptch1 is degraded, removing its inhibition of Smo. Smo migrates to primary cilia, where it ultimately effects dissociation of SUFU-Gli interactions. Gli2 and Gli3 are retained in their full-length forms as strong or very weak transcriptional activators, respectively, inducing expression of downstream Hh pathway target genes. Among these target genes are several core Hh components, including Gli1, which has only a transcriptional activator form and generates positive feedback in the context of Hh pathway activation.

The Hh signaling pathway and cancer

A large body of literature exists pointing towards a dependence on Hh signaling in multiple solid tumor types [56]. Tumor types suggested to require Hh signaling range from non-small and small cell lung cancer [57, 58], to glioma [59], to melanoma [60], to prostate [61] and pancreatic cancer [62]. A cell autonomous function *via* autocrine Hh signaling was originally posited as an explanation for the requirement for Hh signaling in these solid tumors. However, a report from Yauch *et al.* (2008) subsequently demonstrated that Hh signaling likely plays a cell extrinsic role in these cancers, rather than a cell intrinsic one [56]. Xenograft models of human tumors in mice where Hh signaling was disrupted (*via* small molecule inhibitor, neutralizing antibody for Hh ligand, or genetic ablation of the Hh signal transducer *Smo*) showed a paracrine requirement for Hh signaling in tumor-stroma interactions [56]. The cell-extrinsic effects of Hh signaling on different solid tumors can be directly relevant to therapy targeting these tumors in humans. For example, in the case of pancreatic cancer, Hh signaling from tumor to stroma results in decreased vascularization of the tumor, thereby blocking ingress of chemotherapeutics and aiding in survival and growth of the cancer [63].

Beyond cancers that depend on the Hh pathway for tumor-stroma interactions, the Hh signaling pathway has also been shown since the mid-1990's to be required cell intrinsically in a handful of human cancers. A cell-intrinsic requirement for Hh signaling was first corroborated, for the skin cancer BCC, the cerebellar cancer MB, and the skeletal muscle tumor rhabdomyosarcoma, when

Gorlin's Syndrome, a human heritable syndrome conferring predisposition towards developing rhabdomyosarcoma, MB, and especially BCC, was linked to mutations in the Hh inhibitory receptor *Ptch1* [64-66]. Subsequently, mutations in Hh pathway components leading towards pathway activation were found to be common in sporadic human BCC and MB as well. It has been estimated that ~90% of human sporadic BCC bear mutations in *PTCH1*, with another ~10% bearing presumptive activating mutations in *SMO* [21]. Mutations in Hh signaling pathway genes define an entire subtype of human MB, comprising ~30% of MB cases [67, 68]. Mouse models capable of conditionally deleting inhibitory *Ptch1* or conditionally expressing activated alleles of *Smo* in the skin and cerebellum permitted verification that Hh pathway activation causes BCC and MB development *in vivo* and that Hh-driven BCC and MB originate from stem cells and/or progenitors in the hair follicle or developing cerebellum [8, 10, 11, 20].

The role of the transcription factor Zfx *in Hh pathway-dependent cancers*

The transcription factor Zfx is highly conserved in vertebrates and contains a C-terminal DNA binding domain, consisting of 13 C2-H2 zinc fingers, and a large N-terminal acidic transcriptional activation domain [69]. Zfx recognizes a 5-bp consensus DNA binding sequence, GGCCT [70-72]. *Zfx* is a member of the small Zfy family of transcription factors. The other main member of this family is the Y-linked *Zfy*, a gene that was once investigated as a candidate for the male sex-determining region. Zfy is ubiquitously expressed in human cells but expressed

only in tissue-restricted fashion in the testis in mice [73]. Encoded on the X chromosome, Zfx is ubiquitously expressed in both human and in mouse [73]. That being said, its actions and any requirements for Zfx are cell-type- and tissue-specific.

One of the few known functions for Zfx is in governing a program of self-renewal across multiple distinct stem cell types. Previously published work from our laboratory has demonstrated that *Zfx* is absolutely required for the self-renewal of multiple stem cell types [74, 75]. Murine embryonic stem cells (ESC) bearing a null allele of *Zfx* (*Zfx*^{null}) can differentiate normally. They form tissues of all three germinal layers when injected into mice to make teratomas and contribute to all tissues in chimeric mice [74]. However, *Zfx*^{null} ESC are specifically deficient in maintaining themselves in an undifferentiated state *in vitro* [74]. *Zfx*^{null} ESC are outcompeted for growth in undifferentiating conditions by control *Zfx*^{flox} ESC, and *Zfx*^{null} ESC exhibit increased apoptosis and decreased growth over passages in more restrictive serum-free media [74]. Addition of a transgenic copy of *Zfx* into *Zfx*^{null} ESC rescued the growth defects in undifferentiated and serum-free media conditions [74]. In other words, *Zfx*^{null} ESC are specifically deficient in self-renewal.

Similarly, ZFX is also required for self-renewal in human ESC. Knockdown of ZFX in human ESC using lentivirally-delivered RNAi impaired ESC self-renewal *in vitro* as measured by clonogenic ESC colony growth [75]. In addition, overexpression of ZFX in human ESC appears to enhance their self renewal and block differentiation *in vitro*. Human ESC clones overexpressing ZFX from BAC

transgenes have enhanced clonogenic colony growth and exhibited reduced spontaneous differentiation [75].

Zfx is also absolutely required for the self-renewal of murine hematopoietic stem cells (HSC), the adult stem cell population resident in the bone marrow (BM) and responsible for replenishment of the hematopoietic system throughout the life of the organism [74]. HSC numbers were greatly decreased in mouse BM immediately after *Zfx* was conditionally deleted (Zfx^{CKO}), while myeloid progenitor numbers and total BM hematopoietic cell numbers are not affected. Zfx^{CKO} BM also fails the gold-standard functional test of HSC self renewal, namely reconstitution of hematopoietic lineages after bone marrow transplantation into irradiated recipient mice. Zfx^{CKO} BM fails to reconstitute hematopoietic lineages over the short- and long-term after competitive BM transplantation, confirming loss of HSC self-renewal due to *Zfx* deletion [74]. Zfx is also required for development and maintenance of some more mature hematopoietic lineages. *Zfx* is required for the early development of B lymphocytes and their progression through the pro-B to pre-B-cell transition [76]. *Zfx* is also required for the long-term homeostatic maintenance of B-cells in peripheral blood and secondary lymphoid organs [76]. Loss of *Zfx* also blocks generation and/or maintenance of B-1 cells, an alternative subset of B lymphocytes distinct from the adaptive and memory immune responses and capable of self renewal over the course of the organism's lifetime [76].

While its requirement in the case of stem cell self-renewal is established, the role of Zfx in the context of cancer development remains controversial.

Several studies have shown virally-delivered RNAi targeted against ZFX impairing growth of human laryngeal cancer, glioma, and prostate cancer cell-lines *in vitro* [77-79]. Unpublished work from our laboratory also points towards a requirement for *Zfx* for initiation and maintenance of AML *in vivo* (S. Weisberg, unpublished data). However, a recent report from a transposon-based screen in a MYC-dependent murine liver cancer model found the opposite result, identifying *Zfx* as a potential tumor suppressor gene [80].

Here, we present additional evidence in favor of the former view. Given that Zfx is required for self-renewal in two distinct types of stem cells, we hypothesized that Zfx might also be required for aberrant self-renewal in certain cancers. To test this, we utilized models of cancers initiated by Hh signaling pathway hyperactivation. Specifically, we observed the effects of *Zfx* loss in mouse models of Hh-dependent BCC and MB generated by conditional deletion of inhibitory *Ptch1*. In Chapter I, we demonstrate Zfx loss prevents Hh-dependent BCC development *in vivo*, suggesting a requirement for *Zfx* . In Chapter II, we present data showing that Zfx loss also delays tumor progression in Hh-dependent MB *in vivo*, illuminating a common requirement for *Zfx* shared across two very different Hh-driven cancers. Finally, in Chapter III, we identify conserved downstream targets of Zfx in mouse and human, and we pursue preliminary investigations of some of the candidate targets, such as the Hh signal transducer *Smo,* to determine their contribution (if any) to the molecular underpinning of the requirement for Zfx in Hh-dependent cancers.

CHAPTER I

Zfx is required for Hedgehog (Hh)-dependent basal cell carcinoma (BCC) formation *in vivo*

Introduction

Hair follicles: morphogenesis and cyclical regeneration

Mammalian hair follicles expand and elongate downward into the skin as they initially develop and generate hair shafts, and most hair follicles subsequently recapitulate this process over and over again through the life of the organism in a process of retreat and regrowth called the hair cycle. In the mouse, hair follicle morphogenesis begins during embryogenesis and continues into the first two post-natal weeks. Starting when small groups of dermal fibroblasts, destined to become dermal papillae, localize beneath basal keratinocytes of the embryonic epidermis and help them form into placodes, hair follicle morphogenesis continues with proliferation of epidermal placode cells into hair germs expanding and differentiating inward into the dermis, finishing when the now-recognizable hair follicle has elongated to its full extent down to the subcutaneous muscle and organized itself into component structures and cell-layers [81-83].

Following morphogenesis, hair follicles do not retain a static structure throughout life but instead proceed to involute and then regrow cyclically. Periods of hair follicle retreat (catagen), driven by apoptosis and characterized by the regression of the lower portion of the hair follicle, are followed by “resting” intervals (telogen) when hair follicles are at their smallest and shortest and are largely quiescent [82, 84, 85]. Hair follicles then enter a period of rapid cellular

proliferation (anagen) where they regrow the lower portion of the follicle and the hair shaft, before repeating the cycle all over again.

The cyclical replacement during anagen of the cells lost during catagen is made possible by adult tissue stem cells resident in the hair follicle. Specifically, these stem cells reside in the hair follicle "bulge," a portion of the basal epithelial layer of the follicle (known as the outer root sheath) and the lowermost permanently retained portion of the cycling hair follicle [84, 86]. Originally identified as harboring label-retaining cells and for its ability to regenerate hair follicles after transplant [87-89], the hair follicle bulge is marked by expression of keratin 15 (K15), as well as by CD34 and a marker of intestinal stem cells, Lrg5 [90-93]. Activation of these slow-cycling hair follicle bulge stem cells is responsible for the generation of the transit amplifying cells that regrow the lower portion of the anagen hair follicle [86, 89, 94-96].

The Hedgehog (Hh) pathway and the hair follicle

The Hedgehog (Hh) signaling pathway is critically important for hair follicle development and maintenance. Hh morphogen is required for normal hair follicle morphogenesis, and active Hh signaling is also critically required for hair follicle cycling in adult animals. Loss of functional Hh signaling results in an early block in follicle morphogenesis. In *Shh*$^{-/-}$ mice mutant for the relevant Hh ligand in the skin, initial epidermal placodes and hair germs form, but all subsequent hair follicle morphogenesis is prevented [18, 19]. Shh signal is also crucial for follicle

regrowth during anagen in the hair cycle. Blockade of Shh signaling stops hair follicle regeneration in cycling follicles in adult mice [97], and virally-delivered Shh overexpression generates the opposite phenotype, inducing hair follicle regrowth [98]. The regrowing lower portion of anagen follicle shows signs of receiving Hh signal, from expression of the Hh downstream targets (and pathway components) *Gli1* and *Ptch1* [99]. There is even recent evidence of Gli1 expression (and thus Hh pathway activity) in telogen hair follicle bulge cells which go on to repopulate the hair follicle [100], suggesting a Hh pathway interaction with mostly quiescent hair follicle bulge stem cells.

Hh pathway activation and basal cell carcinoma (BCC)

Given the prominent role the Hh pathway plays in normal hair follicle morphogenesis and maintenance in adult skin, it is a short walk to make to arrive at the question of whether Hh is similarly required in the *abnormal* context of hair follicle-derived cancers. Many studies over the last two decades have shown this emphatically to be so in the case of the hair follicle-derived cancer basal cell carcinoma (BCC). Deriving its name from the resemblance by histology of BCC tumor cells to the basal layer cells of the epidermis, BCC in patients most commonly presents as a slow-growing nodular skin lesion on the body areas receiving heaviest sun exposure [101]. Although BCC is the most commonly diagnosed human cancer among persons of European ancestry, it almost never metastasizes and thus is very rarely fatal [21].

Great progress in understanding the genetic changes causing and molecular mechanisms driving BCC came with the discoveries linking BCC to the Hh pathway. The connection was first made when the underlying mutation of Gorlin syndrome, a genetic disorder conferring a predisposition for developing BCC, was mapped to *Patched1* (*Ptch1),* the gene encoding the inhibitory receptor for Hh ligands [64-66]. From there, it became clear that nearly all sporadic human BCC also bore mutations in Hh pathway genes, with 90% of sporadic human BCC carrying mutations in the inhibitory receptor gene *PTCH1* and another 10% bearing mutations in the gene for the Hh signal transducer Smoothened (SMO) [21].

Mouse models confirmed the importance of Hh pathway aberrant activation as the primary causative agent driving BCC formation. In recapitulation of the human disease, *Ptch1*$^{+/-}$ heterogzygous mice carrying one mutant allele of *Ptch1* develop BCC upon induction with UV or ionizing radiation [102, 103]. Activating the Hh pathway in the skin works all by itself, without the radiation, as demonstrated by the successful generation of BCC-like tumors in mice with conditionally targetable *Ptch1* alleles [20] or inducible constitutively active *Smo* alleles [104].

Analogous to its periodic requirement for maintenance of normal hair follicle through cycles of anagen regrowth, sustained Hh pathway activity is also required for the maintenance of BCC in mouse skin [22]. In an additional parallel to normal hair follicle development, a long-suspected location for the BCC cells-of-

origin is the same locale in which the follicle stem cells that regrow cycling hair follicles reside, namely the hair follicle bulge. Lineage-tracing using a bulge specific marker, coupled with radiation-induced BCC formation in *Ptch1*$^{+/-}$ skin, points towards hair follicle bulge stem cells as the BCC cell-of-origin [8]. However, a recent publication from Youssef *et al*. (2010) has questioned the bulge as the location of BCC cells-of-origin. Using an *in vivo* model of BCC generated by expression of an activated *Smo* allele, their results pointed instead towards progenitor cells residing in the interfollicular epidermis [9].

The role of Zfx *in Hh-dependent BCC in the skin*

The zinc-finger transcription factor *Zfx* is absolutely required for the self-renewal of two highly disparate stem cell types, embryonic stem cells (ESC) and murine adult hematopoietic stem cells (HSC) [74, 75]. The role of *Zfx* in the context of cancer models, however, remains controversial. In this Chapter, we asked whether *Zfx* was required in the context of Hh-dependent BCC. To answer this question, we employed mouse models that would make BCC by deleting inhibitory *Ptch1* or expressing constitutively active *Smo*, while at the same time also deleting *Zfx*. We found that *Zfx* loss prevented BCC formation in the skin after Hh pathway overactivation due to *Ptch1* loss or activated Smo expression. Together, these results identify *Zfx* as a novel transcription factor required cell-intrinsically for the development of Hh-dependent BCC.

Results

Establishing a tamoxifen-inducible system for co-deleting Ptch1 *and* Zfx *and for BCC generation* in vivo

We began by asking whether Zfx was required for the initiation and progression of BCC triggered by Hedgehog pathway activation *in vivo*. To establish a system where we could answer this question, we first obtained mice bearing a "floxed", excisable allele of *Patched1* (*Ptch1*^{flox}) [105], the gene encoding the Hh pathway inhibitory receptor. We crossed these animals to mice carrying a transgene encoding a tamoxifen (Tmx)-inducible allele of Cre recombinase under the control of the ubiquitous *Rosa26* promoter (*R26-CreER*), along with either wild-type (*Zfx*^{WT}) or targetable (*Zfx*^{flox}) [74] alleles of *Zfx*. By crossing together resultant progeny, we established two independent breeding lines where administration of tamoxifen could effect either deletion of *Ptch1* alone (*Ptch1*^{flox} *R26-CreER*$^{+}$)(Fig. 2A) or deletion of both *Ptch1* and *Zfx* (*Ptch1*^{flox} *Zfx*$^{flox/Y}$ *R26-CreER*$^{+}$)(Fig. 2B).

Topical tamoxifen successfully deletes Zfx *from epidermis and hair follicles in treated dorsal skin*

Before investigating the effects of *Zfx* deletion on BCC initiation and progression, we first asked whether administration of tamoxifen to the skin of *Ptch1*^{flox} *R26-CreER*$^{+}$ and *Ptch1*^{flox} *Zfx*^{flox} *R26-CreER*$^{+}$ mice could successfully

ablate targetable alleles from cells in the basal layer of the interfollicular epidermis and in the hair follicle. We shaved dorsal skin of male *Ptch1*^{flox} *R26-CreER*$^{+}$ mice (designated as *Ptch1* in Figures), *Ptch1*^{flox} *Zfx*^{flox} *R26-CreER*$^{+}$ mice (*Ptch1 Zfx*), and *CreER* (Ctrl) littermates and treated it with topical tamoxifen for five consecutive days to enforce deletion. To help ensure that topical tamoxifen infiltrated down through the entire hair follicle, mice were shaved in age-matched cohorts at 7-8 weeks of age, aiming temporally for the second telogen of their hair cycle [85] when most hair follicles should be quiescent and synchronized at their shortest length.

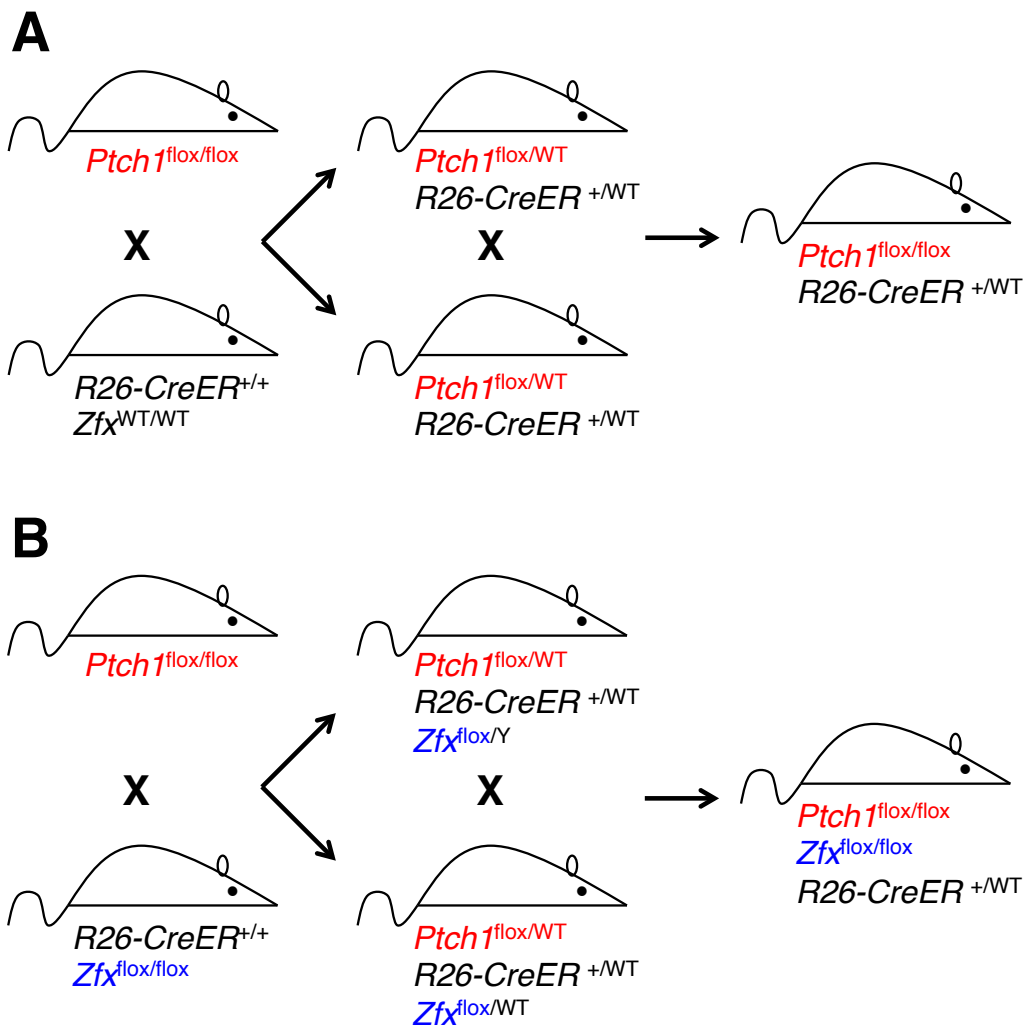

Figure 2. Generation of Tmx-inducible 23elete mice for *Ptch1* and *Zfx*

Mice homozygous for conditionally targetable "floxed" alleles of *Patched1* (*Ptch1*^{flox}) were bred to mice bearing the *Rosa26-CreERT2* transgene (*R26-CreER*), expressing a tamoxifen (Tmx)-inducible Cre recombinase under the control of a ubiquitous promoter, and either wild-type (*Zfx*^{WT}) or targetable (*Zfx*^{flox}) alleles of *Zfx*. Shown are schematics depicting the breedings to generate separate mouse lines for Tmx-induced deletion of *Ptch1* alone (A) or co-deletion of both *Ptch1* and *Zfx* (B).

We subsequently analyzed dorsal skin patches from treated mice 3 days after the termination of tamoxifen treatment, by both immunohistochemistry (IHC) and by qPCR on RNA from bulk epidermis and hair follicles (Fig. 3). In IHC sections from Tmx-treated dorsal skin from Ctrl mice, nuclear staining for Zfx protein can be observed in cells throughout the basal layer of the epidermis and down into the hair follicle (Fig. 4A). In contrast, IHC staining for Zfx in sections from Tmx-treated *Ptch1 Zfx* skin showed the loss of strong nuclear Zfx staining in many (but not all) cells in the epidermis and follicle, including cells in the stem cell-containing hair follicle bulge (Fig. 4B). These data suggest that the applied topical tamoxifen is successfully reaching cells throughout the epidermis and hair follicle of treated mice, to activate CreER-mediated excision and delete targetable "floxed" alleles.

Additional evidence for successful Tmx-mediated deletion came from gene expression analysis of the treated skin patches. Cohorts of *Ptch1*, *Ptch1 Zfx*, and *CreER*$^{-}$ (Ctrl) mice were sacrificed 3 days after Tmx treatment, and bulk epidermis and hair follicles from the treated dorsal skin patch were isolated and processed for RNA isolation and for subsequent gene expression analysis by qPCR. Levels of *Zfx* mRNA were comparable between *Ptch1* and Ctrl samples but were decreased nearly 10-fold in samples from *Ptch1 Zfx* mice carrying the targetable allele of *Zfx* (Fig. 4C). Tmx-treated *Ptch1 Zfx* skin also showed decreased expression of *Dis3L*, a previously validated transcriptional target of Zfx across multiple cell-types [74-76]. Combined with the decreased nuclear Zfx

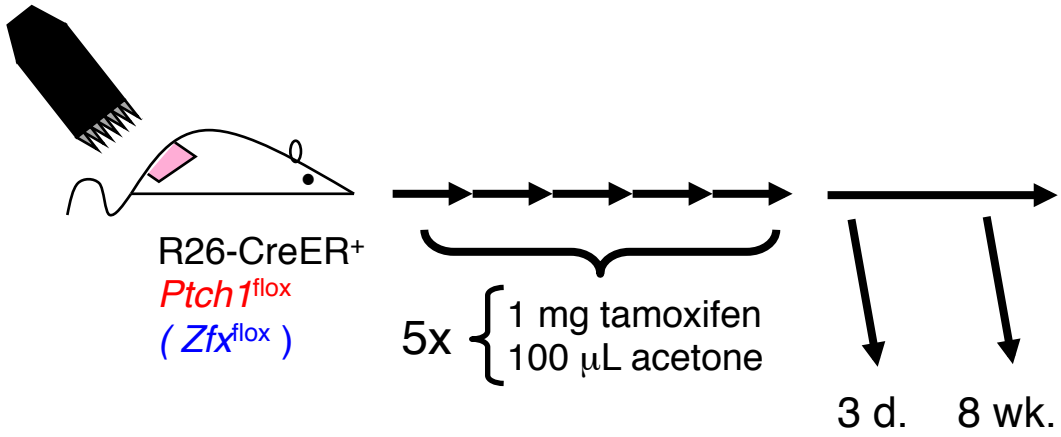

Figure 3. Topical Tmx treatments for BCC induction *in vivo*

Male singly-deleting *Ptch1*$^{flox/flox}$ *Zfx*$^{WT/Y}$ *R26-CreER*$^{+}$ and doubly-deleting *Ptch1*$^{flox/flox}$ *Zfx*$^{flox/Y}$ *R26-CreER*$^{+}$ mice were shaved across their dorsal skin at 7-9 weeks of age and treated with tamoxifen (Tmx) to induce deletion of *Ptch1* in the skin, with or without *Zfx* co-deletion. Shown is a schematic diagram illustrating the treatment regimen of 5 consecutive doses of daily 1 mg tamoxifen, topically applied to shaved dorsal skin, before analysis of treated skin three days (3d) or eight to nine weeks (8 wks) after Tmx by IHC and qPCR.

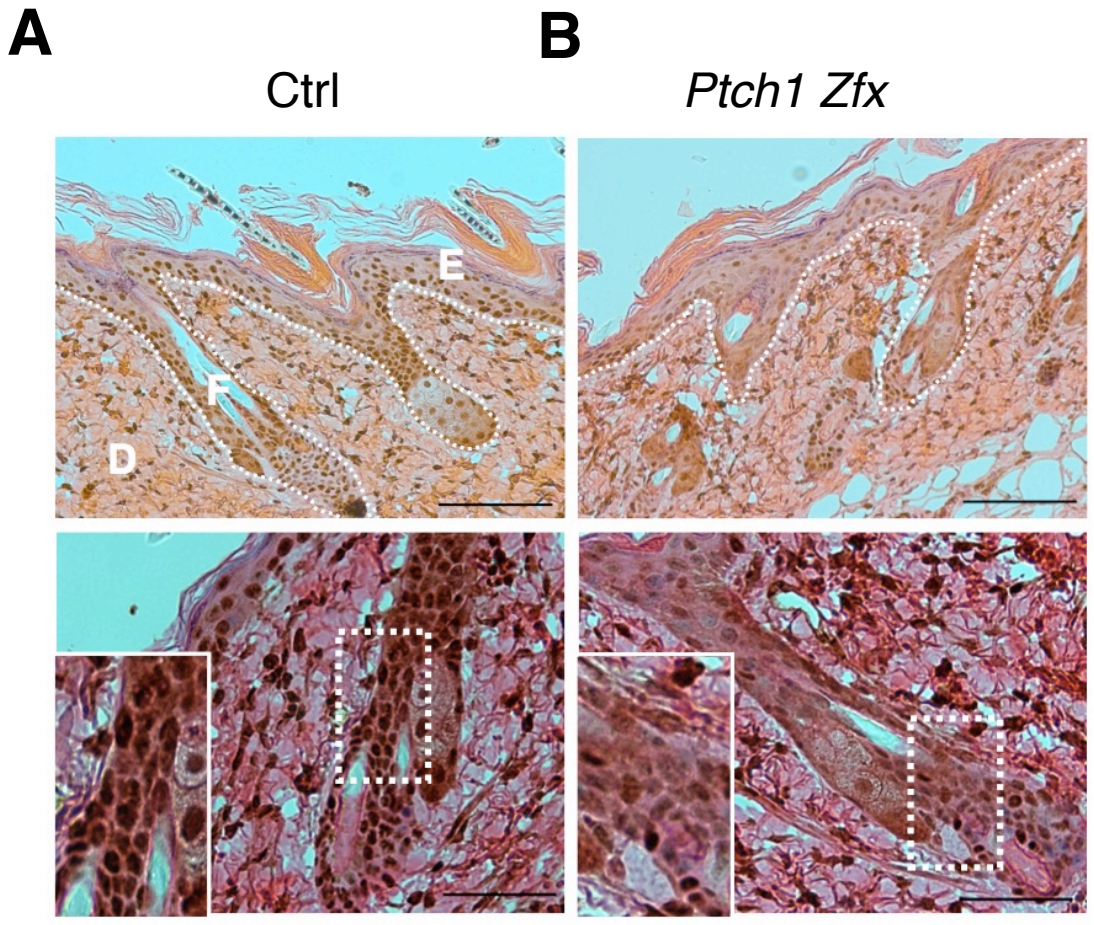
A
B
Ctrl
Ptch1 Zfx
E
F
D

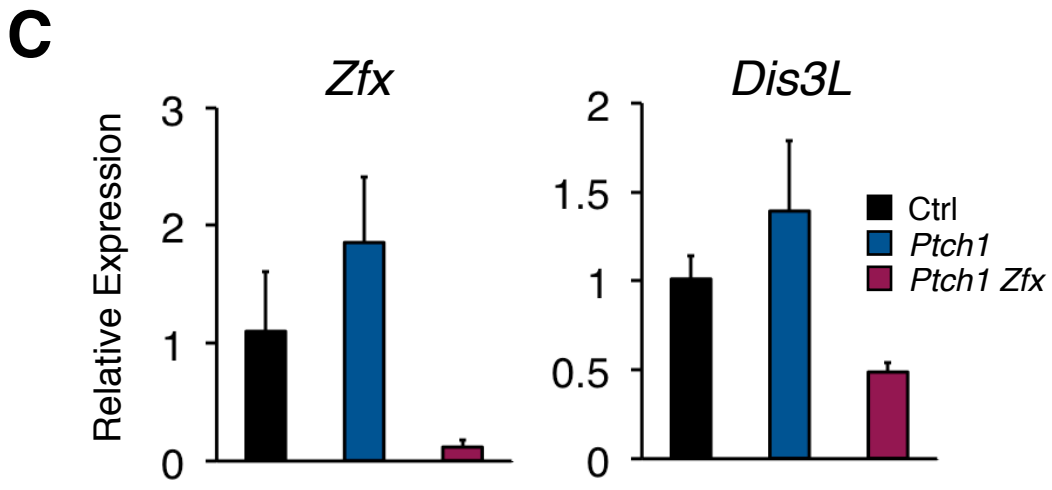
C
Zfx
Dis3L
Relative Expression
3
2
1
0
2
1.5
1
0.5
0
Ctrl
Ptch1
Ptch1 Zfx

Figure 4. **Topical Tmx successfully ablates *Zfx* in treated dorsal skin**

As described in Figure 2, *Ptch1*$^{flox/flox}$ *Zfx*$^{+/y}$ *R26-CreER*$^{+}$ (*Ptch1*) and *Ptch1*$^{flox/flox}$ *Zfx*$^{flox/y}$ *R26-CreER*$^{+}$ (*Ptch1 Zfx*) mice, along with *Ptch1*$^{flox/flox}$ *R26-CreER*$^{-}$ controls (Ctrl), were treated topically with tamoxifen (Tmx) to induce deletion of *Ptch1* alone or of both *Ptch1* and *Zfx* in the skin.

(A&B) Shown is Zfx expression in the skin 3 days after Tmx treatment. Representative micrographs of IHC staining for Zfx in sections from treated Ctrl (A) and *Ptch1 Zfx* (B) dorsal skin are shown. Scale bars represent 100 μm (upper panel) and 50 μm (lower panel). Epidermis (E), dermis (D), and hair follicle (F) are labeled, and the boundary between epidermis/follicles and dermis is marked (dotted line; upper panel). Zoomed insets show decreased nuclear staining for Zfx in the follicle (lower panel).

(C) Expression levels of *Zfx* and the Zfx target gene *Dis3L* in bulk epidermis and hair follicles from shaved dorsal skin 3 days after topical Tmx treatment in *Ptch1*, *Ptch1 Zfx*, and CreER^{-} (Ctrl) mice. Shown are normalized expression levels relative to Ctrl skin as determined by qPCR (mean ± SD of 2-4 mice; representative of four independent experiments).

detected after Tmx treatment by IHC, these qPCR data showing decreased *Zfx* expression confirm that our topical tamoxifen application successfully deletes targetable alleles in shaved, treated dorsal skin.

Co-deletion of Zfx *prevents BCC development after* Ptch1 *deletion* in vivo

After the demonstration from IHC and qPCR data that topical tamoxifen could successfully delete targeted alleles in the interfollicular epidermis and hair follicle, we asked two further questions as logical follow-ups. First, we needed to confirm that topical Tmx administration and resultant deletion of *Ptch1* in treated skin would generate BCC *in vivo* in our hands. Second, if the expected BCC after Tmx was observed, we sought to determine whether co-deletion of *Zfx* in treated skin would impair or prevent BCC development.

To answer these questions, we followed cohorts of shaved male mice as they aged after induction of *Ptch1* and *Zfx* deletion, observing them until 8-9 weeks after Tmx application. During this time period, *Ptch1*$^{flox/flox}$ *Zfx*$^{WT/Y}$ *R26-CreER* (Ctrl) mice re-grew hair throughout the treated dorsal skin patch (Fig. 5A). In stark contrast, *Ptch1* mice, which deleted only *Ptch1* after Tmx, lost the hair on and developed gross induration of the skin over most of their treated dorsal skin (Fig. 5A). Then, looking at the mice that would co-delete *Zfx,* we observed that *Ptch1 Zfx* mice largely retained regrown hair and intact skin in the Tmx-treated dorsal skin patch (Fig. 5A), akin to what we saw with the Ctrl mice.

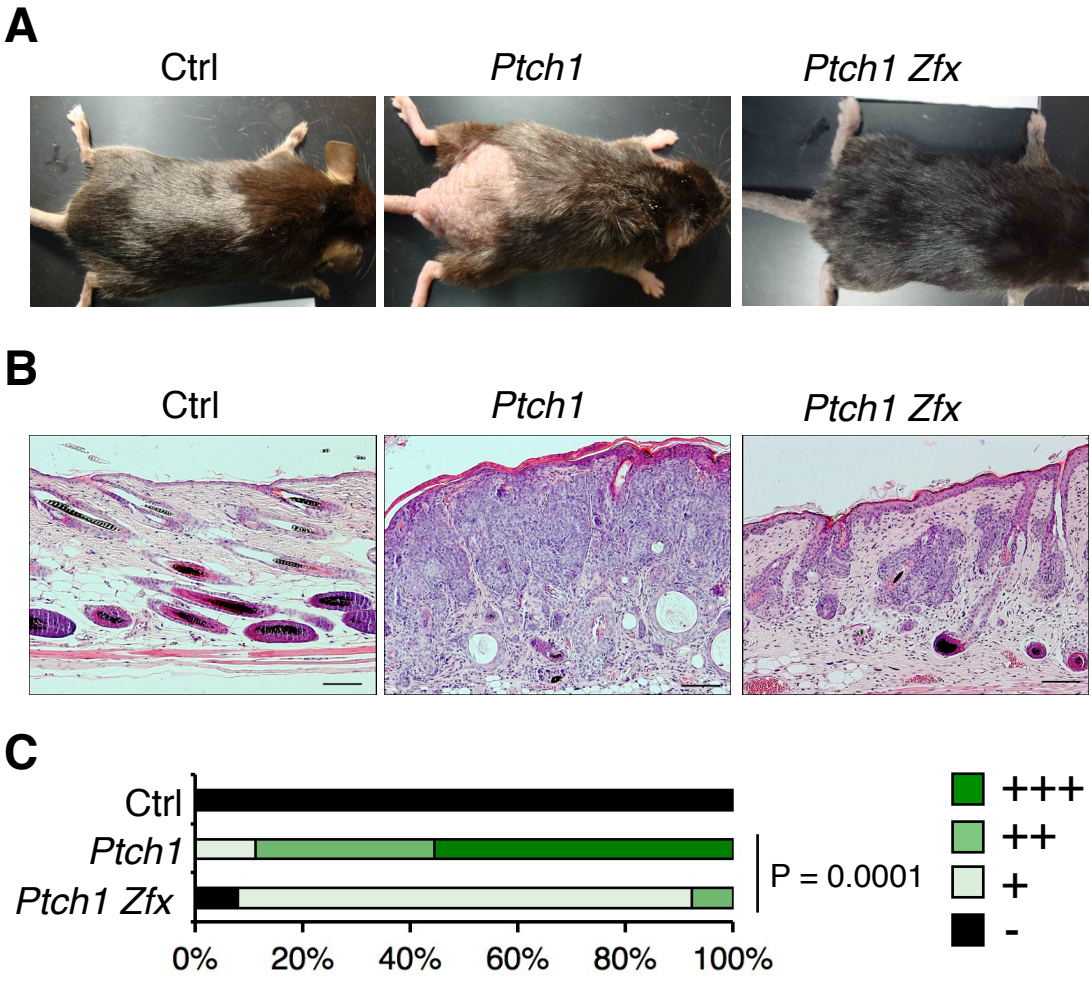
A
Ctrl
Ptch1
Ptch1 Zfx
B
Ctrl
Ptch1
Ptch1 Zfx
C
Ctrl
Ptch1
Ptch1 Zfx
0%
20%
40%
60%
80%
100%
P = 0.0001
+++
++
+
-

Figure 5. Co-deletion of *Zfx* prevents BCC development after *Ptch1* deletion *in vivo*

Mice carrying tamoxifen (Tmx)-inducible Cre recombinase and conditional alleles of *Ptch1* alone (*Ptch1)* or of both *Ptch1* and *Zfx* (*Ptch1 Zfx)*, as well as *R26-CreER*$^{-}$ *Zfx*^{WT} littermate controls (Ctrl), were treated with Tmx on shaved dorsal skin, as described in Figure 3.

(A) Representative photographs showing dorsal skin of mice of the indicated genotypes following euthanasia 8 weeks after Tmx treatment.

(B) BCC development in the mice of indicated genotypes. Shown are sections of dorsal skin isolated 8 weeks after Tmx treatment and stained with H&E. Scale bars represent 100 μm.

(C) Pathology scores of BCC in treated skin 8-9 weeks after Tmx treatment. Shown are the fractions of indicated BCC severity scores in Ctrl, *Ptch1* and *Ptch1 Zfx* mice (n = 5, 9, and 13, respectively).

Next, we looked more closely at treated skin 8-9 weeks after Tmx *via* histology. Histological analysis of paraffin sections from skin of *Ptch1* mice at 8 weeks post-Tmx revealed frank BCC throughout the tissue sections, with massive dermal infiltration and multiple dermal cysts in lieu of the intact hair follicle (Fig. 5B). *Ptch1 Zfx* skin, on the other hand, showed only occasional aberrant follicles or instances of potential incipient BCC (Fig. 5B) and otherwise more closely resembled the wild-type follicles and epidermis seen in *CreER*$^{-}$ (Ctrl) tissue sections.

The differences in BCC development we observed by eye and by histology between *Ptch1* and *Ptch1 Zfx* mice were further supported by pathology scoring of histological sections. Blinded scoring of hematoxylin and eosin (H&E) stained sections from treated dorsal skin 8-9 weeks after tamoxifen confirmed that *Ptch1 Zfx* mice exhibited significantly reduced pathology scores for BCC when compared with *Ptch1* mice (Fig. 5C). The great majority of the *Ptch1 Zfx* sections scored (11/13) received the lowest score above wild-type baseline. Meanwhile, on the side of our positive control in this BCC model, the majority of the *Ptch1* sections (5/9) received the highest pathology score, a score received by none of the *Ptch1 Zfx* sections (Fig. 5C). Combined with the difference in BCC phenotypes observed by eye and in histological sections for *Ptch1* and *Ptch1 Zfx* skin, these data strongly suggested that *Zfx* co-deletion severely impairs or prevents BCC following *Ptch1* inactivation *in vivo*.

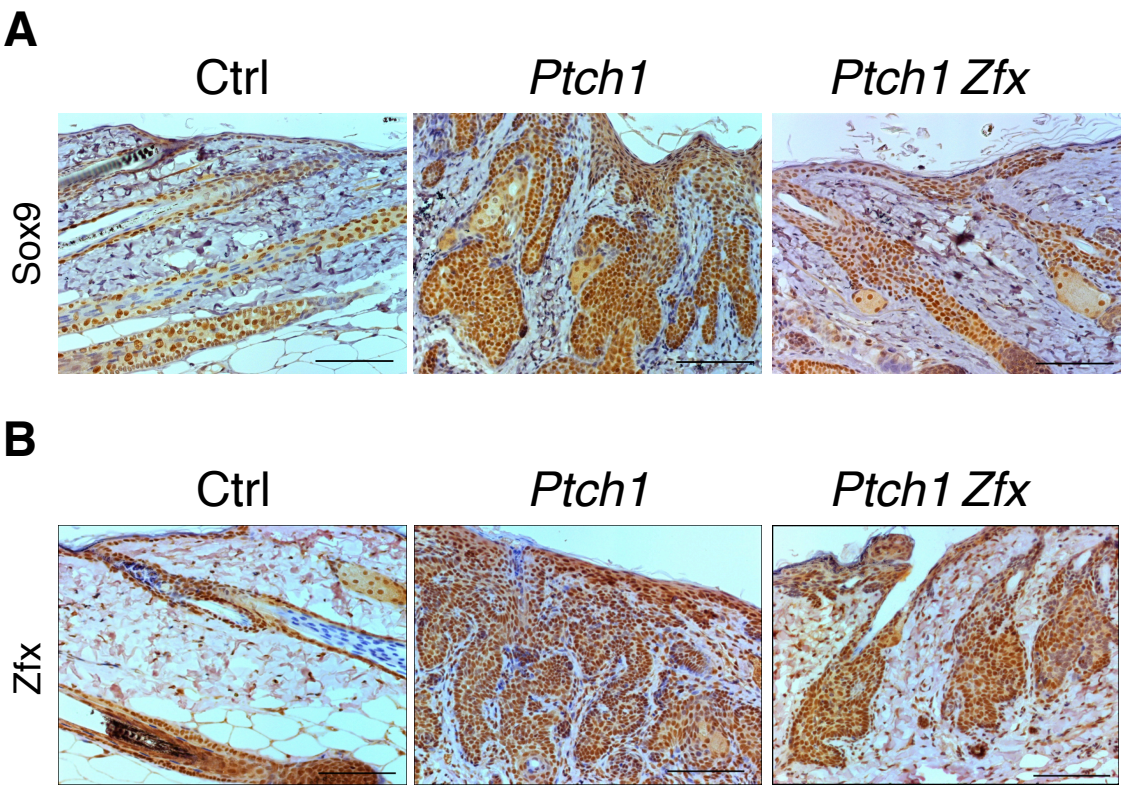

Figure 6. *Zfx*^{null} BCC do not develop following *Ptch1* deletion in the skin

As described in Figure 5, mice were shaved across their dorsal skin at 7-9 weeks of age and were treated with topical Tmx to enforce deletion and induce BCC. Shown are representative micrographs of *Ptch1*$^{flox/flox}$ *R26-CreER*$^{-}$ (Ctrl), *Ptch1*$^{flox/flox}$ *Zfx*$^{WT/y}$ *R26-CreER*$^{+}$ (*Ptch1*), and *Ptch1*$^{flox/flox}$ *Zfx*$^{flox/y}$ *R26-CreER*$^{+}$ (*Ptch1 Zfx*) dorsal skin sections isolated 8-9 weeks after Tmx and stained with antibodies against Sox9 (A) or Zfx (B). Sections are counterstained with hematoxylin, and scale bars represent 100 μm.

Zfx^{null} BCC does not form and Zfx^{null} hair follicles are not maintained in skin after Tmx-induced deletion

We examined sections from 8-9 weeks post-Tmx skin patches by IHC, to confirm that BCC we generated with Tmx-induced *Ptch1* and *Zfx* deletion bore biochemical markers of BCC. We stained slides with antibody raised against Sox9, a marker of the hair follicle stem cell compartment and outer root sheath that also marks BCC tumors [106]. BCC in sections from *Ptch1* skin stained positively for Sox9 (Fig. 6A), as did hair follicles in skin from *R26-CreER^{-}* (Ctrl) and *Ptch1 Zfx* mice (Fig. 6A). Sox9^{+} staining in the tumors supports the conclusion that we have successfully generated model BCC *in vivo* using *Ptch1* deletion, as intended.

We also wanted to examine the expression of Zfx protein in skin sections 8-9 weeks after Tmx-induced deletion. After staining slides with anti-Zfx antibody, we noted nuclear Zfx staining throughout the basal layer of the epidermis and hair follicle in Ctrl skin (Fig. 6B), as we had also observed previously in skin 3 days post-Tmx treatment. Cells in BCC in skin sections from *Ptch1* mice also stained positive for nuclear Zfx (Fig. 6B). Interestingly, however, most cells in the epidermis and in normal and abnormal hair follicles from *Ptch1 Zfx* skin 8-9 weeks post-Tmx also stained positively for nuclear Zfx (Fig. 6B). This unexpected result contrasted with the Zfx deletion we previously observed by IHC in *Ptch1 Zfx* skin 3 days post-Tmx (Fig. 4B). The absence of *Zfx*^{null} hair follicles or incipient BCC in *Ptch1 Zfx* skin 8-9 weeks post-Tmx suggests that there is strong

selection favoring *Zfx* non-deleter cells in the skin following Tmx-induced gene ablation. These data also strengthened the conclusion from histology and pathologist scoring of *Ptch1 Zfx* skin (namely, that *Zfx* co-deletion severely impairs or prevents BCC development), showing that any abnormal follicles or incipient BCC which eventually develop in *Ptch1 Zfx* skin are comprised of cells that fail to delete *Zfx*.

Zfx *loss decreases expression of the Hh pathway signal transducer Smo and blunts Hh pathway activation after* Ptch1 *deletion in the skin*

Because evidence so far suggested that loss of *Zfx* prevented BCC initiation in the skin after Hh pathway activation due to *Ptch1* deletion, we asked whether we could detect changes in the expression of any of the core components or direct targets of the Hh signaling pathway after *Zfx* co-deletion. To answer this question, we again utilized the cohorts of *Ptch1*, *Ptch1 Zfx*, and *CreER*$^{-}$ (Ctrl) mice that we sacrificed 3 days after Tmx, for RNA extraction from bulk epidermis/hair follicles of dorsal skin and subsequent gene expression analysis by qPCR. Notably, *Smo* transcript levels were decreased by approximately 2-fold in *Ptch1 Zfx* samples, compared to *Ptch1* and Ctrl skin (Fig. 7), correlating with decreased *Zfx* levels in *Ptch1 Zfx* skin. Additionally, in skin from *Ptch1* mice, expression levels of the Hh pathway targets *Gli1* and *Mycn* were substantially increased (Fig. 7), consistent with an activation of the Hh pathway following deletion of the inhibitory *Ptch1*. In contrast, in *Ptch1 Zfx* mice

this increase in *Gli1* and *Mycn* expression was blunted nearly down to the levels in *CreER*$^{-}$ (Ctrl) skin (Fig. 7). Together, the decreased *Smo* expression and

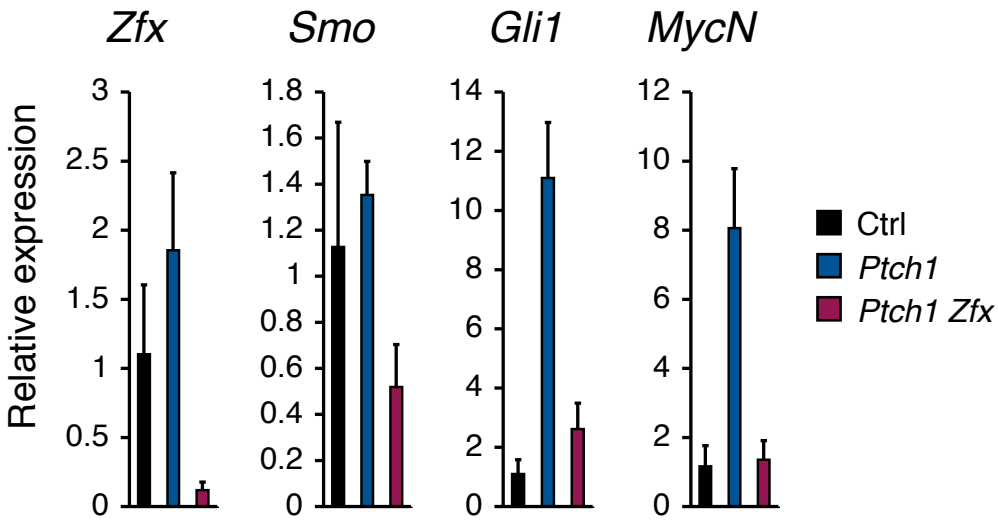

Figure 7. Loss of *Zfx* correlates with decreased *Smo* expression and blunted overexpression of Hh pathway target genes after *Ptch1* deletion in the skin

Expression levels of *Zfx*, *Smo,* and Hh pathway target genes in bulk epidermis and hair follicles from shaved dorsal skin 3 days after topical Tmx treatment in *Ptch1*, *Ptch1 Zfx*, and Ctrl mice (as described in Figure 5). Shown are normalized expression levels relative to Ctrl skin as determined by qPCR (mean ± SD of 2-4 mice; representative of four independent experiments).

blunted overexpression of Hh targets *Gli1* and *Mycn* after *Zfx* co-deletion suggest a simple hypothetical explanation of the observed prevention of Hh-dependent BCC formation after *Zfx* loss. Specifically, the transcription factor *Zfx* could regulate the expression of *Smo* in the skin, and therefore be required for Hh pathway activation after *Ptch1* loss in this *in vivo* model of BCC.

Loss of Zfx *impairs BCC formation caused by an activated* Smo *allele "downstream" of endogenous* Smo

We then attempted some preliminary experiments, to test this new hypothetical explanation for *Zfx* requirement in BCC formation after *Ptch1* deletion. We reasoned that: if transcriptional regulation of *Smo* alone explains the loss-of-*Zfx* phenotypes in Hh-dependent BCC, then BCC models initiated by Hh pathway activation downstream of Smo should be immune to effects from *Zfx* deletion. To investigate this possibility, we obtained transgenic *Rosa26-SmoM2*$^{\text{stop-flox-stop-EYFP}}$ (*R26-SmoM2*) mice [104]. The *SmoM2* allele, a missense mutant allele mimicking a human *SMO* missense mutant identified from BCC patients, encodes a constitutively active Smo that generates BCC in mice [104, 107]. *R26-SmoM2* mice will express this Smo allele, fused with enhanced yellow fluorescent protein (EYFP), from the ubiquitously-expressed *Rosa26* promoter, but only after Cre-mediated excision of a *loxP*-flanked "stop" cassette [104].

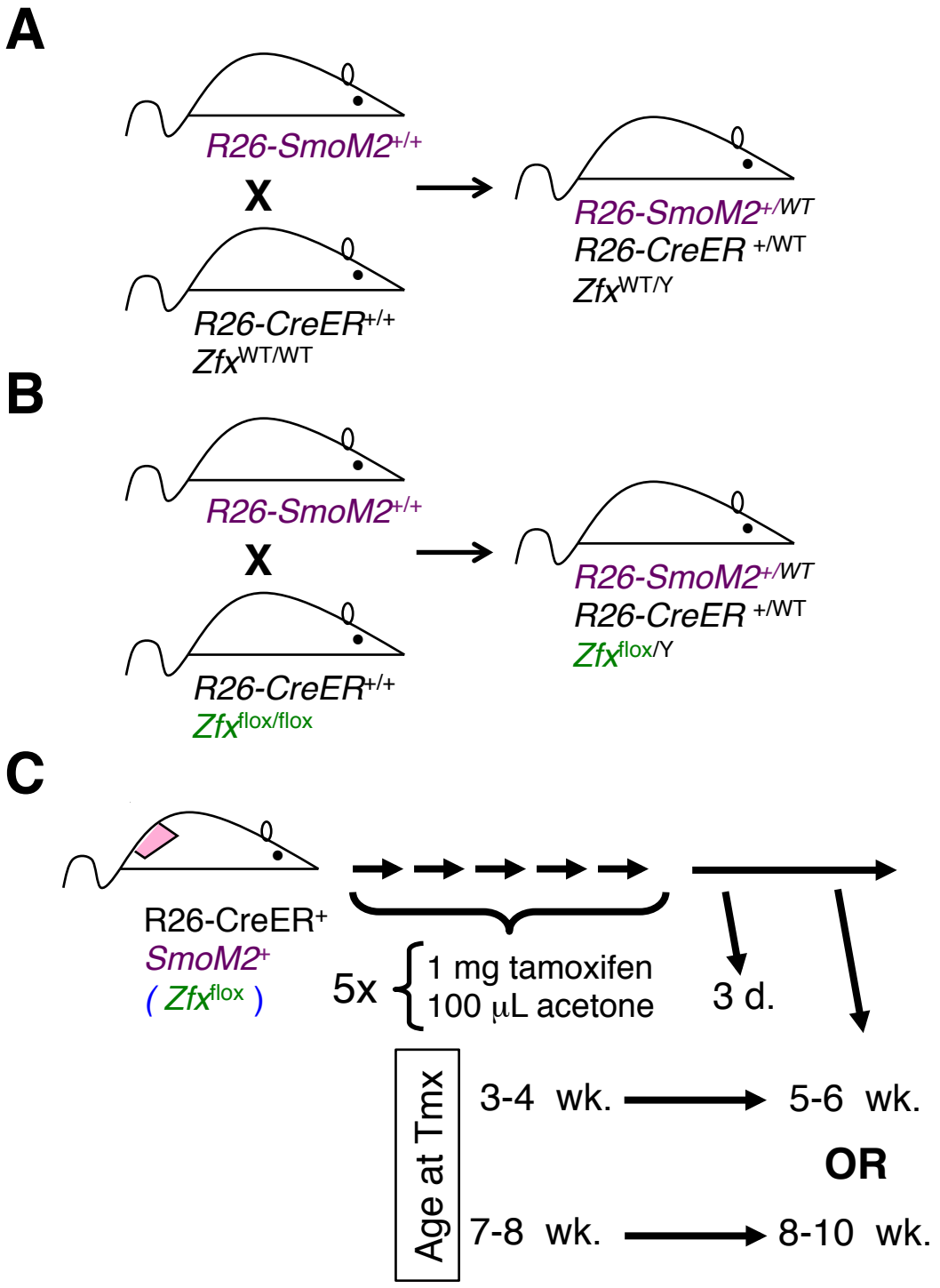
A
R26-SmoM2+/+
X
R26-CreER+/+
Zfx WT/WT
R26-SmoM2+/WT
R26-CreER +/WT
Zfx WT/Y
B
R26-SmoM2+/+
X
R26-CreER+/+
Zfx flox/flox
R26-SmoM2+/WT
R26-CreER +/WT
Zfx flox/Y
C
R26-CreER+
SmoM2+
(Zfx flox)
5x
1 mg tamoxifen
100 μL acetone
3 d.
Age at Tmx
3-4 wk.
5-6 wk.
OR
7-8 wk.
8-10 wk.

Figure 8. Generation of Tmx-inducible *SmoM2* mice for initiating BCC using a constitutively active *Smo* allele

Mice homozygous for inducible “stop-floxed” transgene encoding a constitutively active allele of *Smo* (*R26-SmoM2*) were crossed with Tmx-inducible *R26-CreER* mice that had either wild-type (Zfx^{WT}) or conditional (Zfx^{flox}) alleles of *Zfx*.

(A&B) Shown are schematics depicting the breedings to generate experimental male mice for Tmx-induced excision of the “stop-flox” cassette and expression of the constitutively active SmoM2 allele, with concomitant retention of Zfx^{WT} (A) or deletion of Zfx^{flox} (B) alleles.

(C) Schematic diagram illustrating the treatment regimen of 5 consecutive doses of daily Tmx (1 mg), topically applied to shaved dorsal skin, before analysis of treated skin 3 days after Tmx by qPCR, or 5-6 or 8-10 weeks after Tmx by IHC.

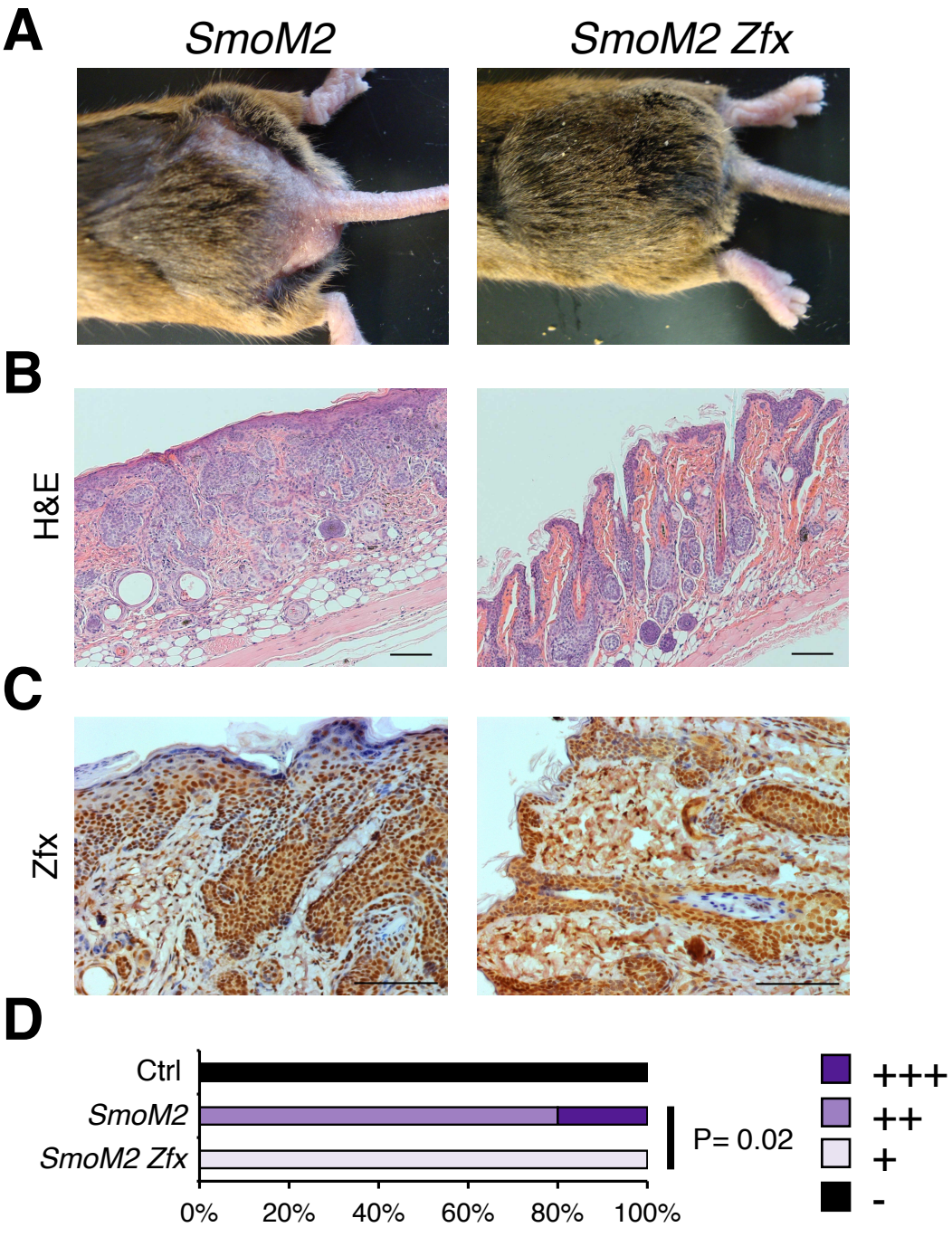
A
SmoM2
SmoM2 Zfx
B
H&E
C
Zfx
D
Ctrl
SmoM2
SmoM2 Zfx
0%
20%
40%
60%
80%
100%
P= 0.02
+++
++
+
-

Figure 9. *Zfx* co-deletion impairs BCC progression after *SmoM2* expression and Hh pathway activation downstream of endogenous *Smo*

Mice carrying tamoxifen (Tmx)-inducible Cre recombinase and an inducible "stop-floxed" transgene encoding the constitutively active *R26-SmoM2* allele, with (*SmoM2 Zfx*) or without a conditional allele of *Zfx*, were treated with Tmx on shaved dorsal skin, as described in Figure 8.

(A) Representative photographs showing dorsal skin of mice of the indicated genotypes following euthanasia 8-10 weeks after Tmx treatment.

(B&C) BCC formation in treated dorsal skin after *SmoM2* induction. Shown are representative micrographs of sections of dorsal skin isolated 8-10 weeks after Tmx treatment from *SmoM2 Zfx* and *SmoM2* mice, then stained with H&E (B) or with anti-Zfx antibody (C). Scale bars represent 100 μm.

(D) Pathology scores in treated skin after Tmx treatment to inititate *SmoM2*-dependent BCC induction. Shown are the fractions of indicated BCC severity scores in *SmoM2* and *SmoM2 Zfx* mice, with *Ptch1*$^{flox/flox}$ *Zfx*$^{WT/Y}$ *R26-CreER*$^{-}$ mice serving as Ctrl (n = 5, 3, and 5, respectively).

We bred homozygous *R26-SmoM2* mice with homozygous *Rosa26-CreERT2* (*R26-CreER*) mice carrying wild-type or conditional alleles of *Zfx* (Fig. 8A,B). Resulting double-heterozygote *R26-CreER*$^{+}$ *R26-SmoM2*$^{+}$ *Zfx*$^{WT/Y}$ (designated *SmoM2*)(Fig. 8A) and *R26-CreER*$^{+}$ *R26-SmoM2*$^{+}$ *Zfx*$^{flox/Y}$ (designated *SmoM2 Zfx*)(Fig. 8B) males were shaved along their dorsal skin and treated topically with Tmx to induce BCC formation, as had been done previously with *Ptch1* conditional mice (Fig. 8C). In this case, a small subset of the *SmoM2* and *SmoM2 Zfx* mice were shaved and painted with Tmx at 3-4 weeks of age during the presumptive 1st telogen of their hair cycle [85], to attempt to induce BCC on a shortened time scale (Fig. 8C).

The effects we observed previously in the *Ptch1*-dependent BCC model, such as hair loss and gross induration over the treated skin patch, were slower to develop and appeared less severe in the *R26-SmoM2* BCC mice. However, by 8-10 weeks post-Tmx (or 5-6 weeks in the younger Tmx-treated mice), hair loss and sclerotic hardening of the skin in Tmx-treated dorsal skin patch was observed in *SmoM2* mice but not in *SmoM2 Zfx* mice (Fig. 9A).
BCC-like tumors could be observed in H&E sections from *SmoM2* treated dorsal skin, where *SmoM2 Zfx* skin had hair follicles closer to wild-type in appearance (Fig. 9B). Similar to the case in *Ptch1 Zfx* mice, co-deletion of *Zfx* was not maintained over time in *SmoM2 Zfx* mice. Anti-Zfx staining of *SmoM2 Zfx* skin sections did not reveal *Zfx*^{null} follicles, normal or aberrant, and Zfx nuclear staining was detected throughout the epidermis in both *SmoM2* and *SmoM2 Zfx*

dorsal skin (Fig. 9C). Furthermore, although the sample sizes were very small, pathologist scoring of *SmoM2* and *SmoM2 Zfx* skin sections from 8-10 (or 5-6) weeks post-Tmx showed a significantly decreased severity in disease score for *SmoM2 Zfx* mice compared to *SmoM2* mice (Fig. 9D). Collectively, these results from the *R26-SmoM2* model of BCC resemble the results from the *Ptch1* model, and they suggest that *Zfx* co-deletion also strongly impairs BCC generated by constitutively active SmoM2 “downstream” of endogenous Smo.

Conversely, preliminary results from qPCR-based gene expression analysis of treated skin in a single cohort of *R26-SmoM2* mice are quite different from those seen previously with the *Ptch1* model (Fig. 10). Decreased expression levels for *Zfx* (~8 to 10-fold) and the Zfx target *Dis3L* (~2-fold) in *SmoM2 Zfx* skin 3 days after Tmx do match the results from the *Ptch1* conditional system, as well as confirm the successful co-deletion of *Zfx* by Tmx application. However, qPCR results for the Hh signal transducer *Smo* and Hh target *Gli1* are strikingly different than we saw previously. *Smo* levels are not reduced after *Zfx* deletion, and increased *Gli1* expression is not blunted after the loss of *Zfx* (Fig. 10). These expression data suggest that impairment in *SmoM2*-dependent BCC development due to *Zfx* co-deletion is not mediated through transcriptional control of *Smo* and subsequent effects on Hh pathway activity.

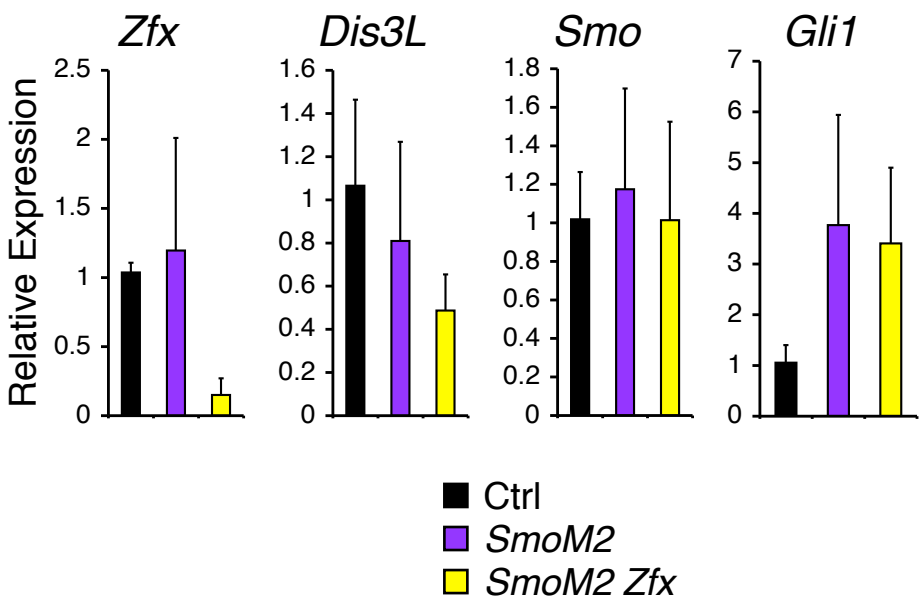

Figure 10. Loss of *Zfx* does not cause decreased expression of *Smo* or Hh target *Gli1* after Tmx-induced *SmoM2* expression in the skin

Expression levels of *Zfx*, the Zfx target *Dis3L*, *Smo,* and Hh pathway target gene *Gli1* in bulk epidermis and hair follicles from shaved dorsal skin 3 days after topical Tmx treatment in *SmoM2* (n= 5), *SmoM2 Zfx* (n= 3), and *R26-CreER*$^{-}$ *Ptch1*^{flox} (Ctrl) (n= 2) mice. Shown are normalized expression levels relative to Ctrl skin as determined by qPCR (mean ± SD of 2-5 mice).

Discussion

We asked whether the transcription factor Zfx was required for tumorigenesis in the Hh-dependent skin cancer basal cell carcinoma. Given the cell-intrinsic requirement for Zfx in the self-renewal of murine HSC and ESC [74, 75], we hypothesized that Zfx might also be required in the context of this Hh-dependent cancer, especially considering that BCC is thought to arise from the stem cell and progenitor compartment in the hair follicle bulge [8]. Here, we demonstrated that formation of Hh-driven BCC was severely impaired or prevented in dorsal skin of *Ptch1 Zfx* (Fig. 5) and *SmoM2 Zfx* mice (Fig. 9), 8-10 weeks after topical Tmx treatment induced *Zfx* co-deletion and Hh pathway activation *via* removal of inhibitory Ptch1 or introduction of activated Smo, respectively. Zfx^{null} BCC were not detected in either the *Ptch1*-dependent (Fig. 6) or *SmoM2*-dependent (Fig. 9) mouse models. These results demonstrated a cell-intrinsic requirement for *Zfx* in the development of the Hh-driven cancer BCC.

A number of established therapies exist for treating BCC, including several forms of surgical excision, radiation treatment, and topical imiquimod or 5-fluorouracil (5-FU) application [108, 109]. While these established therapies have the upside of high effective clearance rates, often approaching 100%, they also have some drawbacks. Surgical excision can leave behind residual tissue damage, and topical imiquimod or 5-FU therapies are only recommended for superficial BCC [108, 109]. The discoveries of the mid- and late-1990s linking BCC to mutations in *PTCH1* or *SMO* [21, 65, 66] paved the way for the addition of a new tool to this

armamentarium: small molecule inhibitors targeting the Hh pathway. Phase I clinical trials of inhibitors targeting the Hh signal transducer, SMO, have shown promising results in treating patients with advanced or metastatic BCC [110]. Since *Zfx* is required for BCC to develop *in vivo*, one future possibility is that Zfx or its relevant downstream transcriptional targets could represent novel druggable molecules for treatment of BCC.

Our preliminary investigations into downstream Zfx targets with functional relevance in BCC pointed towards *Smo*. After inducing *Ptch1* deletion and Hh pathway activation with topical Tmx, *Ptch1 Zfx* mice (which co-delete *Zfx*) had decreased *Smo* expression in treated skin, and the overactivation of Hh pathway as gauged by *Gli1* and *Mycn* expression was prevented (Fig. 7). These data favored a simple explanation of the role of Zfx in Hh-dependent BCC: Zfx is necessary for *Smo* expression after removal of *Ptch1*, and loss of Zfx thus decreases the levels of the Hh pathway signal transducer, blocking the pathway overactivation that initiates BCC. Such an explanation is consistent with previous work in mouse models to generate BCC, whence we know that Hh activation *via* ablation of *Ptch1* is sufficient to successfully generate BCC [20] and that sustained Hh pathway activation is required to maintain them [22].

This first explanation for the role of *Zfx* in BCC development runs up against complications when we consider our experimental results from the generation of BCC using activated *SmoM2* allele. As with the *Ptch1*-dependent BCC model previously, we found that co-deletion of *Zfx* significantly impaired

BCC development after induction of constitutively active SmoM2 in the skin and that *Zfx*^{null} BCC or aberrant follicles were not observed (Fig. 9). In the *SmoM2*-dependent BCC model, however, Hh pathway activity is driven by expression of a constitutively active Smo, "downstream" or at least independently of endogenous Smo. Expression analysis in treated *SmoM2 Zfx* skin showed the same loss of *Zfx* expression as in *Ptch1 Zfx* skin, but *Smo* transcript levels were not decreased and overexpression of Hh targets *Gli1* and *MycN* were not blunted (Fig. 10). Zfx is thus required in BCC initiated by either deletion of inhibitory Ptch1 or activated SmoM2 expression, but evidence for Zfx control of Hh activation *via Smo* is present in only the former case.

There are at least two possible explanations for this discrepancy. One possibility is that *Ptch1*-dependent and *SmoM2*-dependent BCC represent two tumor cell environments distinct enough that the relevant downstream targets of *Zfx* in the two different models are different. There is precedent in the literature suggesting that BCC generated by *Ptch1* loss and *SmoM2* expression are substantially different. A recent study generated BCC in *Ptch1*$^{+/-}$ mutant mice treated with ionizing radiation, mimicking a common etiology of human BCC, and subsequently identified cells of hair follicle bulge stem cell compartment as the predominant BCC cells-of-origin, using cell fate mapping with inducible Cre specific to the bulge (*K15-CrePR1*) or widely expressed in the epidermis (*K14-CreER*) [8]. This study from Wang *et al*. (2011) was a direct response to the previous report from Youssef *et al*. (2010), where the authors generated BCC

using inducible Cre transgenes and the same *Rosa26-SmoM2* transgene we employed in the Results above. In their case, they identified long-lived progenitor cells of the interfolliclular epidermis as the BCC cell-of-origin [9]. By histology, none of the *SmoM2* BCC from Youssef *et al*. (2010) arose from hair follicles, while all did in the *Ptch1*$^{+/-}$ IR model of Wang *et al*. (2011) [8, 9]. These differences between BCC models could be explained by ubiquitous expression of *SmoM2* by the Rosa26 promoter in locales (such as the interfollicular epidermis) where *Smo* is not normally expressed, or by additional non-Hh-specific functions of Ptch1 that are lost in *Ptch1*-deficient BCC but not *SmoM2*-driven BCC [8]. The role of *Zfx* in these two similar but distinct BCC models could be different, with driving of *Smo* expression being crucial in the *Ptch1* model but other downstream targets taking on significance in BCC generated by Rosa26-driven *SmoM2*.

A second possible explanation for the discrepancy is that the same, yet-to-be-identified downstream Zfx targets are responsible for the phenotypes in both the *Ptch1*-dependent and *SmoM2*-driven BCC models. In this case, qPCR results for *Smo*, *Gli1*, and *Mycn* from 3 days post-Tmx skin in *Ptch1 Zfx* mice (Fig. 7) would represent a good exampe of correlation not implying causation. Instead, Zfx targets such as *Dis3L* that are downregulated after *Zfx* co-deletion in both the *Ptch1*-dependent (Fig. 4C) and *SmoM2*-driven (Fig. 10) models of BCC would be the best candidates to explain the prevention of BCC development after *Zfx* loss.

A third and final possible explanation for the discrepancy is that loss of *Zfx* regulation of endogenous *Smo* expression causes the phenotype in both the

Ptch1-dependent and *SmoM2*-dependent models, but that this loss of endogenous *Smo* is masked in the *SmoM2* model by overexpression of the transgenic constitutively active *Smo* allele. Smo has been reported to function as a dimer, with phosphorylation of C-terminal Arg clusters and consequent dimerization of its C-terminal cytoplasmic tails in response to Hh signal being essential for downstream pathway activation [48]. In the *SmoM2*-dependent BCC model, it is possible that the overexpressed, constitutively active *SmoM2* allele still requires endogenous Smo for this dimerization and Hh pathway downstream activation. If this were the case, then decreased expression of endogenous *Smo* following Zfx loss would explain the prevention of BCC formation in *SmoM2*-dependent BCC, as well as in *Ptch1*-dependent. Currently, we are unable to directly confirm that *Zfx* co-deletion decreases expression levels of endogenous *Smo* in *SmoM2* BCC mice, however, since our qPCR primers detect both wildtype transcript and the transcript from the *SmoM2* cDNA. Any lowered levels of endogenous Smo are therefore masked by the abundant levels expressed off the *SmoM2* transgene.

In this Chapter, we demonstrated a requirement for the transcription factor Zfx in the Hh-dependent, hair follicle-derived cancer basal cell carcinoma. The downstream targets of Zfx responsible remain unclear, although the Hh signal transducer *Smo* emerged as candidate. In Chapter II, we examine whether a requirement for *Zfx* is generalizable across cancers driven by aberrant Hh

pathway activation in progenitor compartments, by examining whether *Zfx* is necessary for development of the cerebellar tumor medulloblastoma (MB).

Materials & Methods

Animals

Mice with conditional alleles of the Hh pathway inhibitory receptor gene *Patched1* (*Ptch1*^{flox})[105] and of the transcription factor *Zfx* (*Zfx*^{flox})[74] have been previously described. Tamoxifen (Tmx)-inducible *Rosa26-CreERT2* deleter mice (*R26-CreER*$^{+}$) were kindly provided by Dr. Thomas Ludwig, Columbia University[74]. Homozygous *Ptch1*$^{flox/flox}$ mice were mated separately with *R26-CreER*$^{+}$ *Zfx*^{WT} and *R26-CreER*$^{+}$ *Zfx*^{flox} mice to ultimately generate distinct singly-deleting *R26-CreER*$^{+}$ *Ptch1*^{flox} *Zfx*^{WT} and doubly-deleting *R26-CreER*$^{+}$ *Ptch1*^{flox} *Zfx*^{flox} breeding lines. Male mice with genotypes *R26-CreER*$^{+}$ *Ptch1*$^{flox/flox}$ *Zfx*$^{WT/Y}$ (designated *Ptch1* in Figures) and *R26-CreER*$^{+}$ *Ptch1*$^{flox/flox}$ *Zfx*$^{flox/Y}$ (designated *Ptch1 Zfx* in Figures) were compared in Tmx-painting and BCC induction experiments, with *R26-CreER*$^{-}$ *Ptch1*$^{flox/flox}$ *Zfx*$^{WT/Y}$ littermates (designated Ctrl in Figures) serving as negative controls.

Rosa26-SmoM2 (*R26-SmoM2*) transgenic mice were obtained from Jackson Laboratories. After Cre-mediated excision of a “stop-flox” cassette, these mice will express an enhanced YFP-tagged, constitutively active allele of *Smo* under the control of the ubiquitous *Rosa26* promoter, and the *SmoM2* allele has been demonstrated previously to initiate BCC-type tumors in mice *in vivo* [104, 107, 111]. Homozygous *R26-SmoM2*$^{+/+}$ mice were bred with either *R26-CreER*$^{+/+}$ or

R26-CreER$^{+/+}$ *Zfx*$^{flox/flox}$ mice to generate *R26-CreER*$^{+}$ *R26-SmoM2*$^{+}$ and *R26-CreER*$^{+}$ *R26-SmoM2*$^{+}$ *Zfx*$^{flox/Y}$ males, respectively, for experiments involving Tmx-induced of BCC initiation in dorsal skin *via* activation of the Hh pathway downstream (or independently) of endogenous *Smo*.

All animal studies were performed according to the investigator's protocol approved by the Institutional Animal Care and Use Committee of Columbia University.

RNA Isolation and qPCR

Total cellular RNA was isolated from samples in 0.5-1 mL TriZol LS reagent (Invitrogen). cDNA was synthesized from 1-2 μg RNA per sample using SuperScript III reverse transcriptase (invitrogen). Quantitative real-time PCR (qPCR) assaying for SYBR Green incorporation were run on an Mx3000P instrument (Stratagene) using FastStart Universal SYBR Green Master mix containing Rox (Roche). Triplicate reactions were run for each sample, and replicates with a Ct value >1 Ct from any of the other two replicates (while those two replicates remained within 1 Ct value of one another) was excluded as an outlier. All qPCR results were analyzed using the ΔΔCt method as previously[74]. The expression values for all genes were scaled to total RNA content using Ct for the housekeeping genes β-Actin (*Actb*), β2-microglobulin (*B2m*), hypoxanthine guanine phosphoribosyl transferase (*HPRT*), or *GAPDH*, and then normalized to the indicated control samples. The qPCR primers are listed below.

Species	Gene	Forward	Reverse
Mouse	Actb	ATCCTGACCCTGAAGTACC	TACGACCAGAGGCATACAG
	B2m	ACCCTGGTCTTTCTGGTGCTTG	TATGTTCGGCTTCCCATTCTCC
	HPRT	GCCCCAAAATGGTTAAGGTTGC	TCAAGGGCATATCCAACAACAAAC
	GAPDH	AAGGTCGGTGTGAACGGATTTG	CTCGCTCCTGGAAGATGGTGAT
	Zfx	GCAGTGCATGAACAGCAAGT	GCAAGGTGTTCAGGATGGTT
	Dis3L	AGGGGGAAGCCATGGAGAAG	GATTTGATGCCCGCTTCCAG
	Ube2j1	GACGCATAGTACTGCCACCA	ATGGCCCCCTCTCCTTTAGT
	Smo	CTCGGACTCGCAGGAGGAAG	TCAGGGAAGTGGTCCGGTGT
	Gli1	CATTGGGGAGGTTGCTCCAG	CCGAAGGTGCGTCTTGAGGT
	Mycn	GGAGAGGATACCTTGAGCGACTC	CGCCTTGTTGTTAGAGGAGGAAC
	Mnx1	AGGCGCAGTCGAACCTCTTG	TCCATTTCATTCGGCGGTTC
	Isl1	CAAGCGGTGCAAGGACAAGA	CAGGGCGGCTGGTAACTTTG
	Olig2	CACCTCCTCGTCCACGTCCT	GGCGATCTTGGAGAGCTTGC
	Tubb3	GGCCATTCTGGTGGACTTGG	GCCCTGCAGGCAGTCACAAT
Human	GAPDH	AAGGTGAAGGTCGGAGTCAACG	CCCACTTGATTTTGGAGGGATC
	Zfx	GCAGGATGATGACAAAGGCAAC	CAAGGATCAATTTCCGACTCTGTG
	Dis3L	CCAGGACAGGATGCCAATTGTT	CGTGGGCAGCTTTTAAATCAGG
	Ube2j1	GAAACTTGGCAGCCTTCGTG	ATGGCAGAGCCACATCCTTC
	Smo	GCTCATCGTGGGAGGCTACTTC	AGCATGGTCTCGTTGATCTTGC
	Gli1	CTCGGGCACCATCCATTTCTAC	GCCAGTCATTTCCACACCACTG

Tamoxifen Treatment of Dorsal Skin

Adult male mice of the designated genotypes were shaved across their dorsal skin at 7-9 weeks of age (with the great majority shaved at postnatal day 50 or P50), temporally situating tamoxifen (Tmx) treatment within the second telogen of the hair cycle[85]. Animals were then treated for five consecutive days topically with 100 μL per day of 10 mg/mL tamoxifen (Sigma) in acetone (i.e. – 1 mg tamoxifen q.d.). In the case of experiments with mice bearing the *SmoM2* "stop-flox" allele of *Smo*, some mice were shaved instead during their first telogen at

approximately 3-4 weeks of age (e.g.- P21 or P22), in an attempt to accelerate initiation of BCC.

For gene expression analysis in bulk epidermis and hair follicles, Tmx-treated mice were sacrificed three days after final Tmx treatment. Tmx-treated dorsal skin was removed, and connective/adipose/vascular tissue was stripped from the dermis in cold PBS (Gibco). The remaining dermis and epidermis were floated in 0.25% trypsin - 1x EDTA (Gibco), with epidermis/hair follicles up, at 37°C, 7.5% CO_2 for 2 hours, and bulk hair follicles and epidermis were separated from dermis into DMEM with 10% FBS using sterile disposable scalpels. Bulk follicles/epidermis were minced, collected by centrifugation, and lysed in 2 mL TriZol LS reagent (Invitrogen).

For histological analysis, at 8-9 weeks after Tmx-treatment, mice were re-shaved if dorsal hair had regrown, and the Tmx-treated patch was removed, flattened, and fixed before processing for histology. Again, some exceptions to this time-scale occurred in the case of *SmoM2*$^{+}$ mice, where mice painted during their first telogen (beginning at approximately P21) were instead sacrificed 5-6 weeks post-Tmx. Additionally, BCC initiation in mice painted during their

Immunohistochemistry

Dorsal skin from topically Tmx-treated mice was fixed for 24 hrs in zinc formalin (Thermo Scientific) and then 24 hours in 70% ethanol. Tissue segments were subdissected from the Tmx-treated region, with the long dimension following the spinal column midline, and embedded on edge in paraffin. Paraffin sections (5

μm) from Tmx-treated skin were stained with hematoxylin and eosin (H&E), or were immunostained with anti-Zfx (1:500) or with anti-Sox9 (Santa Cruz, 1:500) antibodies, incubated with biotinylated anti-rabbit secondary antibody (Vector Labs), visualized ABC and DAB Peroxidase Substrate Kits (Vector Labs), and counterstained with hematoxylin.

Micrographs of histological sections were recorded using an AxioImager.M2 microscope with attached AxioCam MRc camera (Zeiss).

Statistics

Pathology scores were analyzed using Fisher's Exact Test extended to a 2x4 contingency table.

CHAPTER II

A requirement for *Zfx* for optimal growth of medullblastoma (MB) models *in vivo* and *in vitro*

Introduction

Hedgehog (Hh) signaling is required for growth and patterning of the cerebellum

The Hedgehog (Hh) family of secreted, intercellular morphogens is critical for numerous processes during mammalian development [26]. Classic examples of Hh function during development include patterning of the distal limb and digits by Sonic hedgehog (Shh) secreted from the zone of polarizing activity (ZPA) [112-114], or specification of motor neuron (MN) and ventral interneuron progenitor pools in the developing spinal cord [55, 115, 116]. In Chapter I we touched on another example when discussing the requirement for Hh signaling for the original morphogenesis and subsequent cycling of the hair follicle [18, 19, 97].

Shh signaling is also critically important during the development of the cerebellum. The cerebellum is a region of the brain most associated with balance and sensorimotor function, although it may have additional roles in other cognitive functions [117]. The different cell types of the cerebellum derive from distinct germinal regions. A progenitor domain in the ventricular zone or the IVth ventricle gives rise to Purkinje neurons, as well as various cerebellar interneurons and glia, while progenitors in the rhombic lip give rise to granule neurons, the most numerous neuronal subtype in not only the cerebellum but also the entire central nervous system (CNS) [10, 117, 118]. Mature granule neurons are generated from proliferation of granule neuron precursors (GNP), which migrate from the rhombic lip during embryogenesis and form an external granular

layer (EGL) on the cerebellar surface [117-119]. While there, GNP undergo extensive proliferation post-natally (until postnatal day 15 in mice and postnatal ***year*** 2 in humans), before differentiating into granule neurons and migrating inward to constitute an internal granule layer [117-119]. Shh signaling is critically required during this process. Hh pathway activation, from Shh signal received from Purkinje cells, is required for the expansion of GNP in the EGL and for normal growth and patterning of the cerebellum [24, 119]. The characteristic lobed foliation pattern of the cerebellum also depends on the levels of functional Hh signaling during development, as demonstrated in mouse models where graded decrease in Shh signaling generated increasingly stunted cerebellar foliation [23].

The cerebellar tumor medulloblastoma (MB) is linked to Hh pathway activation

In another parallel with the discussion of hair follicles and the follicle-derived cancer basal cell carcinoma (BCC) from Chapter I, aberrantly activated Hh signaling also acts as the etiological agent for a cancer of the cerebellum, namely medulloblastoma (MB). Primarily a pediatric cancer, MB is the most common malignant brain tumor in infants and children [117, 118]. Survival rates for MB following conventional therapy with surgery, radiation, and chemotherapy approach 70-80%, but surviving patients are consequently subject to an array of long-term side effects [67].

Genome-wide analyses over the last decade have revealed the name “medulloblastoma” to be something of an umbrella term, encompassing four

molecularly distinct cancer subtypes [68, 120-123] that originate from different cell-types and regions of the brain [10-12, 124]. These MB subtypes include a WNT subtype, a SHH subtype, and two other groups yet to be definitively named, although one bears a MYC mutation signature [67]. Hh-driven MB account for approximately 30% of all MB, carry an intermediate prognosis, cluster primarily in infant or in adult patients, and are marked primarily by a desmoplastic/nodular histological appearance, although they can less frequently exhibit large cell anaplastic or “classic” histology [67, 68].

The first connection between the Hh pathway and MB was actually established well before its confirmation in these genomics studies, from the same studies linking the hereditary condition Gorlin Syndrome to mutations in the inhibitory receptor *PTCH1* that also linked Hh pathway activation to the skin cancer BCC [65, 66]. When MB development was observed in mice heterozygous for mutant *Ptch1* [125, 126], or in mice with tissue-specific, Cre-mediated *Ptch1* deletion or constitutively active *Smo* expression [10, 11], it confirmed Hh pathway activation as a driver of MB. Creative use of mouse models also led to identification of the cell-of-origin for Hh-dependent MB. Mice deleting *Ptch1* or expressing activated Smo in neural stem cells, or later in granule neuron precursors using the GNP-specific Math1-Cre, revealed that Hh-dependent MB arise from GNP in the developing cerebellar EGL [10, 11]. Thus, mirroring intriguingly the situation with Hh-dependent BCC formation from cells of the hair follicle bulge, MB also develops following uncontrolled activation of Hh signaling

in a progenitor-bearing compartment of the cerebellum that is sensitive to Hh signal during its normal development.

An incomplete requirement for Zfx *in Hh-dependent MB*

In Chapter I, we observed that co-deletion of *Zfx* prevented the formation of BCC *in vivo* following tamoxifen (Tmx)-induced activation of the Hh pathway in the skin. In this Chapter, we asked whether *Zfx* was similarly required for initiation and maintenance of a Hh-dependent MB. Using a previously validated *in vivo* model for generating Hh-dependent MB [11], we established mouse lines that initiated MB *via* nearly CNS-wide deletion of the inhibitory receptor *Ptch1*, with or without concomitant deletion of *Zfx.* Co-deletion of *Zfx* significantly delayed, but did not prevent, MB growth after *Ptch1* deletion. Loss of ZFX also impaired growth of human MB cells *in vitro*. *Zfx* was not required, however, for development in a model of *PTEN*-dependent glioblastoma, a different brain tumor. Combined with our data from BCC models in Chapter I, these models suggest that there is a common cell-intrinsic requirement for *Zfx* shared by two distinct Hh-dependent cancers.

Results

Establishing a CNS-specific model for co-deleting Ptch1 *and* Zfx *and for Hh-dependent MB generation* in vivo

Having previously observed a requirement for *Zfx* in BCC development stemming from Hh pathway activation in the skin, we asked whether *Zfx* was similarly required for the formation and growth of Hh-dependent MB. To answer this question, we utilized mouse strains carrying the same conditionally targetable "floxed" alleles of *Patched1* (*Ptch1*^{flox})[105] and *Zfx* (*Zfx*^{flox})[74] that we used previously to generate Hh-dependent BCC *in vivo*. In the case of MB, since the cerebellum does not afford the same ease of access for tissue-targeted tamoxifen (Tmx) treatments as the skin, we eschewed the Tmx-inducible but ubiquitously expressed *Rosa26-CreER* and instead obtained the non-inducible but CNS-specific *hGFAP-Cre.*

Originally intended to be an astrocyte-specific Cre transgene, *hGFAP-Cre* begins expressing Cre recombinase under the control of the human glial fibrillary acid protein (hGFAP) promoter in the developing mouse brain at embryonic day 13.5 (E13.5), and it instead effects deletion of targeted alleles in nearly all cell types in the brain, with the exception of cerebellar Purkinje neurons and cells of the choroid plexus [127]. Included on the list of CNS cell-types covered by *hGFAP-Cre* are the granule neuron precursor (GNP) cells which are the cells-of-origin in Hh-dependent MB, and hGFAP-Cre-mediated deletion of *Ptch1* has been successfully used previously as a system to generate MB *in vivo* [10, 11].

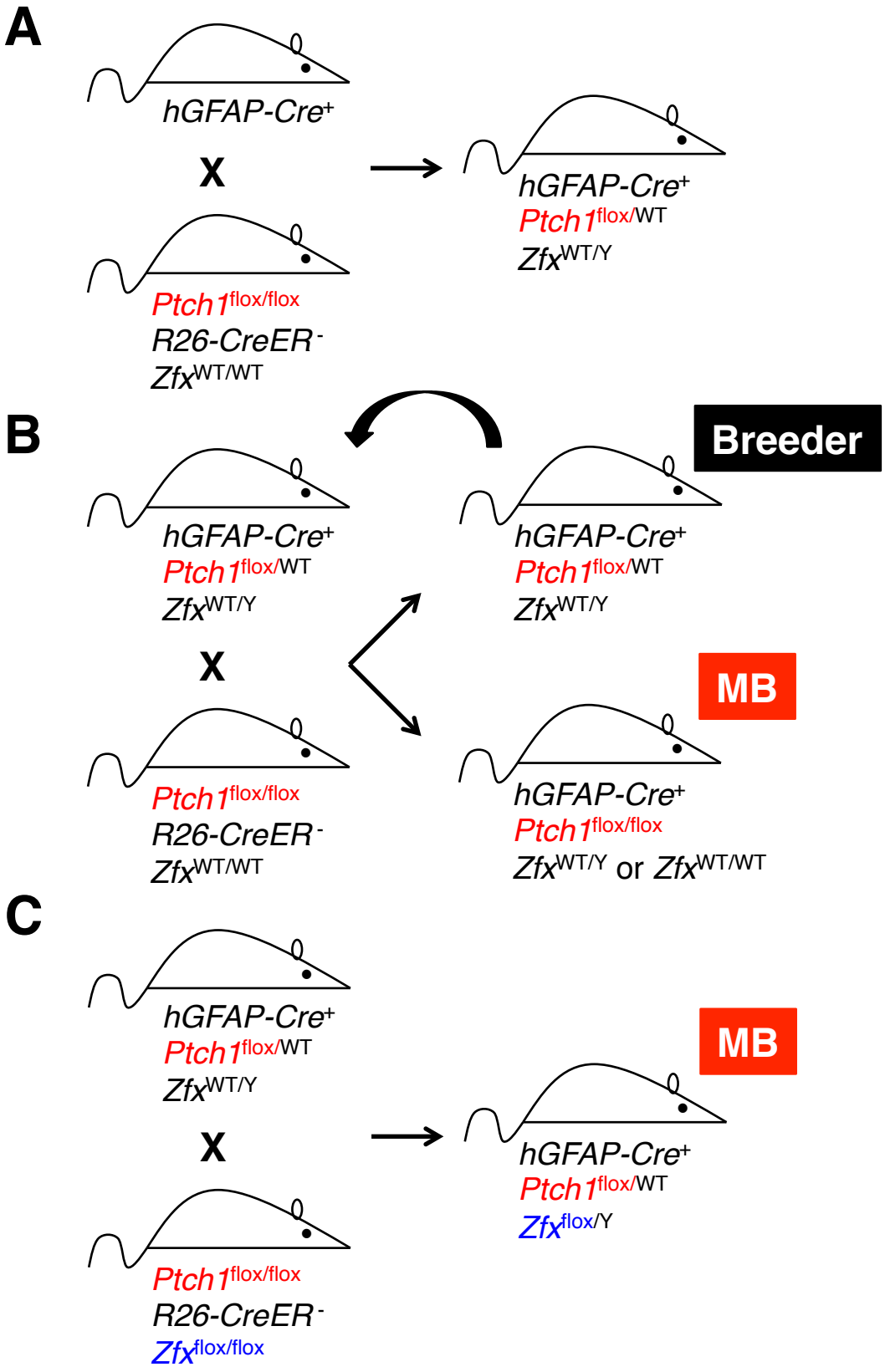
A
hGFAP-Cre+
X
Ptch1flox/flox
R26-CreER-
ZfxWT/WT
hGFAP-Cre+
Ptch1flox/WT
ZfxWT/Y
B
Breeder
hGFAP-Cre+
Ptch1flox/WT
ZfxWT/Y
X
Ptch1flox/flox
R26-CreER-
ZfxWT/WT
MB
hGFAP-Cre+
Ptch1flox/flox
ZfxWT/Y or ZfxWT/WT
C
hGFAP-Cre+
Ptch1flox/WT
ZfxWT/Y
X
Ptch1flox/flox
R26-CreER-
Zfxflox/flox
MB
hGFAP-Cre+
Ptch1flox/WT
Zfxflox/Y

Figure 11. Generation of CNS-specific deleter mice for *Ptch1* and *Zfx*

Mice bearing the *hGFAP-Cre* transgene, which expresses Cre recombinase and effects deletion in nearly all CNS cell-types, were bred with mice bearing conditional alleles of *Patched1* (*Ptch1*^{flox}) and *Zfx* (*Zfx*^{flox}) to generate single- or double-deleter mice that would develop Hh-dependent medulloblastoma (MB).

(A) Schematic depicting generation of *hGFAP-Cre*$^{+}$ *Ptch1*$^{flox/WT}$ *Zfx*$^{WT/Y}$ breeder males for the crosses generating Hh-dependent MB mice.

(B) Generation of positive control *hGFAP-Cre*$^{+}$ *Ptch1*$^{flox/flox}$ *Zfx*^{WT} mice. Breeder males generated in (A) were bred with *Ptch1*$^{flox/flox}$ *Zfx*$^{WT/WT}$ *Rosa26-CreER*$^{-}$ mice (Fig. 2A), yielding singly-deleting MB mice and also regenerating breeder males.

(C) Generation of experimental *hGFAP-Cre*$^{+}$ *Ptch1*$^{flox/flox}$ *Zfx*$^{flox/Y}$ mice. . Breeder males generated in (A) were bred with *Ptch1*$^{flox/flox}$ *Zfx*$^{flox/flox}$ *Rosa26-CreER*$^{-}$ mice (Fig. 2B), yielding doubly-deleting experimental MB mice.

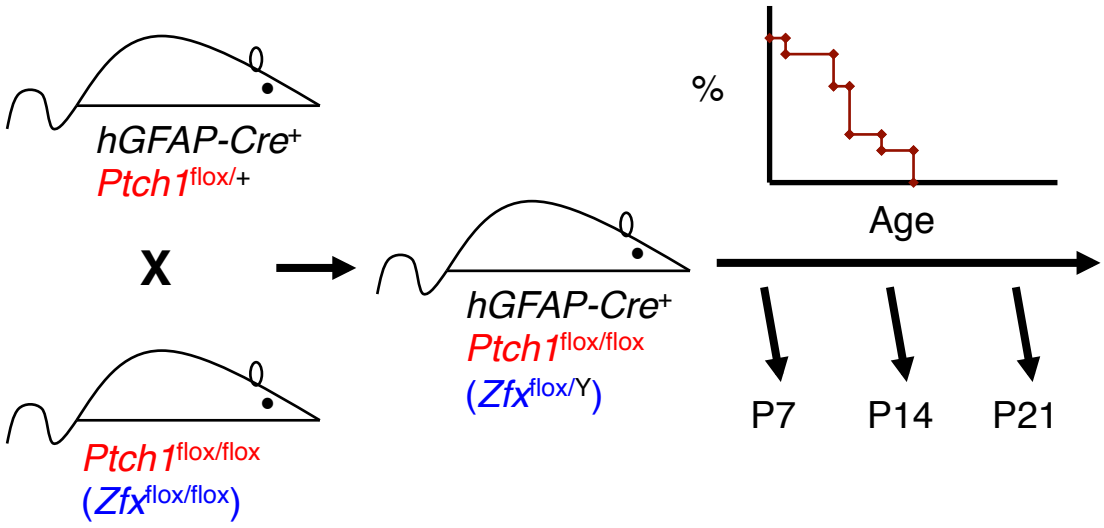

Figure 12. Hh-dependent MB induction by *Ptch1* deletion *in vivo*

Experimental setup for observation of mice that delete *Ptch1* with or without *Zfx* co-deletion and that develop Hh-dependent MB. Animals were followed for survival curve and sacrificed at defined postnatal days of age (P7, P14, P21) for analysis by histology, immunohistochemistry (IHC), and qPCR.

To begin to replicate this model of Hh-dependent MB, we obtained *hGFAP-Cre* mice and bred them to *Ptch1*$^{flox/flox}$ *Zfx*$^{WT/WT}$ *R26-CreER*$^{-}$ mice generated by our BCC model crosses, yielding *Ptch1*$^{flox/WT}$ *Zfx*$^{WT/Y}$ *hGFAP-Cre*$^{+}$ breeder males (Fig. 11A). These breeder males could then be crossed to other *Ptch1*$^{flox/flox}$ *Zfx*$^{WT/WT}$ *R26-CreER*$^{-}$ females, yielding both additional breeder males and also *Ptch1*$^{flox/flox}$ *Zfx*^{WT} *hGFAP-Cre*$^{+}$ (designated *Ptch1* in Figures) males and females that would delete *Ptch1* throughout their cerebella and develop MB (Fig. 11B). Breeder males were also crossed with *Ptch1*$^{flox/flox}$ *Zfx*$^{flox/flox}$ *R26-CreER*$^{-}$ females, generating *Ptch1*$^{flox/flox}$ *Zfx*$^{flox/Y}$ *hGFAP-Cre*$^{+}$ mice (designated *Ptch1 Zfx*) that co-delete *Zfx* along with *Ptch1* (Fig. 11C). *Ptch1* and *Ptch1 Zfx* mice, along with *hGFAP-Cre*$^{-}$ or *Ptch1*$^{flox/WT}$ littermate control animals (Ctrl), were monitored closely for disease progression and survival, and some mice were sacrificed at defined post-natal timepoints for analysis of their cerebella by histology (Fig. 12).

Co-deletion of Zfx *slows MB development and enhances survival after* Ptch1 *deletion* in vivo

To see whether *Zfx* co-deletion affected MB generation after *Ptch1* deletion in the cerebellum, we examined sagittal sections from cerebella of *Ptch1*, *Ptch1 Zfx*, and Ctrl mice at post-natal day 7 and 14 (P7 and P14)(Fig. 13). Unlike in the BCC model in the skin, co-deletion of *Zfx* did not prevent or drastically impair MB formation following *Ptch1* deletion.

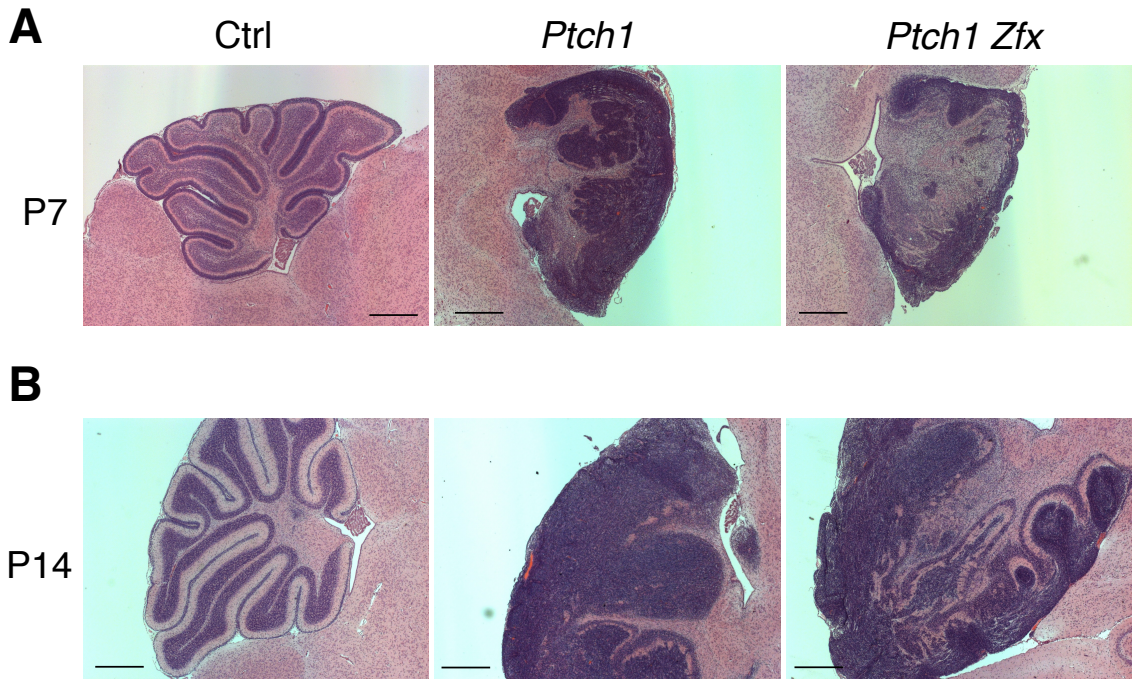

Figure 13. Loss of *Zfx* delays Hh-induced MB development

MB development was followed in mice with CNS-specific *hGFAP*-Cre and conditional alleles of *Ptch1* alone (*Ptch1*) or of both *Ptch1* and *Zfx* (*Ptch1 Zfx*), as well as in Cre^- control mice (Ctrl).

(A&B) H&E-stained sagittal sections of cerebella from P7 (A) and P14 (B) mice of the indicated genotypes. Scale bars represent 500 μm.

The massive expansion of the EGL and disruption of normal cerebellar foliation seen in P7 *Ptch1* cerebella compared with P7 Ctrl cerebella was present also in P7 *Ptch1 Zfx* cerebella (Fig. 13A). Expansion of hyperproliferative EGL and disruption of normal cerebellar morphology was even more pronounced in both *Ptch1* and *Ptch1 Zfx* cerebella at P14 (Fig. 13B).

While loss of *Zfx* did not appear, as with BCC, to stop MB formation in its tracks, visual inspection of sagittal sections from P7 and P14 *Ptch1 Zfx* cerebella suggested that loss of *Zfx* did result in reduced size of the MB-like expanded EGL and better preservation of cerebellar architecture (Fig. 13A&B). To confirm this observation, we quantified the size of MB tumor induced by *Ptch1* deletion by measuring the cross-sectional area of the EGL (Fig. 14A) and non-EGL cerebellar tissue (Fig. 14B) in sagittal sections from *Ptch1*, *Ptch1 Zfx*, and Ctrl P7 cerebella. Both *Ptch1* and *Ptch1 Zfx* cerebella had significantly larger MB burden than Ctrl mice, as gauged by both cross-sectional area of the EGL (Fig. 14C) and by the percent of total cerebellar area occupied by EGL (Fig. 14D). However, *Ptch1 Zfx* P7 pups also had significantly smaller hyperproliferative EGL than pups that deleted only *Ptch1*, by EGL area (Fig. 14C) and percent cerebellar area (Fig. 14D). These data suggested that *Zfx* loss did not prevent but did slow the growth of MB after *Ptch1* deletion.

Results from monitoring *Ptch1* and *Ptch1 Zfx* MB mice for survival were concordant with the reduced MB tumor burden in *Ptch1 Zfx* mice observed by cross-section area measurements. All *Ptch1* mice developed MB, with symptoms

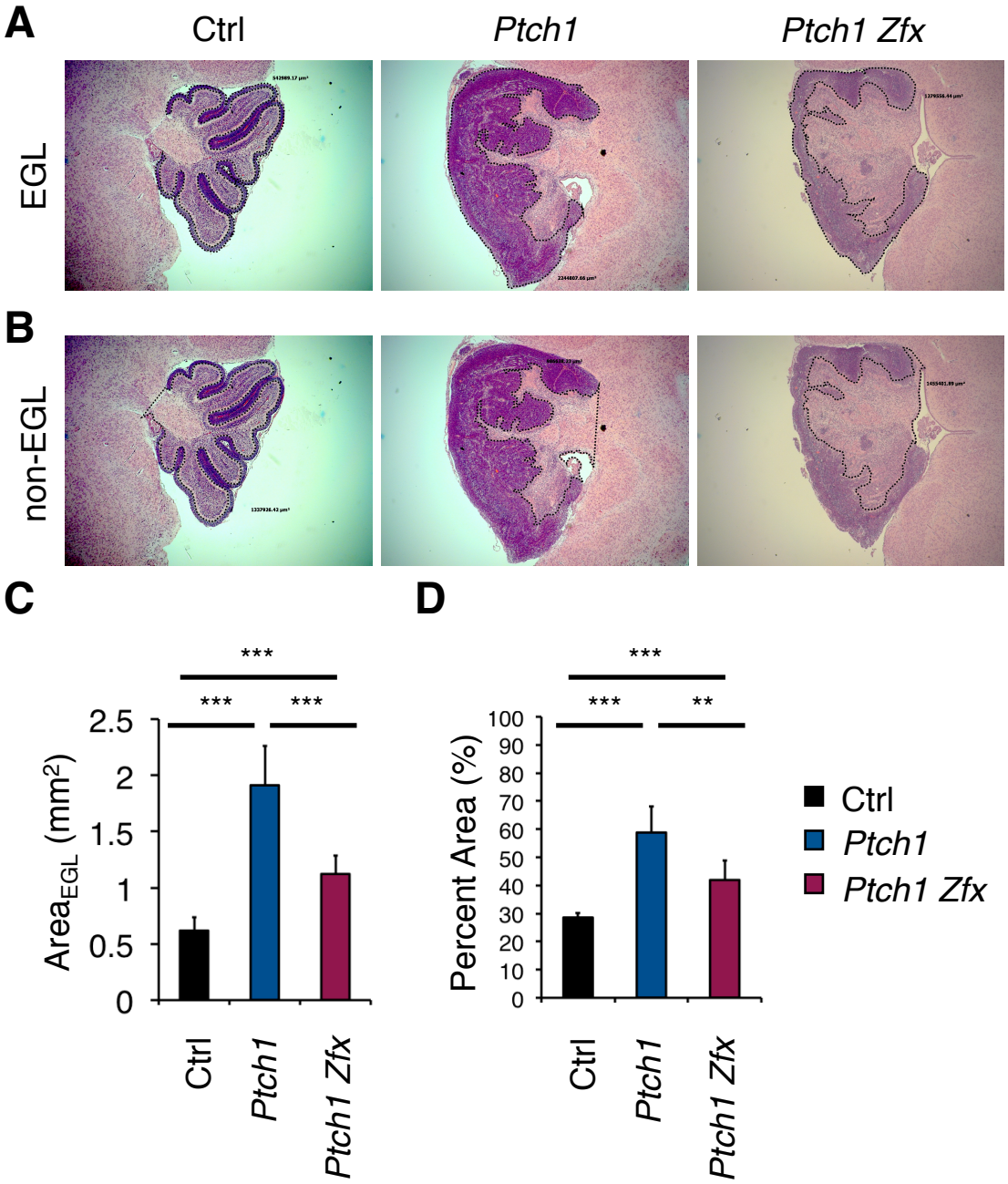
A
Ctrl
Ptch1
Ptch1 Zfx
EGL
B
non-EGL
C
***
***
***
Area$_{EGL}$ (mm^2)
2.5
2
1.5
1
0.5
0
Ctrl
Ptch1
Ptch1 Zfx
D
***
***
**
Percent Area (%)
100
90
80
70
60
50
40
30
20
10
0
Ctrl
Ptch1
Ptch1 Zfx
Ctrl
Ptch1
Ptch1 Zfx

Figure 14. Hh-dependent MB that co-delete *Zfx* have significantly smaller cross-sectional areas.

To quantify the size of MB tumors generated in *hGFAP-Cre*$^{+}$ *Ptch1*$^{flox/flox}$ *Zfx*^{WT} (*Ptch1*), *hGFAP-Cre*$^{+}$ *Ptch1*$^{flox/flox}$ *Zfx*$^{flox/Y}$ (*Ptch1 Zfx*), and *Cre*$^{-}$ or *Cre*$^{+}$ *Ptch1*$^{flox/+}$ (Ctrl) mice, we measured the cross-sectional area of hyperprolerative EGL in sagittal sections from P7 cerebella.

(A) Representative micrographs showing measurement of cross-section area of external granular layer (EGL) or hyperproliferative EGL/MB tumor in sagittal cerebellar sections from P7 Ctrl, *Ptch1*, and *Ptch1 Zfx* pups. Sections are from same level (2nd out of 4 level sections through half cerebellum). 20x objective used, and area measurements made directly in Axionvision 4.8.2 software.

(B) Representative micrographs showing measurement of cross-section area of all cerebellar tissue *excluding* the EGL (non-EGL), in sagittal cerebellar sections from P7 Ctrl, *Ptch1*, and *Ptch1 Zfx* pups. Sections are from Level 2 out of 4 Level sections through half cerebellum. 20x objective used, and area measurements made directly in Axionvision 4.8.2 software.

(C) Cross-section area of EGL in sagittal sections from P7 Ctrl, *Ptch1*, *Ptch1 Zfx* cerebella (n=7, 7, 6, respectively; mean $\pm$ SD shown). Measurements made on sections from Level 2 of 4. ***, P<0.001.

(D) Percent total cerebellar area comprised of EGL in sagittal sections from P7 Ctrl, *Ptch1*, *Ptch1 Zfx* cerebella (n=7, 7, 6, respectively; mean $\pm$ SD shown). Percent area computed as $Area_{EGL}/(Area_{EGL} + Area_{nonEGL})*100$. Measurements made only on sections from Level 2 of 4. **, P< 0.01; ***, P<0.001.

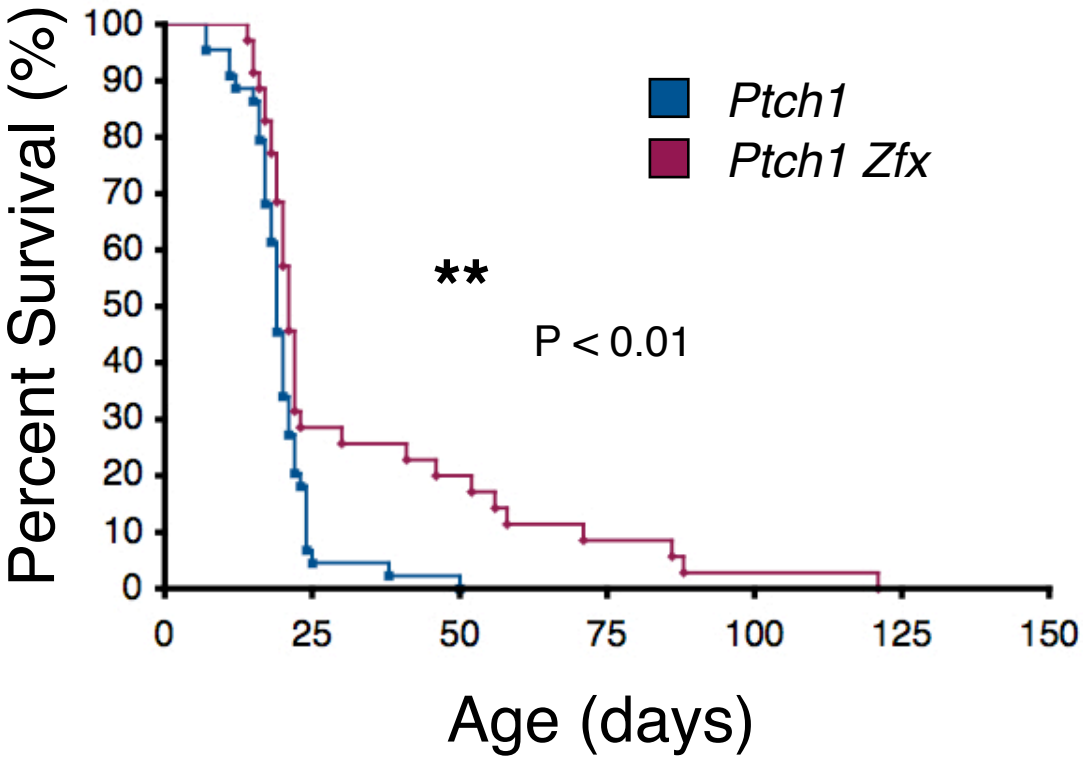

Figure 15. *Zfx* co-deletion enhances survival in mice with MB induced by *Ptch1* deletion

Shown is a Kaplan-Meier survival plot for *hGFAP-Cre*$^{+}$ *Ptch1*$^{flox/flox}$ *Zfx*^{WT} (*Ptch1)* mice versus *hGFAP-Cre*$^{+}$ *Ptch1*$^{flox/flox}$ *Zfx*$^{flox/Y}$ (*Ptch1 Zfx)* mice. **, P<0.01.

including enlarged cranium, flattening of ears on the skull, and progressively worsening ataxia observable by eye by P14, and nearly all *Ptch1* mice died or were sacrificed as moribund by 25 days of age (Fig. 15). This is an age consistent with the maximum survival age (~4 weeks) previously observed with this MB model [11], and one which corresponds to 4-6 days post-weaning, suggesting a possible failure to thrive independent of the dam. Meanwhile, all *Ptch1 Zfx* mice also developed MB, with the majority of *Ptch1 Zfx* mice (~70%) died around the same time (Fig. 15), likely also due to inability to survive the threshold effect of weaning. However, ~30% of *Ptch1 Zfx* mice survived past weaning and ~20% lived for >50 days, resulting in a significant improvement in survival (Fig. 15). Overall, these data suggest that the loss of *Zfx* slows MB tumor formation and prolongs survival in MB caused by Hh activation.

Ptch1 Zfx *mice develop* Zfx^{null} *MB after* Ptch1 *deletion* in vivo

Previously we observed an outgrowth of *Zfx* non-deleter cells and failure to maintain *Zfx*^{null} cells in skin over the long-term following Tmx-induced co-deletion of *Zfx*. Given that we observed Hh-dependent MB develop and ultimately cause the death of *Ptch1 Zfx* mice *in vivo*, we asked whether MB tumors in doubly-deleting *Ptch1 Zfx* mice would, as in the BCC model, be comprised of *Zfx* non-deleters. We stained sagittal sections from P7 cerebella of Ctrl, *Ptch1*, and *Ptch1 Zfx* mice with anti-Zfx antibody. While cells staining positive for nuclear Zfx were visible throughout normal EGL in Ctrl and MB-like EGL in *Ptch1* cerebella, cells throughout the expanded EGL in *Ptch1 Zfx* cerebella stained negatively for

Zfx (Fig. 16A). Thus, in contrast with the results from our BCC model in the skin, *Zfx*^{null} MB do successfully develop following *Ptch1* deletion in the cerebellum.

We also examined whether sections from *Ptch1* and *Ptch1 Zfx* cerebella exhibited different levels of staining for proliferation markers. Towards this end, we stained sagittal sections from P7 cerebella of Ctrl, *Ptch1*, and *Ptch1 Zfx* mice with antibody against phosphohistone-3 (pH3), to mark cells in M-phase (Fig. 16B). Counts of pH3^{+} cells in expanded EGL of *Ptch1* and *Ptch1 Zfx* cerebellar showed no significant difference in frequency of proliferative cells between MB that did or did not co-delete *Zfx* (Fig. 16C). The above results from anti-pH3 staining argued against any prolonged, global decrease in proliferative index as an explanation for the decrease in *Zfx*^{null} MB tumor size observed in doubly-deleting *Ptch1 Zfx* cerebella (Fig. 14).

In the *in vivo* model of BCC initiated by *Ptch1* deletion, *Zfx* co-deletion coincided with decreased expression of the signal transducer *Smo* and blunted overexpression of Hh targets *Gli1* and *Mycn*. We asked whether the same changes in *Smo* and *Gli1* expression occurred in our Hh-dependent MB model after *Zfx* co-deletion. Unlike the Tmx-inducible *R26-CreER* transgene used to induce BCC in the skin, *hGFAP-Cre,* the Cre line we employed to generate MB, does not allow for temporal control of its activity *via* Tmx administration and begins effecting Cre-mediated deletion in the mouse brain starting around E13.5 [127]. As a result, instead of collecting tissue for gene expression analysis at a defined timepoint after induced deletion, as in the skin, we instead collected bulk

cerebella from a single, small cohort of Ctrl, *Ptch1*, and *Ptch1 Zfx* mice at P14, when the majority of cerebella of *Ptch1* and *Ptch1 Zfx* mice are comprised of Hh-dependent MB cells (Fig. 13B). Gene expression analysis on bulk P14 cerebella by qPCR showed decreased levels of *Zfx* mRNA in all *hGFAP-Cre*$^{+}$ *Zfx*$^{flox/Y}$ mice, confirming successful *Zfx* ablation by *hGFAP-Cre* (and perdurance of *Zfx*^{null} cells in developing cerebella after *Ptch1* deletion)(Fig. 17A). However, expression of the high-confidence Zfx target *Dis3L* was not substantially decreased in *Ptch1 Zfx* P14 cerebella when compared with cerebella that delete *Ptch1* alone (Fig. 17B). Interestingly, *Smo* expression levels were higher in both *Ptch1* and also in *Ptch1 Zfx* P14 cerebella (Fig. 17C). The Hh targets *Gli1* and *Mycn* were also overexpressed comparably in both *Ptch1* and *Ptch1 Zfx* P14 cerebella, compared with Ctrl mice (Fig. 17D&E).

Collectively, these preliminary expression data suggest that, by P14 in the MB model system, *Ptch1 Zfx* cerebella exhibit neither the decreased *Dis3L* expression levels observed after *Zfx* loss in all tissues we've previously examined, nor reduced *Smo* levels or blunted activation of *Gli1* and *Mycn* expression that we observed 3 days after *Zfx* co-deletion in the BCC model. To look at global changes in gene expression in P14 *Ptch1 Zfx* cerebella compared with *Ptch1* and Ctrl (*hGFAP-Cre*$^{-}$) cerebella, we performed a microarray analysis using RNA isolated from bulk cerebellar cells from P14 *Ptch1 Zfx* (n=2), *Ptch1*, and Ctrl cerebella (Fig. 18). Hierarchical clustering analysis of microarray data showed *Ptch1* and *Ptch1 Zfx* P14 cerebella clustering closely together and

separately from Ctrl cerebella (Fig.18A). Only 10 genes were overexpressed $\geq$ 2-fold specifically in the *Ptch1 Zfx* cluster, compared to other nodes in the dendrogram (Fig. 18A). Direct comparison of expression data revealed that only 64 genes were overexpressed and 29 genes underexpressed by more than 2-fold in *Ptch1* versus *Ptch1 Zfx* P14 cerebella (Fig. 18B). Additionally, principle component analysis of microarray data for a curated list of 9765 significant genes demonstrated that the first principle component, accounting for the great majority of the variation in the expression data (83%), corresponded to genes whose expression changes similarly in both *Ptch1* and *Ptch1 Zfx* cerebella compared to Ctrl (Fig. 18C). Thus, microarray analysis from P14 cerebella suggests that the gene expression signature of *Ptch1* and *Ptch1 Zfx* are very close to identical, and that doubly-deleting *Ptch1 Zfx* MB express very few genes differentially compared to *Ptch1* MB by the time the affected mice reach post-natal day 14.

Loss of Zfx *alone does not impair normal cerebellar development in mouse*

Data collected up to this point showed that *Zfx* co-deletion delayed (but did not stop) MB progression following *Ptch1* deletion. One possible explanation for this phenotype, given the almost global range of deletion by *hGFAP-Cre* in the cerebellum, is that *Zfx* loss negatively affects normal cerebellar development and thereby causes delayed MB development without the need for any interaction

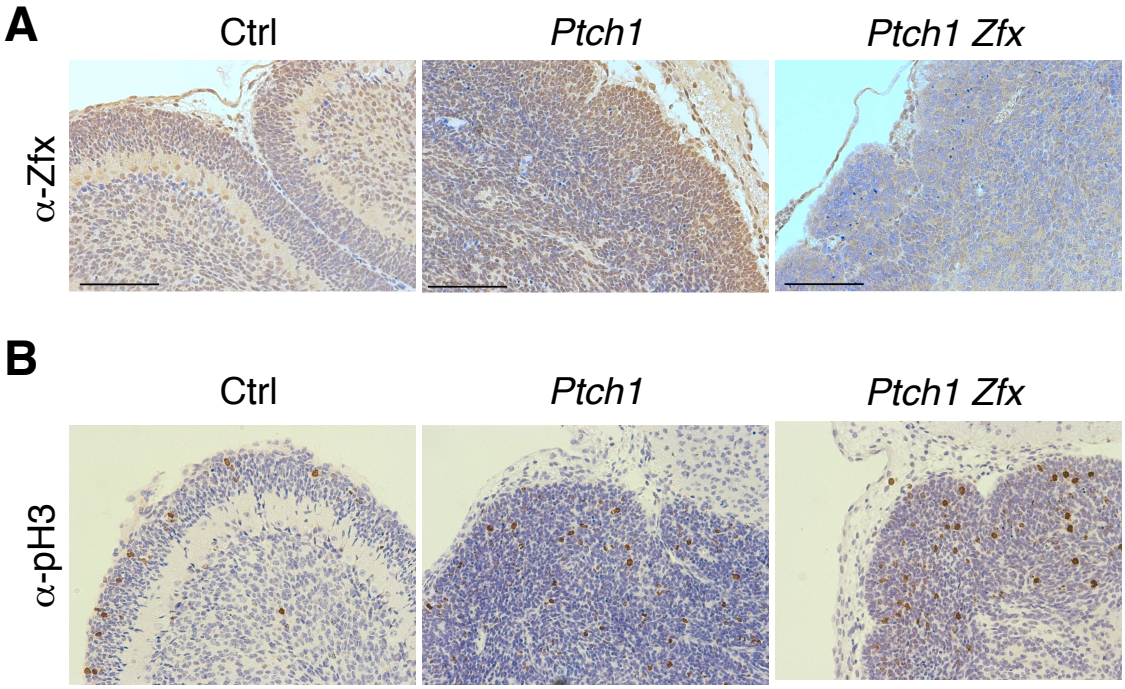
A
Ctrl
Ptch1
Ptch1 Zfx
α-Zfx
B
Ctrl
Ptch1
Ptch1 Zfx
α-pH3

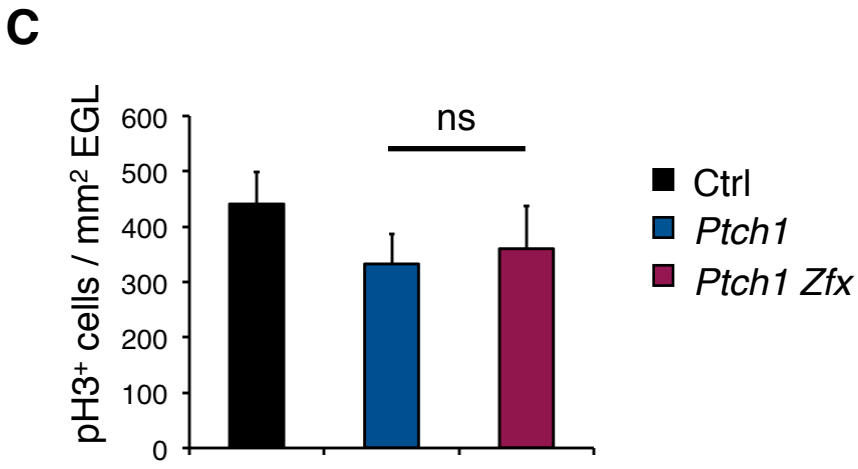
C
pH3+ cells / mm2 EGL
600
500
400
300
200
100
0
ns
Ctrl
Ptch1
Ptch1 Zfx

Figure 16. Co-deletion of *Zfx* does not prevent MB development or alter proliferation profile after *Ptch1* deletion *in vivo*

(A) Zfx expression in cerebella after *Ptch1* deletion, with or without *Zfx* co-deletion. Shown are representative micrographs of anti-Zfx immunostainings of sagittal sections from P7 cerebella from *Ptch1*, *Ptch1 Zfx*, and *hGFAP-Cre*$^{-}$ or *hGFAP-Cre*$^{+}$ *Ptch1*$^{flox/WT}$ (Ctrl) mice. Scale bars represent 100 μm.

(B) Expression of the proliferation marker phosphohistone 3 (pH3) in P7 cerebella after *Ptch1* deletion and *Zfx* co-deletion. Shown are representative micrographs of anti-pH3 IHC stainings of sagittal sections from P7 cerebella from *Ptch1*, *Ptch1 Zfx*, and *hGFAP-Cre*$^{-}$ or *hGFAP-Cre*$^{+}$ *Ptch1*$^{flox/WT}$ (Ctrl) mice.

(C) Density of pH3^{+} proliferating cells in hyperproliferative EGL of P7 cerebella. Sagittal sections from corresponding level sections (2 of 4) from *Ptch1* (n=7), *Ptch1 Zfx* (n=6), and *Cre*$^{-}$ (Ctrl) (n=3) P7 cerebella were stained with anti-pH3 antibody, and cells in EGL with DAB-marked, pH3^{+} nuclei were counted. Density of pH3^{+} mitotic cells was computed by dividing the counts by cross-section EGL area (cf. Figure 14). Error bars represent SD.

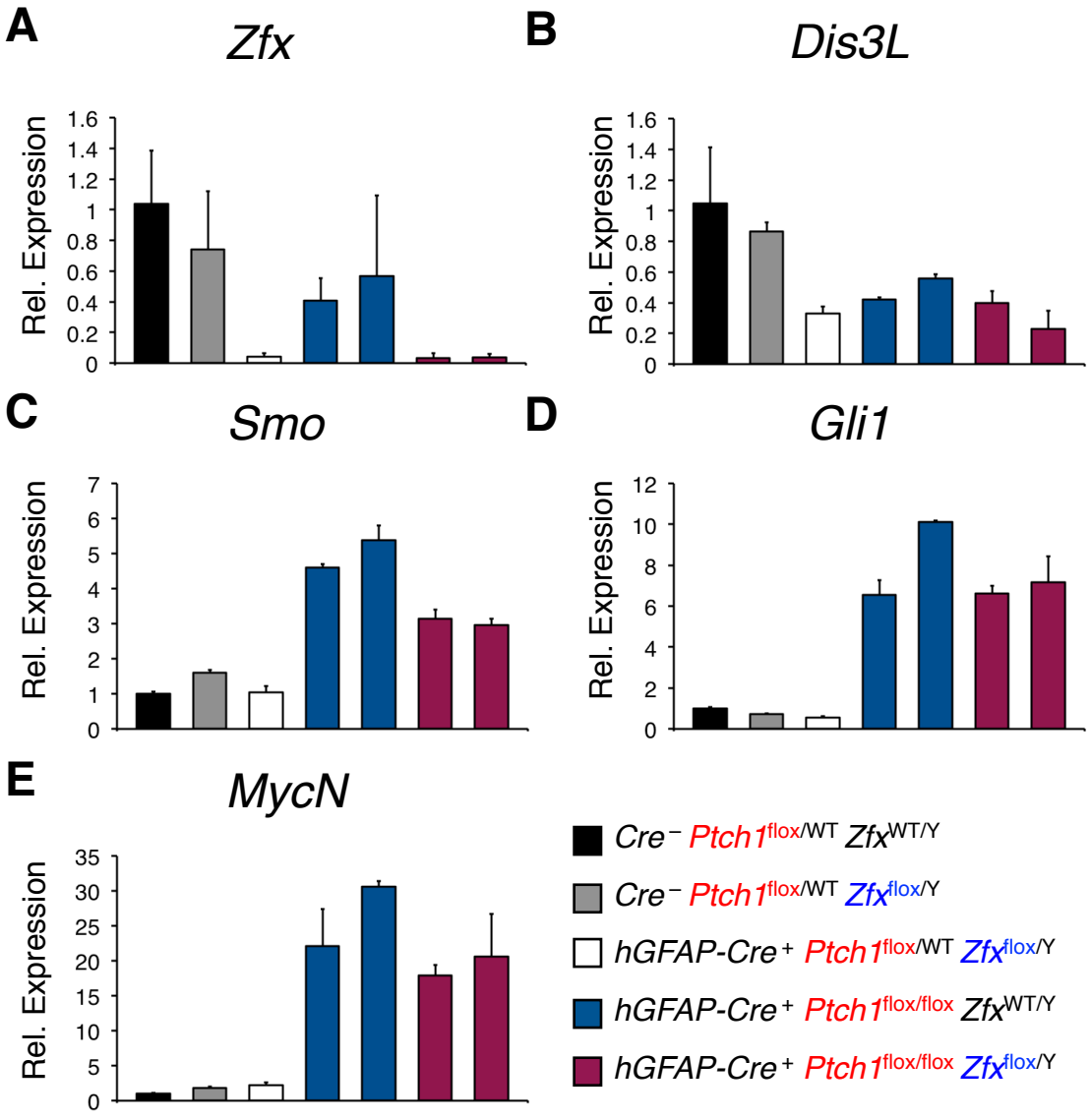
A
Zfx
B
Dis3L
C
Smo
D
Gli1
E
MycN
Rel. Expression
Cre− Ptch1flox/WT ZfxWT/Y
Cre− Ptch1flox/WT Zfxflox/Y
hGFAP-Cre+ Ptch1flox/WT Zfxflox/Y
hGFAP-Cre+ Ptch1flox/flox ZfxWT/Y
hGFAP-Cre+ Ptch1flox/flox Zfxflox/Y

Figure 17. *Zfx* loss does not blunt increase in expression *Smo* and Hh target *Gli1* in cerebella after *Ptch1* deletion

Expression levels of *Zfx* (A), the Zfx target *Dis3L* (B), *Smo* (C), and Hh pathway target genes *Gli1* (D) and *MycN* (E) in RNA from bulk cerebellum isolated from P14 mice with the genotypes: *Cre*$^{-}$ *Ptch1*$^{flox/WT}$ *Zfx*$^{WT/Y}$ (n= 1), *Cre*$^{-}$ *Ptch1*$^{flox/WT}$ *Zfx*$^{flox/Y}$ (n=1), *hGFAP-Cre*$^{+}$ *Ptch1*$^{flox/WT}$ *Zfx*$^{flox/Y}$ (n=1), *hGFAP-Cre*$^{+}$ *Ptch1*$^{flox/flox}$ *Zfx*$^{WT/Y}$ (n=2), and *hGFAP-Cre*$^{+}$ *Ptch1*$^{flox/flox}$ *Zfx*$^{flox/Y}$ (n=2). Shown are expression levels for individual mice, standardized for total RNA content using *HPRT* as a control gene and normalized to expression levels in *Cre*$^{-}$ *Ptch1*$^{flox/+}$ *Zfx*$^{WT/Y}$ cerebellum, as determined by qPCR. Error bars represent SD of triplicate rxns.

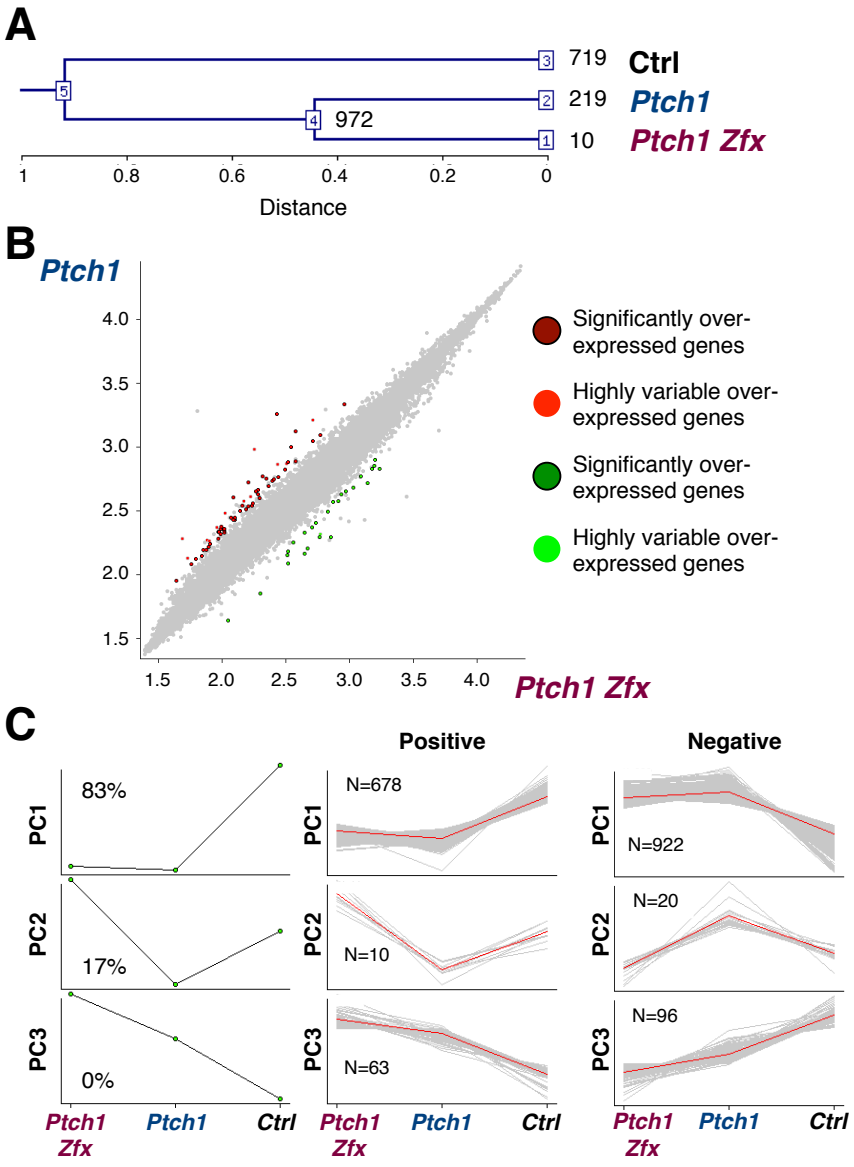
A
719
Ctrl
219
Ptch1
10
Ptch1 Zfx
972
1
0.8
0.6
0.4
0.2
0
Distance
B
Ptch1
4.0
3.5
3.0
2.5
2.0
1.5
1.5
2.0
2.5
3.0
3.5
4.0
Ptch1 Zfx
Significantly over-expressed genes
Highly variable over-expressed genes
Significantly over-expressed genes
Highly variable over-expressed genes
C
Positive
Negative
PC1
PC2
PC3
83%
17%
0%
N=678
N=10
N=63
N=922
N=20
N=96
Ptch1 Zfx
Ptch1
Ctrl

Figure 18. Minimal changes in gene expression signature in P14 cerebella co-deleting *Zfx* compared to P14 cerebella that delete *Ptch1* alone

Gene expression analysis was performed using Affymetrix Mouse Gene ST1.0 arrays on RNA purified from bulk cerebellar cells, isolated from postnatal day 14 (P14) pups that delete *Patched1* alone (*Ptch1*, n = 2), P14 pups that delete both *Patched1* and *Zfx* (*Ptch1 Zfx*, n = 2), or control P14 pups that are *hGFAP-Cre*$^-$ (Ctrl, n = 2). The breeding scheme to generate these mice is explained in Figure 11. Analysis of microarray data was performed using NIA Array.

(A) Clustering analysis on gene expression array data from Ptch1, Ptch1 Zfx, and Ctrl P14 cerebella. Minimal fold change threshold was 2-fold. Numerical values at each node indicate the number of specific genes $\geq$ 2-fold overexpressed in that nodal cluster compared to all samples outside that cluster.

(B) Scatterplot depicting comparison of array data from *Ptch1* (n = 2) and *Ptch1 Zfx* (n = 2) P14 cerebella. Shown are genes significantly overexpressed (n = 64) or underexpressed (n=29) in *Ptch1* cerebella compared to *Ptch1 Zfx*. Threshold fold-change in expression was set to 2-fold.

(C) Principal component analysis of microarray data from P14 *hGFAP-Cre* cerebella. Shown are principal components from a 3-component analysis of the *Ptch1*, *Ptch1 Zfx*, and Ctrl microarray data. Percent contribution from each component is shown in the lefthand panels. Fold-change threshold was set at 2-fold, and the NIA Array-curated list of 9765 significant genes were analyzed.

with Hh or other pathways activated by *Ptch1* deletion. To examine this possibility, we generated *hGFAP-Cre*$^{+}$ *Zfx*$^{flox/Y}$ mice that delete *Zfx* alone, without any concomitant *Ptch1* deletion or MB generation. These mice survived up until 293 days of age (P293), and H&E staining of sagittal sections from P24 and P293 *hGFAP-Cre*$^{+}$ *Zfx*$^{flox/Y}$ cerebella showed no gross abnormalities in cerebellar growth or foliation (Fig. 19). Immunohistochemical staining of P293 cerebellar sections for Zfx confirmed that *hGFAP-Cre*$^{+}$ *Zfx*$^{flox/Y}$ cerebella were indeed comprised of Zfx^{null} cells (Fig. 19). Together, these results demonstrated deletion of *Zfx* alone throughout the cerebellum did not derail normal cerebellar development.

Zfx *is not required for tumor progression in a* PTEN-*dependent glioblastoma model* in vivo

Another possibility, given the delaying effect on MB progression due to *Zfx* deletion, was that there existed a general requirement for *Zfx* across brain tumor types. To explore this possibility, we collaborated with researchers in the Canoll laboratory to generate a system to induce *PTEN*-dependent glioblastoma (GBM) in adult mice, with or without concomitant deletion of *Zfx* in the GBM tumor. Mice homozygous for a conditional *Pten*^{flox} allele (designated *Pten* mice) were bred to conditional *Zfx*$^{flox/flox}$ mice, yielding doubly-conditional *Pten*$^{flox/flox}$ *Zfx*^{flox} mice (designated *Pten Zfx*). Stereotactic injection of retrovirus delivering platelet-

derived growth factor (PDGF) and Cre recombinase was performed into the brains of young adult *Pten* and *Pten Zfx* mice, which treatment results in

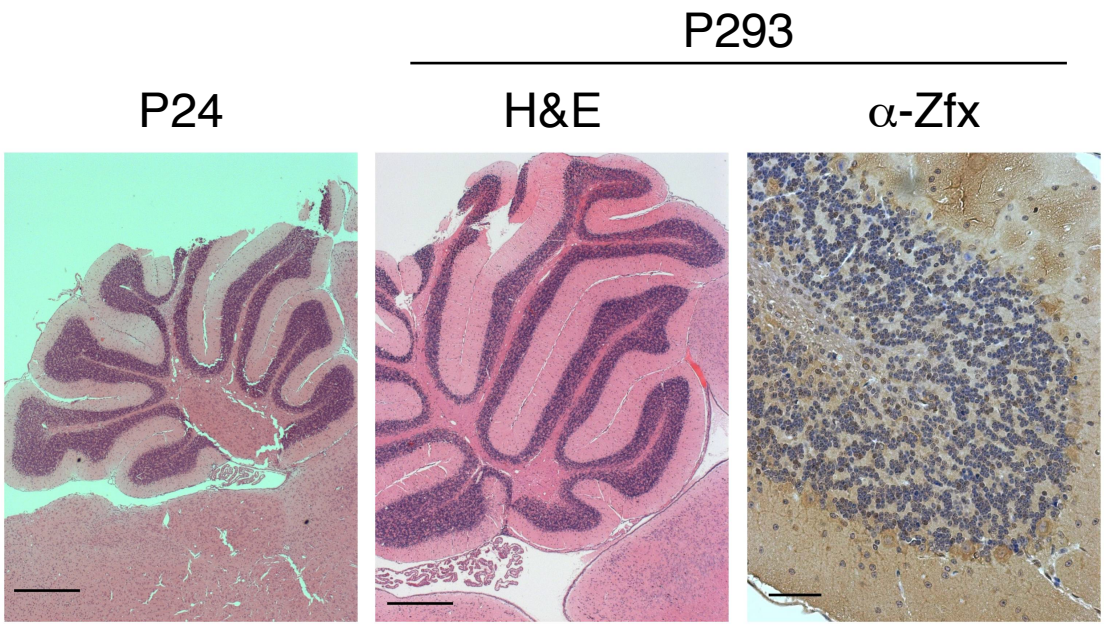

Figure 19. Loss of *Zfx* does not affect normal cerebellar growth

hGFAP-Cre^{+} *Zfx*^{flox}/y mice with brain-specific Zfx deletion have normal lifespan and lack obvious pathology (not shown). *hGFAP*-Cre^{+} *Zfx*^{flox}/y mice were sacrificed at post-natal days 24 (P24, n=2) and 293 (P293, n=2). Shown are representative cerebellar sections stained with H&E or immunostained with anti-Zfx antibody. Scale bars represent 500 μm (H&E) or 50 μm (anti-Zfx).

aggressive Pten-deficient GBM of the proneural subtype [128]. After viral delivery and GBM initiation, *Pten Zfx* mice did not exhibit enhanced survival compared to the Zfx-retaining *Pten* mice (Fig. 20A), displaying instead a tendency towards slightly worsened survival. IHC staining with anti-Zfx antibody confirmed that GBM that developed in *Pten Zfx* mice were indeed comprised of Zfx^{null} cells, not *Zfx* non-deleters (Fig. 20B). These results suggested that Zfx is not required in *Pten*-dependent GBM *in vivo* and argue against a generalizable requirement for *Zfx* across all different brain tumor types.

ZFX *knockdown impairs cell proliferation in a human MB cell line in vitro*

Finally, given the delay in MB progression after *Zfx* deletion in mouse cerebella *in vivo*, we asked whether loss of *ZFX* would impair growth of human medulloblastoma *in vitro*. We used the commercially available human MB cell-line DAOY [129], which has the advantage of having lost the Y chromosome, thereby removing possible confounding effects from the *ZFX* homolog, *ZFY*. To determine whether loss of *ZFX* effects human MB cells *in vitro*, we knocked down ZFX in DAOY cells using lentivirally-delivered short hairpin RNAs (shRNA), a recently validated system used to knock down ZFX in human embryonic stem cells (ESC) [75].

DAOY human MB cells were transduced with lentiviral vectors encoding one of three ZFX-specific shRNAs (H2, H3, H4), or a control “scrambled” (SCR) shRNA. Two ZFX-specific shRNAs (H2, H3) strongly reduced Zfx protein (Fig. 21A) and transcript (Fig. 21B) levels in transduced DAOY cells, whereas the third

(H4) caused a more moderate reduction (Fig. 21B). Additionally, these ZFX-targeting shRNAs impaired the growth of DAOY cells, compared to cells transduced with SCR control shRNA (Fig. 21C). The degree of growth impairment scaled roughly proportionately to the degree of ZFX knockdown observed by qPCR (Fig. 21B,C). Taken together, results from lentiviral knockdown in DAOY cells suggest that ZFX is required for optimal growth of a human MB cell line *in vitro*.

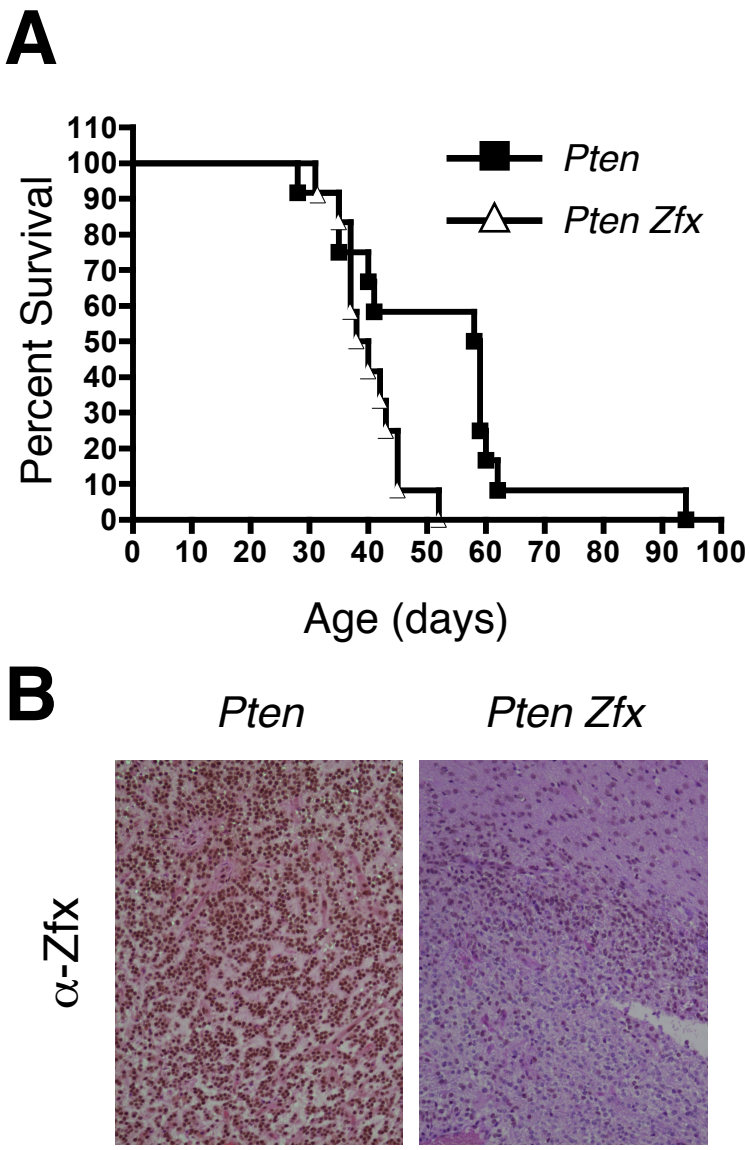

Figure 20. Loss of Zfx does not impair Pten-dependent glioblastoma development

(A) Kaplan-Meier survival curve for retrovirus-injected *Pten* and *Pten Zfx* mice. Glioblastoma was induced *via* stereotactic injection of retrovirus encoding PDGF and Cre recombinase into brains of young adult mice with conditional null alleles of *Pten* only (*Pten*) or of both *Pten* and *Zfx* (*Pten Zfx*).

(B) Immunohistochemical staining for Zfx in sections of glioblastomas from retrovirus-injected *Pten* and *Pten Zfx* mice.

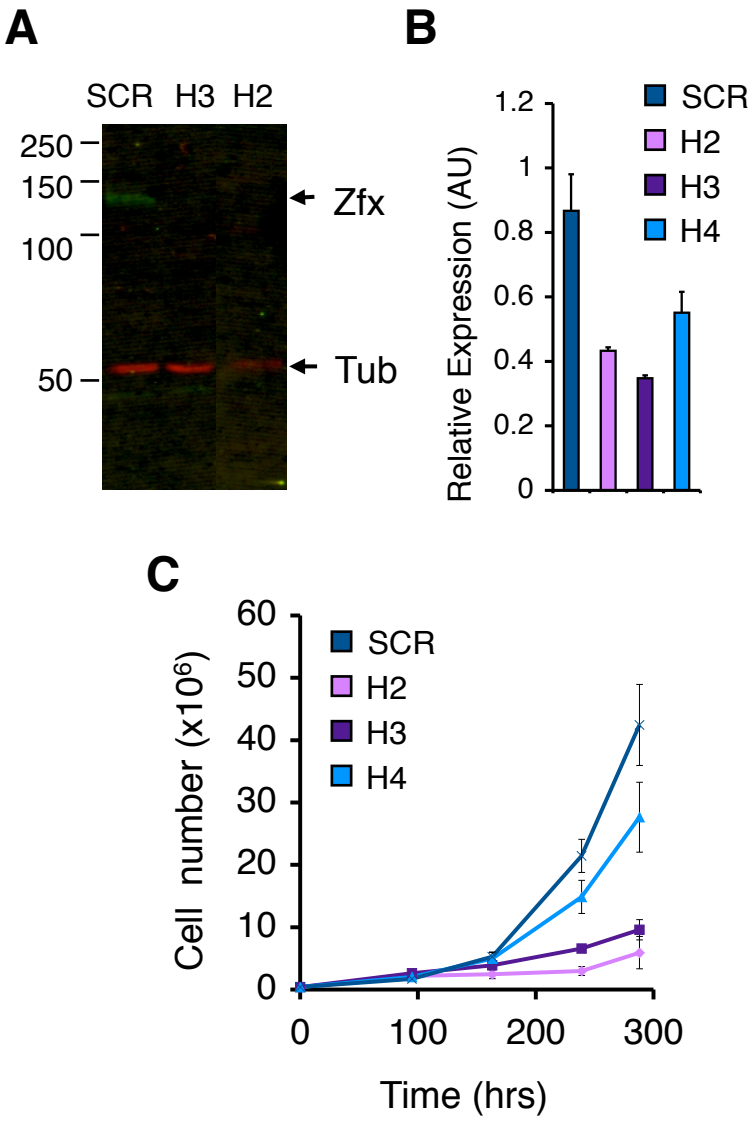
A
SCR H3 H2
250
150
100
50
Zfx
Tub
B
Relative Expression (AU)
1.2
1
0.8
0.6
0.4
0.2
0
SCR
H2
H3
H4
C
Cell number (x10^6)
60
50
40
30
20
10
0
0
100
200
300
Time (hrs)
SCR
H2
H3
H4

Figure 21. Zfx knockdown impairs cell proliferation in a human MB cell line *in vitro*

The human MB cell line DAOY was transduced *in vitro* with lentiviruses encoding short hairpin RNAs (shRNAs) targeting ZFX transcript (H2, H3, H4) or a scrambled control shRNA (SCR). Transduced cells were selected for by growth in puromycin-containing medium.

(A) Western Blot for ZFX (green) and tubulin control (Tub, red) in DAOY cells transduced with control (SCR) or ZFX-targeting (H2, H3) lentivirus.

(B) Expression of *ZFX* in DAOY cells after shRNA knockdown. Shown are *ZFX* expression levels 4 days after transduction, as determined by qPCR (mean ± SD of triplicate parallel cultures; representative of three independent experiments).

(C) Growth curves for DAOY cells transduced with lentivirus expressing control (SCR) or ZFX-targeting (H2, H3, H4) shRNA (mean ± SD of triplicate parallel cultures, representative of three independent experiments).

Discussion

In this Chapter, we investigated whether the transcription factor Zfx was required for the development of a second type of Hh pathway-driven cancer, using mouse models of MB. MB were generated using nearly CNS-wide ablation of Hh inhibitory receptor Ptch1 by *hGFAP-Cre*, and co-deletion of *Zfx* in cerebella of *Ptch1 Zfx* mice delayed but did not stop MB progression (Fig. 13). Mice co-deleting *Zfx* along with *Ptch1* had smaller MB tumors, or hyperproliferative EGL (Fig. 14), which correlated with a significant enhancement in survival times (Fig. 15). In contrast, *Zfx* co-deletion conferred no survival enhancement in a PTEN-dependent model of glioblastoma (Fig. 20). These results argue in favor of a requirement for *Zfx* for the optimal growth of Hh-driven MB *in vivo*, but against a generalized requirement for Zfx across all brain tumor types.

In Chapter I, we reported a requirement for *Zfx* for Hh-driven BCC development in the skin. Combined with our results from the *Ptch1*-dependent MB model summarized above, we have evidence for a common requirement for *Zfx* across two very different Hh pathway-driven cancers. Other genes outside of Hh pathway components have been shown to affect both MB and BCC, such as the tumor suppressor p53, whose loss in $p53^{-/-}$ $Ptch1^{+/-}$ mice has been shown to promote Hh-driven MB [130] and BCC formation [8]. *Zfx* is an interesting case, however, as it is neither an oncogene nor a tumor suppressor gene in this context, but merely an unmutated “normal cellular function” gene which is required in both MB and BCC. This dual requirement across MB and BCC

highlights *Zfx* and its downstream transcriptional targets as a novel cell-intrinsic machinery linking Hh-dependent cancers.

Although *Zfx* is required for optimal growth of both BCC and MB, there are clear qualitative differences between the effects of *Zfx* loss on Hh-driven BCC and those on Hh-driven MB. In BCC models, co-deletion of *Zfx* was incompatible with BCC development. In the case of MB, Zfx^{null} MB clearly develop and grow out (Fig. 16A). Expanded EGL in *Ptch1 Zfx* mice are significantly smaller than in the *Ptch1* only mice at P7, but they are still clearly expanded, full of hyperproliferative GNP, and significantly larger than wild-type EGL (Fig. 14). A fraction of *Ptch1 Zfx* mice survive far longer with their Hh-driven MB than do mice which only delete *Ptch1*, but they all still succumb to MB (Fig.15). Loss of Zfx more weakly impairs Hh-driven MB than it does BCC.

In searching for an explanation for the effects of *Zfx* loss on Hh-driven MB models *in vivo*, one possibility is that phenotypes we observe in *Ptch1 Zfx* cerebella are the result of continual effects from *Zfx* loss spanning the entire embryonic and post-natal development of the cerebellum. If this were to be the case, we could draw some conclusions from analyses of P7 and P14 cerebella. *Ptch1 Zfx* P14 cerebella exhibit the same heightened expression of *Smo* and Hh targets *Gli1* and *Mycn* as *Ptch1* singly-deleting cerebella (Fig. 17C-E), arguing against transcriptional regulation of *Smo* by Zfx in this MB model. Lack of major disruption in cerebellar development in P21 and P293 *hGFAP-Cre*$^{+}$ $Zfx^{flox/Y}$ mice (which delete *Zfx* alone)(Fig. 19) supports the conclusion that *Zfx* does not

regulate *Smo* expression throughout cerebellar development, since even graded disruption of the Hh pathway will generate observable defects in cerebellar foliation patterns [23].

Additionally, decreased GNP proliferation does not appear to account for the delayed growth of MB in *Ptch1 Zfx* doubly-deleting mice, since counts of mitotic $pH3^+$ GNP from expanded EGL are not significantly different between P7 cerebella in *Ptch1* and *Ptch1 Zfx* mice (Fig. 16B,C). In place of a difference in proliferation profile, the delayed MB growth following *Zfx* loss could also be accounted for by increased cell-death, or by introduction of a bias in transformed $Ptch1^{CKO}$ GNP away from self-renewal and towards differentiation in mature neurons. The expanded EGL in *Ptch1*-dependent MB mice is not a monoculture of hyperproliferative GNP but also included regions of differentiated neurons, which can be distinguished by staining for markers like NeuN or synaptophysin [11]. Staining sections from *Ptch1 Zfx* cerebella for markers of mature neurons could determine whether *Zfx* co-deletion slows Hh-driven MB *via* biasing transformed GNP towards differentiation. A similar bias towards differentiation after *Zfx* deletion has already been observed in unpublished work from our laboratory in a different cancer model, where leukemic blasts from MLL-AF9-driven acute myeloid leukemia (AML) adopt a more differentiated myeloid phenotype following *Zfx* deletion (S. Weisberg, unpublished data).

Alternatively, *Zfx* loss could have its effects on Hh-driven MB development over a restricted time-period, perhaps very early after targeted co-deletion of

Ptch1 and *Zfx*. At P14, there is no difference in *Smo* expression between *Ptch1* and *Ptch1 Zfx* cerebella, and they have the same density of mitotic $pH3^{+}$ GNP at P7. However, while placed near the peak and near the eventual fall-off in post-natal GNP proliferation for wild-type cerebella, these time-points are actually capturing relatively late events in the *hGFAP-Cre Ptch1*^{flox} mouse model. The *hGFAP-Cre* transgene begins deleting in the brain as early as E13.5 [127], and hyperproliferation of GNP and expansion of the EGL is already readily observable in E16.5 cerebella [11]. The requirement for Zfx in Hh-driven MB - - whether through regulation of *Smo*, proliferation-related genes, or other downstream targets altogether - - could be temporally restricted to some portion of embryogenesis after E13.5, or to earliest post-natal days. Subsequently, the Hh-driven MB in *Ptch1 Zfx* mice could escape a requirement for Zfx, looking like MB in *Ptch1* only mice by P7 and P14. Additional transcription factors could also compensate for *Zfx* loss, supplementing expression of *Zfx* targets in its absence. Expression analyses of P14 cerebella by both qPCR and microarray argue support the hypothesis that *Zfx* loss has temporally-restricted effects that are lost or compensated for by other transcription factors by P14. For example, there is only a minimal decrease in the expression of the Zfx target gene *Dis3L* in *Ptch1 Zfx* P14 cerebella (Fig. 17B). Furthermore, microarray analysis comparing gene expression in P14 cerebella showed *Ptch1* and *Ptch1 Zfx* samples clustering together and separately from Ctrl samples (Fig. 18A). Microarray data also revealed very few gene expression differences by P14 between singly- and

doubly-deleting cerebella (Fig. 18B, C). These results argue in favor of a temporally-restricted role for *Zfx* in this Hh-driven MB model (one which is lost by P14), and they suggest that further investigation is warranted into transcription factors that could bind to GGCCT-rich Zfx binding sites and compensate for Zfx.

Math1-CreER Ptch1^{flox} mice, a previously validated model for generating Hh-driven MB [11], offer many attractions as a system for validating this putative temporally-restricted role for *Zfx* in MB. *Math1-CreER* is expressed specifically in GNP, the MB cells-of-origin, and its Cre recombinase activity is Tmx-inducible, allowing for controlled MB induction at defined post-natal time-points and exploration of early events following *Ptch1* ablation and *Zfx* co-deletion. Additionally, the kinetics of MB disease generated by *Math1-CreER* are much slower, with pups induced with Tmx at P4 having 12 weeks median survival, compared to 3-4 weeks maximum in *hGFAP-Cre Ptch1*^{flox} mice [11]. Thus, generation of *Zfx*-deficient MB using *Math1-CreER* is an attractive possibility also for its ability to bypass threshold effects of weaning on survival curves, as well as for its potential to verify that the biphasic survival curve in *Ptch1 Zfx* mice (Fig. 15) is indeed an artifact due to weaning age and not attributable to issues with the mixed mouse background.

In Chapter I, we showed a requirement for *Zfx* in Hh-dependent BCC. In this Chapter, we demonstrated that *Zfx* loss delays Hh-driven MB development *in vivo*. In Chapter III, we will explore further the downstream direct targets of Zfx and their functional relevance in these two Hh-dependent cancers. Evidence for

the transcriptional regulation of *Smo* by Zfx will be examined and evaluated as an explanation of the phenotypes from *Zfx* loss in BCC and MB. Additionally, the sensitivity of DAOY human MB cells to *ZFX* loss (Fig. 21) will be utilized, in concert with ChIP-seq and gene expression microarray assays, to identify conserved direct transcriptional targets of ZFX that are candidate members of a novel cell-intrinsic machinery shared by MB and BCC.

Materials & Methods

Animals

Mice with a conditional allele of *Ptch1* (*Ptch1*^{flox})[105] were bred with conditional *Zfx*^{flox} mice[74] to generate singly- and doubly-conditional *Ptch1*$^{flox/flox}$ and *Ptch1*$^{flox/flox}$ *Zfx*^{flox}/y mice. *Pten*^{flox} mice[131] were similarly crossed to *Zfx*^{flox} mice to generate *Pten*$^{flox/flox}$ and *Pten*$^{flox/flox}$ *Zfx*^{flox}/y mice. To generate Hh-dependent medulloblastoma (MB) *in vivo, hGFAP-Cre* mice[127] were obtained from the Jackson Laboratory and crossed with *Ptch1*^{flox} and *Ptch1*^{flox} *Zfx*^{flox} mice to generate *hGFAP*-Cre^{+} *Ptch1*$^{flox/flox}$ (hGFAP-*Ptch1*) and *hGFAP*-Cre^{+} *Ptch1*$^{flox/flox}$ *Zfx*^{flox}/y (hGFAP-*Ptch1*-*Zfx*) experimental animals, along with *hGFAP*-Cre^{-} littermate controls (Ctrl). All animal studies were performed according to the investigator's protocol approved by the Institutional Animal Care and Use Committee of Columbia University.

Cell Culture

DAOY cells were obtained from the ATCC and propagated in complete DMEM medium with 10% FBS, and replated by trypsinization.

RNA Isolation and qPCR

Total cellular RNA was isolated from samples in 0.5-1 mL TriZol LS reagent (Invitrogen). cDNA was synthesized from 1-2 μg RNA per sample using SuperScript III reverse transcriptase (invitrogen). Quantitative real-time PCR (qPCR) assaying for SYBR Green incorporation were run on an Mx3000P instrument (Stratagene) using FastStart Universal SYBR Green Master mix containing Rox (Roche). Triplicate reactions were run for each sample, and all qPCR results were analyzed using the ΔΔCt method. The expression values for all genes were scaled to total RNA content using Ct for the housekeeping genes β-Actin (*Actb*), β2-microglobulin (*B2m*), hypoxanthine guanine phosphoribosyl transferase (*HPRT*), or *GAPDH*, and then normalized to the indicated control samples. The qPCR primers are listed below.

Species	Gene	Forward	Reverse
Mouse	Actb	ATCCTGACCCTGAAGTACC	TACGACCAGAGGCATACAG
	B2m	ACCCTGGTCTTTCTGGTGCTTG	TATGTTCGGCTTCCCATTCTCC
	HPRT	GCCCCAAAATGGTTAAGGTTGC	TCAAGGGCATATCCAACAACAAAC
	GAPDH	AAGGTCGGTGTGAACGGATTTG	CTCGCTCCTGGAAGATGGTGAT
	Zfx	GCAGTGCATGAACAGCAAGT	GCAAGGTGTTCAGGATGGTT
	Dis3L	AGGGGGAAGCCATGGAGAAG	GATTTGATGCCCGCTTCCAG
	Ube2j1	GACGCATAGTACTGCCACCA	ATGGCCCCCTCTCCTTTAGT
	Smo	CTCGGACTCGCAGGAGGAAG	TCAGGGAAGTGGTCCGGTGT
	Gli1	CATTGGGGAGGTTGCTCCAG	CCGAAGGTGCGTCTTGAGGT

	Mycn	GGAGAGGATACCTTGAGCGACTC	CGCCTTGTTGTTAGAGGAGGAAC
	Mnx1	AGGCGCAGTCGAACCTCTTG	TCCATTTCATTCGGCGGTTC
	Isl1	CAAGCGGTGCAAGGACAAGA	CAGGGCGGCTGGTAACTTTG
	Olig2	CACCTCCTCGTCCACGTCCT	GGCGATCTTGGAGAGCTTGC
	Tubb3	GGCCATTCTGGTGGACTTGG	GCCCTGCAGGCAGTCACAAT
Human	GAPDH	AAGGTGAAGGTCGGAGTCAACG	CCCACTTGATTTTGGAGGGATC
	Zfx	GCAGGATGATGACAAAGGCAAC	CAAGGATCAATTTCCGACTCTGTG
	Dis3L	CCAGGACAGGATGCCAATTGTT	CGTGGGCAGCTTTTAAATCAGG
	Ube2j1	GAAACTTGGCAGCCTTCGTG	ATGGCAGAGCCACATCCTTC
	Smo	GCTCATCGTGGGAGGCTACTTC	AGCATGGTCTCGTTGATCTTGC
	Gli1	CTCGGGCACCATCCATTTCTAC	GCCAGTCATTTCCACACCACTG

Microarray

RNA for microarray analysis of cerebella and MB after *Zfx* loss was obtained from bulk cerebellar cell suspensions from P14 cerebella of *hGFAP-Cre*$^{+}$ *Ptch1*$^{flox/flox}$ *Zfx*$^{flox/Y}$ (*Ptch1 Zfx*), *hGFAP-Cre*$^{+}$ *Ptch1*$^{flox/flox}$ *Zfx*^{WT} (*Ptch1*), and *hGFAP-Cre*$^{-}$ (Ctrl) mice . Labeled cDNA was analyzed on Affymetrix Mouse Gene 1.0 ST arrays. Analysis of microarray data was performed using NIA Array Analysis web tools [132].

Glioblastoma Model

Glioblastoma was induced by stereotactic injection into brain of young adult *Pten*$^{flox/flox}$ and *Pten*$^{flox/flox}$ *Zfx*^{flox}/y mice of retrovirus coding for PDGF-IRES-Cre as described.[128] Treated animals were followed for survival, and brains from sacrificed animals were fixed and processed for histology and immunohistochemistry.

shRNA Constructs and Lentiviral infection of DAOY human MB cells

Lentiviral constructs containing *Zfx*-targeting (H2, H3, H4) and non-specific (SCR) short hairpin RNAs (shRNAs) in the pLKO.1 backbone were purchased from Open Biosystems. To generate high-titer lentivirus, HEK293T cells were co-transfected with three plasmids encoding viral packaging proteins (pCMVΔ8.9), envelope proteins (pVSVg) and the pLKO.1 shRNA sequences using the lipid-based transfection reagent Transit-293 (Mirus, LLC). After 48 hours incubation at 37°C, transfected cells were shifted to 32°C for 24 hours. Then viral supernatant was cleared using 0.45 micron filters and ultracentrifuged (50,000 x g, 2 hrs) to concentrate viral particles.

Triplicate cultures of $4x10^5$ DAOY cells were plated out overnight and then incubated with concentrated lentiviral supernatant and 7 μg/mL polybrene for 16-24 hrs, for a Mock, virus-less condition and for each lentiviral construct. Cells were allowed to rest for 2 days and then replated and grown henceforth in selective media containing 2 μg/mL puromycin (invitrogen). At 4 or 6 days post-infection (d.p.i.), plates were washed with 1x DPBS, and cells were collected in TriZol LS reagent for gene expression analysis or scraped, collected by centrifugation, and lysed in RIPA buffer for Western Blot.

Immunohistochemistry

Brains isolated from P7 and P14 pups were fixed whole in zinc formalin for 24-48 hrs, then cut in half sagittally and fixed for an additional 24-96 hrs before embedding each half separately in paraffin. Mice sacrificed after P19 were

cardiac perfused with zinc formalin prior to brain extraction. Sagittal paraffin sections (5 μm) were cut at 4 levels equally spaced across the cerebellum, with one slide stained with H&E at each level and with several blank slides cut and saved. For IHC, paraffin blanks were dewaxed and rehydrated, and antigens were unmasked by boiling for 15-20 minutes in 0.01 M sodium citrate buffer. Slides immunostained with rabbit polyclonal anti-Zfx antibody (1:500) or with anti-phosphohistone 3 (pH3) antibody (Cell Signaling #9701, 1:200) were incubated overnight at 4 C in primary antibody, incubated with biotinylated anti-rabbit secondary antibody (Vector Labs) for one hour, visualized using ABC and DAB Peroxidase Substrate Kits (Vector Labs), and finally counterstained with hematoxylin.

Micrographs of histological sections were recorded using an AxioImager.M2 microscope with attached AxioCam MRc camera (Zeiss). Measurements of cross-section area in cerebellar paraffin sections were made using Axiovision 4.8.2. Scales bars were added in directly with the Axiovision 4.8.2 software package.

Statistics

Cross-section cerebella area and percent area data and phosphohistone 3 staining density data were analyzed by unpaired, two-tailed Student's *t*-tests. Kaplan-Meier survival curves were analyzed with the LogRank test.

CHAPTER III

Zfx regulation of Hedgehog (Hh) signal transducer *Smoothened* (*Smo*) and novel downstream targets in the context of Hh-dependent cancers

Introduction

Molecular targeting of Hh-dependent BCC and MB

As discussed previously in Chapters I and II, basal cell carcinoma (BCC) and the Hh-dependent subtype of medulloblastoma (MB) represent a case of two very different cancers, highly divergent in cell-of-origin, age of onset, and clinical prognosis. BCC are slow-growing, rarely metastatic skin tumors that form mostly in adults and are rarely life-threatening [21]. MB primarily develop in the cerebella of infants and children, and, while combination of chemotherapy and radiation therapies bring overall survival rates for Hh-driven MB to 60-80%, it is at the cost of often severe cognitive side effects in the treated children [67]. Nevertheless, it has been shown that both BCC and a subset of MB are marked by a single root molecular alteration, the activation of the Hh signaling pathway [21, 67], with generation of BCC and MB by targeted activation of the Hh pathway confirmed in multiple mouse models [8, 10, 20, 133].

Molecular therapies targeting the Hh pathway thus offer the promise of an alternative avenue of attack against BCC and MB. Phase I clinical trials for vismodegib (GDC-0449), an orally-delivered small molecule inhibitor targeting the Hh signal transducer Smo, showed encouragingly positive outcomes, especially in the case of BCC [134]. The majority of patients with local or metastatic BCC who were treated (18 out of 33, >50%) had either a partial or complete response to the vismodegib therapy [110]. Trials in an adult patient with metastatic MB also provoked regression of the tumor following vismodegib treatment, although the

effect was temporary [135]. Subsequently, efficacy and safety for vismodegib was confirmed in phase II trials [136], and vismodegib has since been approved by the Food and Drug Administration for treatment of patients with metastatic or locally advanced basal cell carcinoma [137].

Caveats and side-effects pertaining to the use of Hh pathway small molecule inhibitors in treating BCC and MB do exist, however, and must be considered. One problem is outgrowth of tumor cells that have acquired additional mutations (often in the targeted gene) that confer resistance to the small molecule therapy. This effect was already observed in small molecule targeting of Hh-dependent cancers, in the case of adult MB that transiently responded to Smo inhibitor vismodegib, where acquired resistance in the MB was linked to mutation of *Smo* [138].

Small molecule targeting of Smo and the Hh pathway is also problematic given its potentially adverse side effects, both during development in young patients and in adult patients. As was discussed in Chapter II, Hh signaling is essential for post-natal patterning of the developing cerebellum [117]. MB is primarily a pediatric malignancy, potentially coinciding temporally with normal developmental stages in the post-natal cerebellum. Small molecule targeting of Hh pathway in pediatric MB could therefore risk negative side effects on patients' cerebellar development [117], along with other developmental processes such bone growth, where defects have been detected after inhibition of the Hh pathway in young mice [139].

Furthermore, phase II trials with the Smo-targeting vismodegib in adult BCC patients showed that all treated adults exhibited at least one adverse side effect event [136]. While the majority (57%) of treated patients exhibited only the milder Grade 1 or Grade 2 adverse events [136], these side effects included muscle spasms, alopecia, and dysgeusia, all conditions that are unpleasant to endure for the patient and that can prompt discontinuation of drug treatment.

Targeting non-oncogene addiction for cancer therapy

An alternative to targeting molecular therapies against the oncogenes or tumor suppressors mutated in and driving different cancers is to instead identify and then target non-mutated housekeeping genes that are often dispensable in most normal cells but that become preferentially or essentially required in tumor cells. This phenomenon where certain genes involved in normal cellular processes become absolutely required in the context of proliferating cancer cells, without being mutated as either a tumor suppressor gene or oncogene, has been referred to as non-oncogene addiction [140]. Cell-intrinsic non-oncogene addiction often centers on genes pertaining to stresses occurring in tumor cells, such as metabolic stress, DNA damage/repair, proteotoxic stress, or oxidative stress [140]. Examples of targeting cell-intrinsic non-oncogene addiction in these stress scenarios include inhibiting proteasome function with bortezomib to increase proteotoxic stress and kill multiple myeloma [141], or inhibiting an enzyme like PARP1, important in DNA single strand break repair, to exacerbate DNA damage

stress in cancer cells that have mutated BRCA2 and are already deficient in DNA repair by homologus recombination [142, 143]. Identification of similar cases of non-oncogene addiction spanning BCC and MB could provide alternative avenues for delivery of targeted therapies against the two different Hh-dependent tumors, beyond small molecule inhibitors that hit Smo directly and through it Hh pathway activity.

Conserved direct targets of Zfx and their functional relevance in MB & BCC

In results from Chapters I and II, we showed a partial or complete requirement for the transcription factor Zfx in the development of MB and BCC after Hh pathway activation in mouse brain and skin. Here, we propose *Zfx* as a candidate for an example of non-oncogene addiction common across the two disparate Hh-dependent cancers. In this Chapter, we sought to identify direct downstream transcriptional targets of Zfx which had functional relevance in BCC and MB models and could explain the requirement for *Zfx* in Hh-dependent cancers. Using massively parallel sequencing of genomic DNA captured by anti-ZFX chromatin immunoprecipitation (ChIP-seq) from human DAOY MB cells, we found 3000+ conserved direct binding targets of ZFX that were shared in ChIP-seq from mouse ESC [70]. Among the direct ZFX targets, we identified the Hh pathway signal transducer, *SMO,* whose altered expression after *Zfx* deletion in BCC *in vivo* and in MB *in vitro* suggested that Zfx regulation of *Smo* could explain in part the observed requirement for Zfx in BCC and MB. Additionally, we

identified a shortlist of 30 target genes which are bound in Zfx ChIP-seq from both mouse and human and which are also downregulated after *ZFX* knockdown in human MB cells *in vitro*. Knockdown of two target genes from this list, *DIS3L* and *UBE2J1*, impaired growth of human MB *in vitro*. Preliminarily, our results pointed towards the shortlisted downstream targets of ZFX, such as *DIS3L* and *UBE2J1,* as novel candidates for potential molecular targeting in treatment of Hh-dependent cancers.

Results

Finding direct ZFX targets with ChIP-Seq in DAOY human MB cells

In the preceding chapters, data was presented showing a requirement for the transcription factor *Zfx* in mouse models of Hh-dependent BCC and MB *in vivo*, as well as in the human MB cell-line DAOY *in vitro*. In order to understand why the loss of *Zfx* has these effects, we proposed to identify downstream direct transcriptional targets of *Zfx*, some subset of which are presumably relevant in causing the observed phenotypes in BCC and MB models *in vivo* and *in vitro*. As a first step, we set out to identify genomic direct binding targets of ZFX protein using chromatin immunoprecipitation assays followed by massively parallel DNA sequencing of the chromatin-bound genomic DNA fragments (ChIP-seq).

We performed ChIP-seq on anti-ZFX ChIP samples from nuclear lysate of DAOY human MB cells, using nuclear lysate that wasn't subjected to ChIP as a control (Input). Analysis of resulting ChIP-seq data using MACS peak-picking

software[144] yielded over 14,400 sequence-read enrichment peaks in anti-ZFX ChIP-seq compared with Input control. We began basic characterization and analysis of this dataset, in an effort to whittle a bewilderingly long list of binding peaks down to more tractable shortlists of potentially relevant ZFX targets.

First, we looked at the proximity of ZFX ChIP-seq enrichment peaks to adjacent genes. When we grouped ZFX binding peaks into 200 bp-wide "bins" ranging in either direction away from the transcriptional start site (TSS) of the nearest gene, we found that the majority of ZFX binding peaks identified by ChIP-seq in DAOY were located very close to TSS of the nearest adjacent gene (Fig. 22A), with the majority residing within 500 bp of TSS. Additionally, we applied the *ChIPseeqer FIRE* analysis module to our ZFX ChIP-seq dataset to identify short oligonucleotide binding motifs over- or underrepresented in the ZFX binding peaks. Encouragingly, the two highest-scoring motifs picked as overrepresented in our ZFX enrichment peaks from ChIP-seq included AGGCC (Fig. 22B, 23), the reverse complement of the GGCCT consensus sequence previously identified as the motif recognized by Zfx [70,71, 72].

We next asked how our list of ZFX binding targets identified in a human MB cell-line compared against other lists of ZFX binding targets generated by ChIP-seq in different biological contexts. Specifically, we compared our ZFX ChIP-seq target genes from DAOY cells with Zfx direct targets identified by another laboratory from ChIP-seq in murine embryonic stem cells (ESC) [70]. Given that the great majority of ZFX binding peaks occurred very close to TSS of the

nearest gene (Fig. 22A), we focused our comparison only on ChIP-seq peaks within 1 kb of TSS. We found that there was a high degree of overlap between the two lists of Zfx ChIP-seq binding peaks, with 62% of Zfx targets in mESC (3038) also bound in DAOY cells (Fig. 22C). Together, this overlap ChIP-Seq gene-list comprised a pool of Zfx direct binding targets conserved across species.

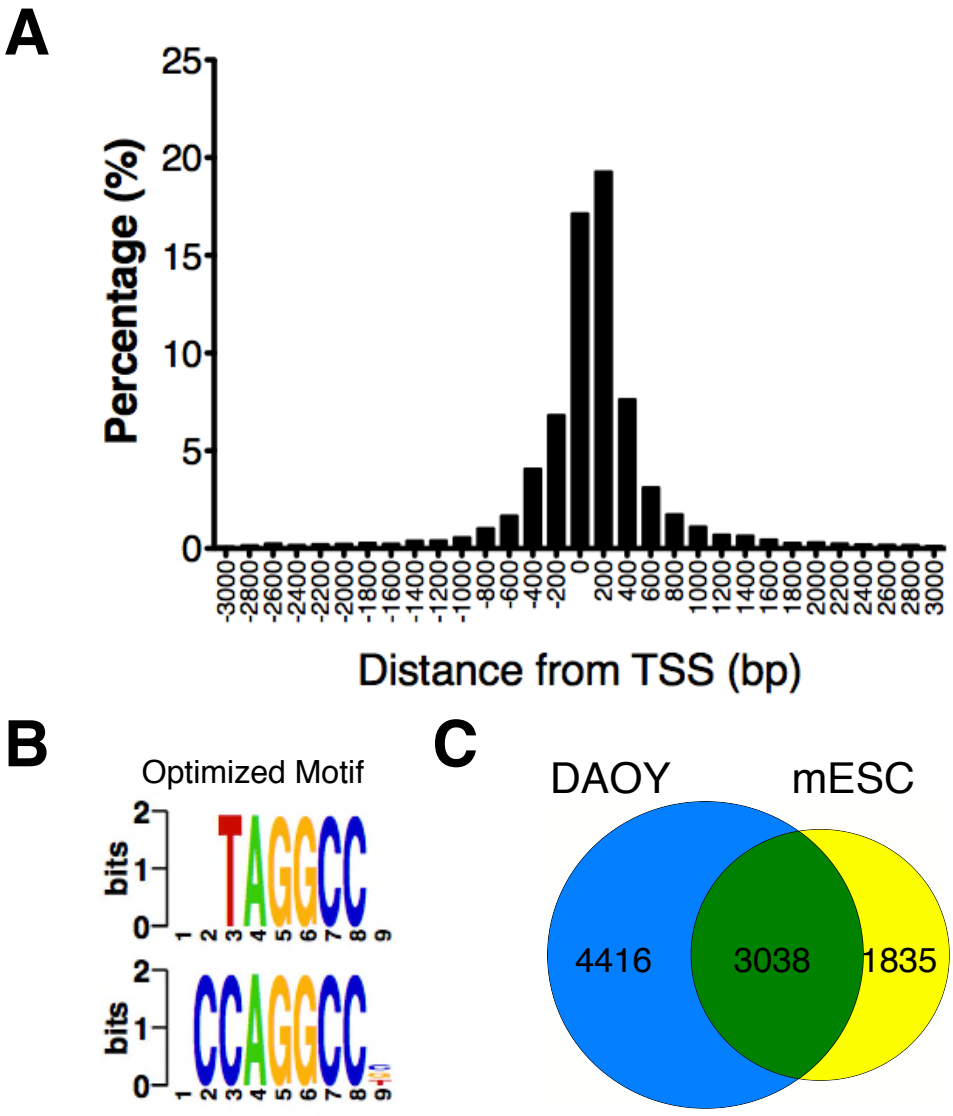
A
Percentage (%)
25
20
15
10
5
0
-3000 -2800 -2600 -2400 -2200 -2000 -1800 -1600 -1400 -1200 -1000 -800 -600 -400 -200 0 200 400 600 800 1000 1200 1400 1600 1800 2000 2200 2400 2600 2800 3000
Distance from TSS (bp)
B
Optimized Motif
bits
2
1
0
1 2 3 4 5 6 7 8 9
TAGGCC
bits
2
1
0
1 2 3 4 5 6 7 8 9
CCAGGCC
C
DAOY
mESC
4416
3038
1835

Figure 22. Direct binding targets of ZFX from ChIP-Seq in human MB and murine ESC

(A) Distribution of ZFX binding peak distances from gene transcription start sites (TSS) from anti-ZFX ChIP-seq in DAOY human MB cells. Shown are percentages of total ZFX binding peaks at binned 200 bp distances from TSS.

(B) Motifs overrepresented in ZFX binding enrichment peaks from ChIP-seq in human DAOY cells, identified by unbiased analysis with *ChIPseeqerFIRE* module.[145]

(C) Comparison of non-redundant ZFX binding enrichment peaks $\geq$1 kb from TSS in ChIP-seq from DAOY human MB and from murine ESC.[70]

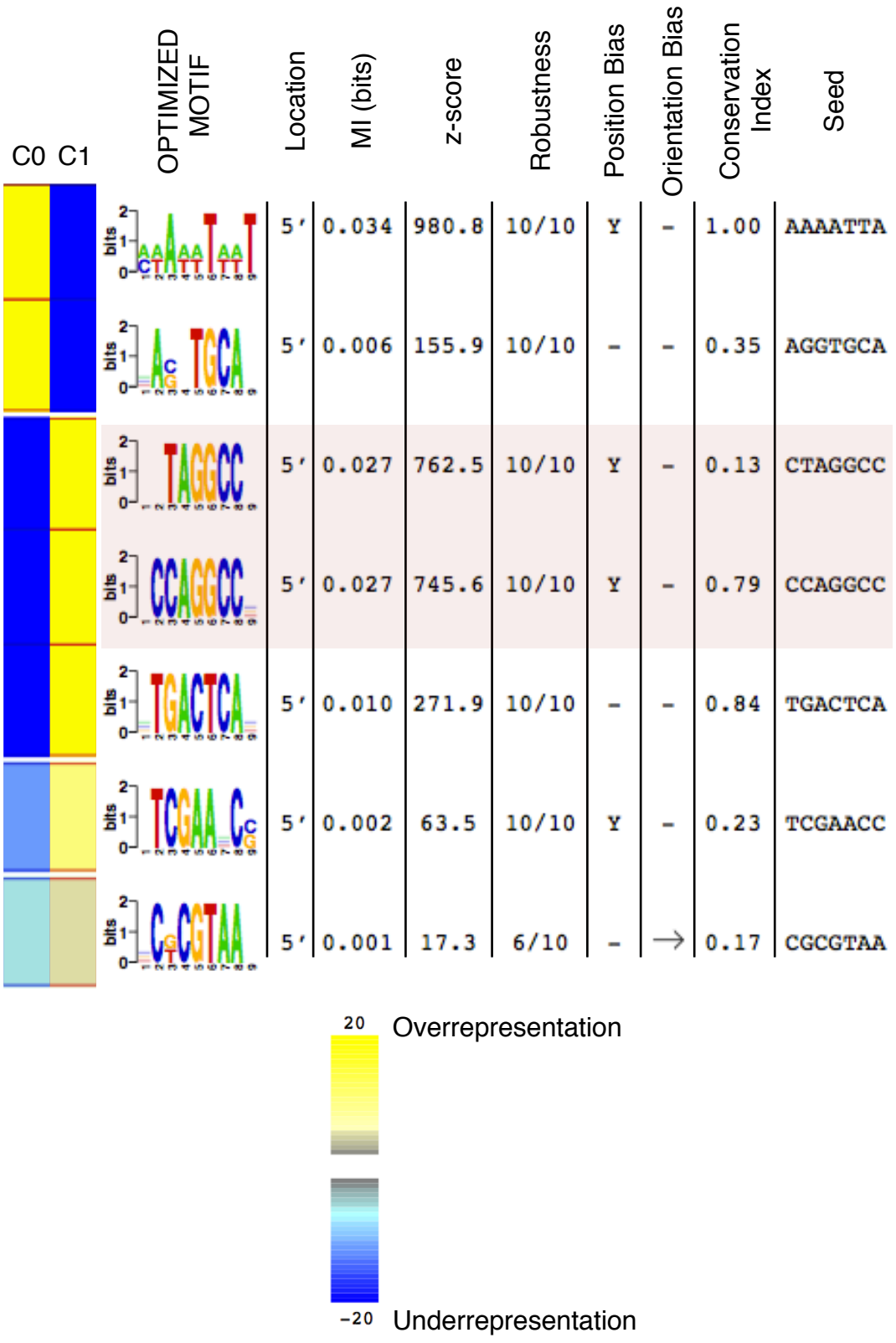
C0 C1
OPTIMIZED MOTIF
Location
MI (bits)
z-score
Robustness
Position Bias
Orientation Bias
Conservation Index
Seed
5′ 0.034 980.8 10/10 Y - 1.00 AAAATTA
5′ 0.006 155.9 10/10 - - 0.35 AGGTGCA
5′ 0.027 762.5 10/10 Y - 0.13 CTAGGCC
5′ 0.027 745.6 10/10 Y - 0.79 CCAGGCC
5′ 0.010 271.9 10/10 - - 0.84 TGACTCA
5′ 0.002 63.5 10/10 Y - 0.23 TCGAACC
5′ 0.001 17.3 6/10 - → 0.17 CGCGTAA
20
Overrepresentation
-20
Underrepresentation

Figure 23. *de novo* motif analysis of ZFX ChIP-seq in DAOY human MB

ZFX binding peaks identified using MACS (1.4.0) from ChIP-seq in human DAOY medulloblastoma cells were analysed for unbiased/*de novo* discovery of binding motifs using the *ChIPseeqerFIRE* module of *ChIPseeqer* (2.0).[145] Shown are the summarized results displaying optimized motifs picked by *ChIPseeqerFIRE* for underrepresentation (uppermost two entries) or overrepresentation (lower five entries) in the ZFX binding peaks sequence from ChIP-seq in DAOY cells. Highlighted motifs (red) had the highest z-score of motifs overrepresented in ZFX ChIP-Seq peaks, and they contain sequence complementary to the GGCCT previously identified as the Zfx binding motif [70, 71, 72].

Zfx *facilitates the expression of the Hh signal transducer* Smo

We refocused our search for downstream targets of ZFX with potential explanatory power onto these 3038 conserved Zfx binding targets. Given observed effects of *Zfx* loss in Hh-dependent MB and BCC cancer models *in vivo*, we first scanned the common ChIP-seq gene-list for core components of the Hh signaling pathway. A core pathway component found in the overlap list was *Smo*, a promising candidate given that it encodes the non-redundant signal transducer of the Hh signaling pathway. There were Zfx binding enrichment peaks near the TSS of *Smo* in ChIP-seq data from both mESC (Fig. 24A) and DAOY human MB (Fig. 24B), confirming *Smo* as a Zfx-bound gene in both mouse and human cells *in vitro*.

We then asked whether we could find evidence for changes in the expression levels of *Smo* and Hh pathway components following *Zfx* loss, particularly in the context of BCC or MB models *in vivo* and *in vitro*. Looking again at the human MB cell-line DAOY, decreased *ZFX* expression after lentiviral shRNA knockdown (KD) of ZFX correlated with reduced *SMO* expression (Fig. 24C). We also saw additional evidence for transcriptional regulation of *Smo* by Zfx earlier in Chapter I. When we examined gene expression by qPCR in bulk epidermis and hair follicles from *Ptch1* and *Ptch1 Zfx* mice 3 days after Tmx application to induce Hh-dependent BCC, co-deletion of Zfx in *Ptch1 Zfx* skin decreased *Smo* expression levels and prevented the induction of Hh pathway targets *Gli1* and *MycN* (Fig. 25). These data point towards a requirement for Zfx

for optimal Smo expression, in both DAOY MB cells *in vitro* and also in the context of a model of Hh-dependent BCC in mouse skin.

Given the correlation of *Zfx* loss with decreased *Smo* expression observed across cell-types and species, we next investigated whether Zfx was generally required for Hh signaling during normal development. Previous work from our laboratory suggested that *Zfx* is dispensable for Hh signaling during normal embryonic development [74]. Pups deleting *Zfx* throughout the embryo-proper die perinatally [74], but they exhibit none of the major skeletal or nervous system defects associated with the complete blockade of the Hh pathway that would results from loss of *Smo* expression [26]. To confirm that *Zfx* is dispensable for Hh signaling during normal development, we tested whether Zfx^{CKO} embryos had defects in the specification of floor plate and of motor neuron pools in the developing ventral spinal cord, a process known to depend on active Hh signaling [55, 116]. $Shh^{-/-}$ or $Smo^{-/-}$ embryos that lack active Hh signaling fail to develop floor plate and have smaller and highly disorganized motor neuron pools in their ventral spinal cord [55, 116]. We examined Zfx^{CKO} embryos at E13.5/E14.5 to determine whether they establish floor plate and motor neuron pools in their developing spinal cord (Fig. 26). Embryos that conditionally deleted *Zfx* stained positively for floor plate in their developing spinal cord comparably to *Sox2-Cre*$^{-}$ littermate control embryos (Fig. 26A), as confirmed by immunostaining for the established floor plate marker FOXA2/HNF-3β [146, 147]. Furthermore, immunostainings for the motor neuron marker HB9/Mnx1 reveal that Zfx^{CKO}

embryos also successfully form motor neuron pools that are grossly comparable to Ctrl embryos (Fig. 26B).

While *Zfx* loss may not impair Hh signaling during normal embryonic development, *Zfx*-dependent regulation of *Smo* expression could still play a role in the context of biological systems where the Hh pathway is overactivated. Heterozygous $Smo^{+/-}$ embryos are wild-type in appearance and display none of the defects associated with $Smo^{-/-}$ full knockouts [44, 116], suggesting that decreases in Smo levels on the order of 2-fold may not significantly impair Hh-dependent developmental processes. However, modest decreases in *Smo* expression levels due to *Zfx* loss could impact systems with hyperactivated Hh signaling from superabundance of Hh ligand or constitutive activation of the pathway upstream of *Smo*, where Smo itself could take on the roll of rate limiting reagent in activated Hh signaling. We next asked whether Zfx was wholly or partially required for a known Hh-dependent biological process in the context of superabundance of Hh ligand or constitutive pathway activation. To answer this question, we made use of a previously described assay, where motor neurons (MN) are generated in a Hh-dependent fashion *in vitro* by means the treatment of murine ESC with retinoic acid (RA) and Sonic Hedgehog (Shh) or a synthetic Hh agonist [148]. Zfx-deficient (Zfx^{null}) ESCs generated fewer MNs than ESCs with non-excised conditional *Zfx* (Zfx^{flox})(Fig. 27A), especially at low concentrations of Hh agonist, as gauged by immunofluorescent staining for the motor neuron marker Mnx1 (HB9). Zfx^{null} ESCs also expressed lower levels of MN- and MN progenitor-specific transcription factors *Mnx1, Isl1*, and *Olig2* after Shh-induced

differentiation (Fig. 27B), again particularly at low concentrations of Hh agonist or recombinant Shh ligand. Replacement of Zfx with a FLAG-tagged allele in *Zfx*^{null} ESC (*Zfx*^{TAG}) rescued this defect (Fig. 27B). Meanwhile, expression of a pan-neuronal tubulin, *Tubb3*, was largely unaffected in *Zfx*^{null} ESC (Fig. 27B). *Zfx*^{null} ESC also expressed higher levels of *Pax6* and *Irx3* (Fig. 28), transcription factors expressed widely across neuronal progenitor domains more dorsally-fated relative to MN progenitors in the developing mouse spinal cord [115, 116]. These results suggest that the loss of *Zfx* specifically impairs Hh-dependent differentiation of ESC into motor neurons, but not their differentiation into neurons generally or differentiation into more dorsally-fated interneurons.

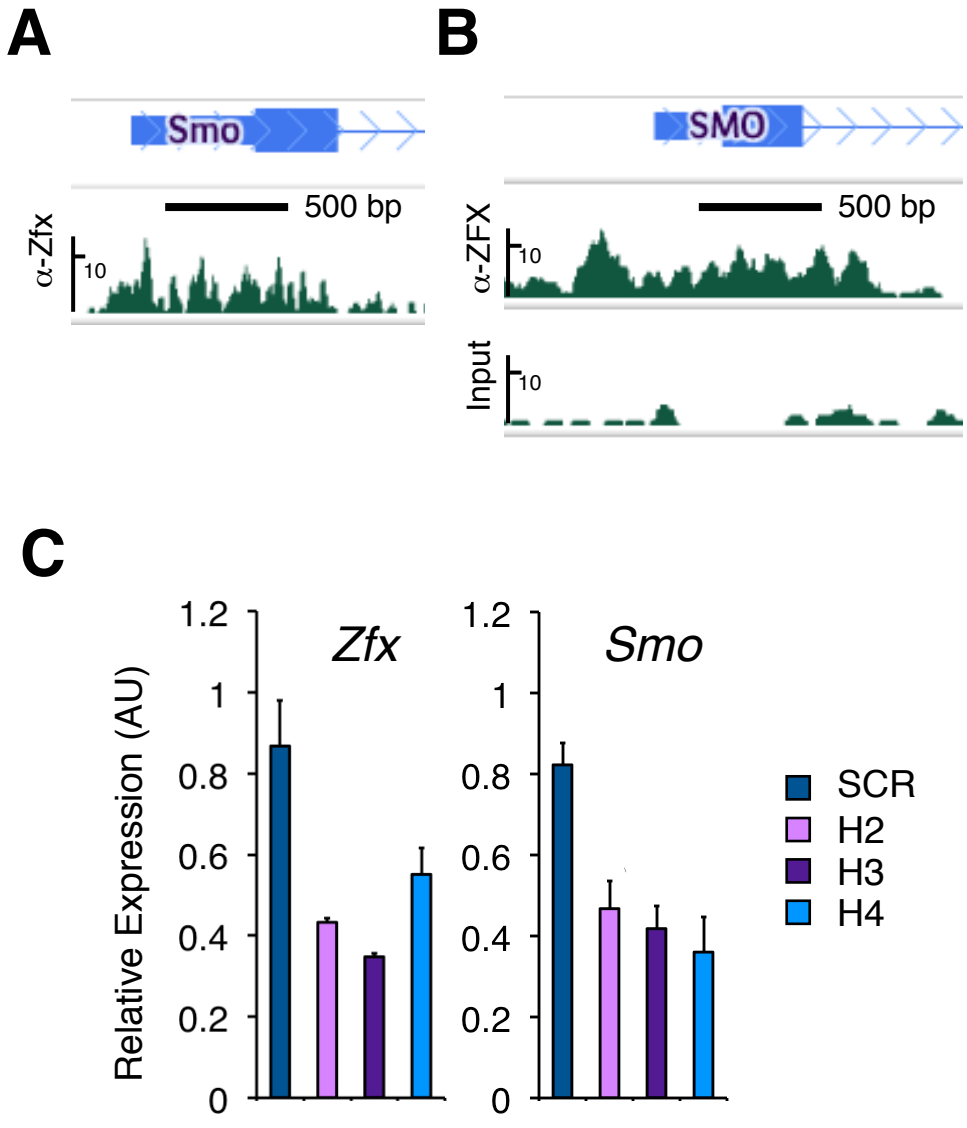
A
Smo
500 bp
α-Zfx
10
B
SMO
500 bp
α-ZFX
10
Input
10
C
Zfx
Smo
Relative Expression (AU)
1.2
1
0.8
0.6
0.4
0.2
0
SCR
H2
H3
H4

Figure 24. ZFX binds directly to *Smo* and regulates *Smo* expression in human DAOY MB cells

(A&B) Zfx binding to *Smo* in murine and human ChIP-seq. Shown are sequencing-read enrichment peaks near TSS of *Smo* in anti-Zfx ChIP-seq from murine ESC (Chen *et al.*, 2008) (A) and near TSS of *SMO* in anti-ZFX ChIP-seq and sheared nuclear lysate control (Input) from DAOY human MB cells (B).
(C) Expression of *ZFX* and *SMO* in DAOY cells after ZFX knockdown. Shown are *ZFX* (left) and *SMO* (right) expression levels by qPCR 4 days after transduction with lentivirus with ZFX-targeting (H2, H3, H4) or scrambled control (SCR) shRNA (mean ± SD of triplicate parallel cultures; representative of three independent experiments).

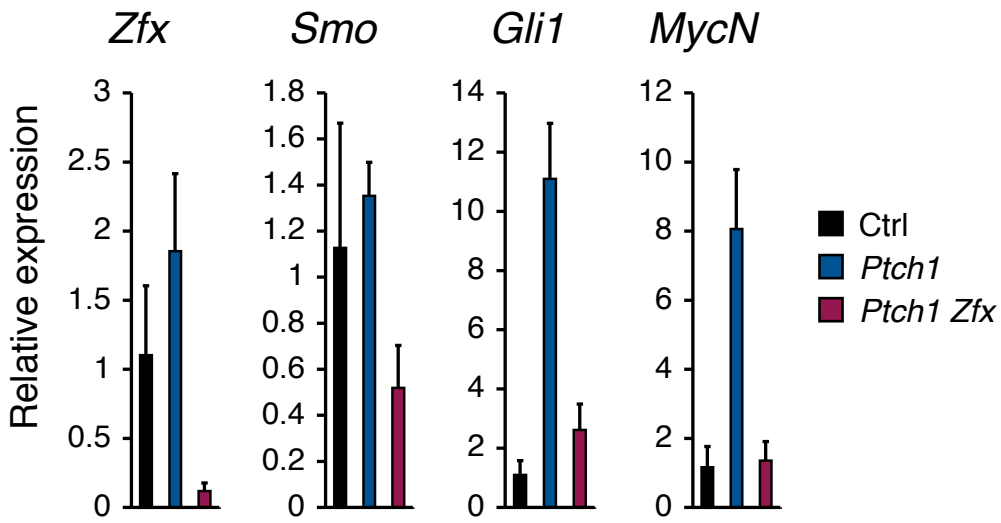

Figure 25. Co-deletion of *Zfx* decreases *Smo* expression and blunts Hh pathway activation in mouse skin after *Ptch1* deletion

Expression levels of *Zfx*, *Smo,* and Hh pathway target genes *Gli1* and *Mycn* in bulk epidermis and hair follicles from shaved dorsal skin 3 days after topical Tmx treatment in *Ptch1*, *Ptch1 Zfx*, and Ctrl mice (as described in Fig. 5). Shown are normalized expression levels for the indicated genes relative to Ctrl skin as determined by qPCR (mean ± SD of 2-4 mice; representative of four independent experiments).

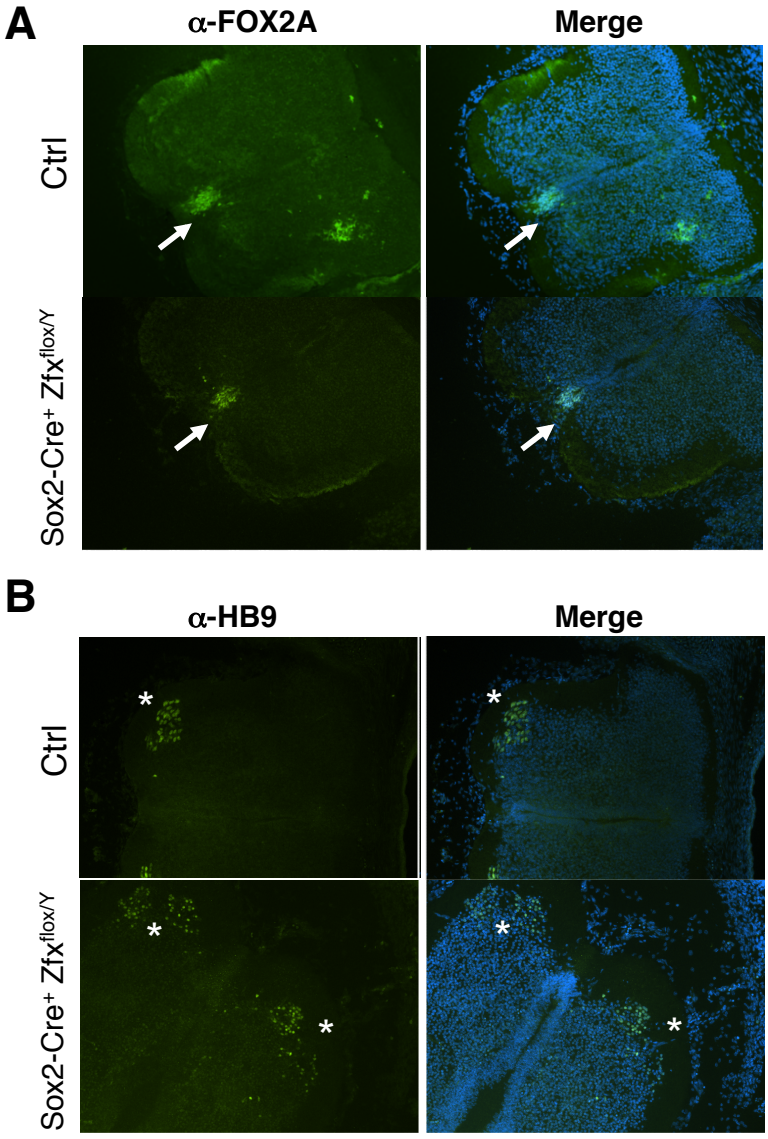
A
α-FOX2A
Merge
Ctrl
Sox2-Cre+ Zfxflox/Y
B
α-HB9
Merge
Ctrl
Sox2-Cre+ Zfxflox/Y

Figure 26. *Zfx*^{CKO} embryos develop floor plate and motor neuron pools in their developing spinal cord.

Embryos were collected at embryonic day 13.5 or 14.5 (E13.5/E14.5) and fixed for immunofluorescence staining analysis. Spinal cords from *Sox2-Cre*$^{-}$ *Zfx*$^{flox/Y}$ embryos (Ctrl) and *Sox2-Cre*$^{+}$ *Zfx*$^{flox/Y}$ embryos were embedded in OCT and cryosectioned. Sections were stained with antibodies against the floor plate marker, FOXA2/HNF3-β (Seven Hills Bioreagents), or against the motor neuron marker HB9/Mnx1. Nuclei were marked with DAPI.

(A) Floor plate in spinal cord from *Zfx*^{CKO} embryos. Shown are representative micrographs from Ctrl (n = 4) and *Sox2-Cre*$^{+}$ *Zfx*$^{flox/Y}$ (n = 3) E13.5/E14.5 spinal cord sections, stained for floor plate marker FOXA2 (green) and with nuclear stain DAPI (blue). White arrows indicate FOXA2^{+} floor plate.

(B) Developing motor neuron pools from *Zfx*^{CKO} embryos. Shown are representative micrographs from Ctrl (n = 2) and *Sox2-Cre*$^{+}$ *Zfx*$^{flox/Y}$ (n = 1) E13.5/E14.5 spinal cord sections, stained for motor neuron marker HB9 (green) and with nuclear stain DAPI (blue). White stars indicate motor neuron pools.

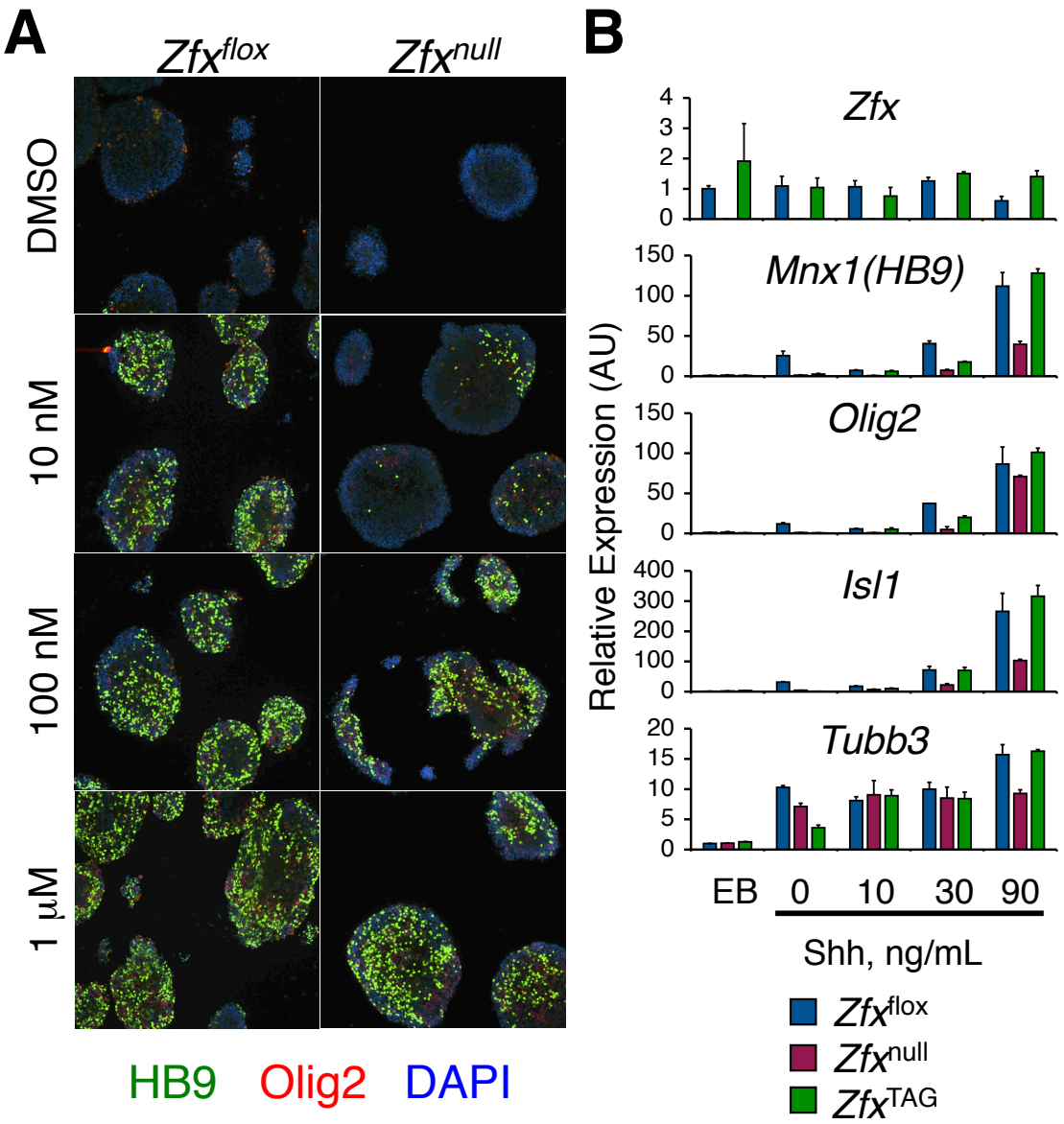
A
Zfx^flox
Zfx^null
DMSO
10 nM
100 nM
1 μM
HB9 Olig2 DAPI
B
Zfx
Mnx1(HB9)
Olig2
Isl1
Tubb3
Relative Expression (AU)
EB 0 10 30 90
Shh, ng/mL
Zfx^flox
Zfx^null
Zfx^TAG

Figure 27. Loss of *Zfx* impairs Shh-dependent formation of MNs from murine ESC *in vitro*

Murine ESC carrying conditional (Zfx^{flox}) or null (Zfx^{null}) Zfx alleles and Zfx^{null} ESC rescued with a tagged *Zfx* transgene (Zfx^{TAG}) were differentiated into embryoid bodies (EB) and treated with synthetic Smo agonist (SAG) or recombinant Shh to induce motor neuron (MN) differentiation.

(A) Immunofluorescence staining for DNA (DAPI, blue), MN progenitors (Olig2; red) and MN (Mnx1/HB9, green) in EB following treatment with SAG at the indicated concentrations.

(B) Expression of MN-specific transcription factors in differentiated ESC of the indicated genotypes prior to (EB) or 3 days after treatment with the indicated concentrations of Shh. Shown are normalized expression levels relative to untreated Zfx^{flox} EB as determined by qPCR (mean ± SD of triplicate reactions; representative of three independent experiments).

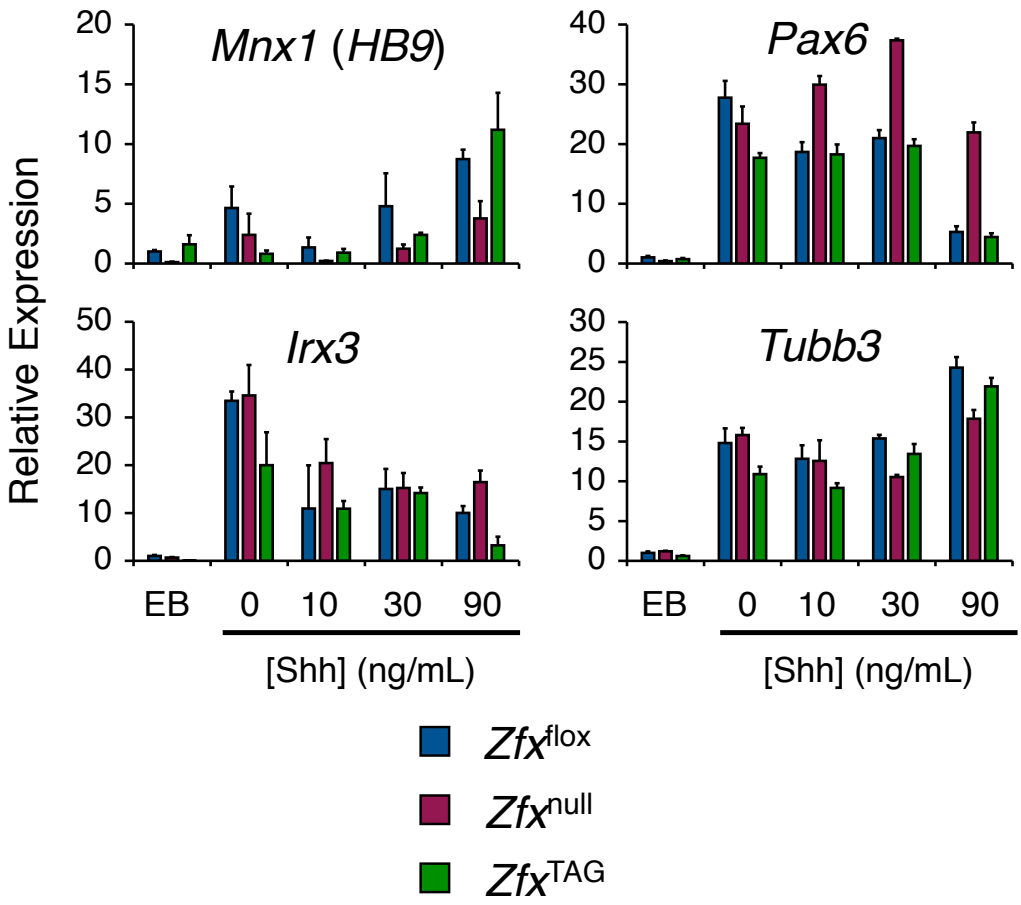

Figure 28. *Zfx*^{null} EBs have increased expression of dorsal spinal cord neuronal fate transcription factors in Shh-dependent MN assay *in vitro*

Expression levels for the MN-specific transcription factor *Mnx1*, for two transcription factors characteristic of neuronal progenitor pools more "dorsally-fated" and distal to Shh ligand source in the developing spinal cord (*Pax6*, *Irx3*), and for the pan-neuronal β3-tubulin (*Tubb3*). Shown are qPCR results for *Zfx*^{flox}, *Zfx*^{null}, and *Zfx*^{TAG} embryoid bodies (EBs) harvested prior to or following 3 days of treatment with retinoic acid (RA) and recombinant Shh ligand. GAPDH was used as the control gene, and expression results were normalized to those for untreated *Zfx*^{flox} EBs (mean ± SD of triplicate reactions).

Identifying candidates for functional conserved direct targets of ZFX in MB

Decreased expression of *Smo* in mouse skin and human DAOY cells, coupled with impaired MN generation from *Zfx*^{null} ESC *in vitro*, all argue in favor of an explanation for the effects of *Zfx* loss in our BCC and MB models that centers around transcriptional regulation of *Smo.* However, recalling results from mouse skin and cerebella presented in Chapters I and II, co-deletion of *Zfx* also impaired formation of BCC after Hh pathway activation by constitutively active *SmoM2* downstream of *Smo* (Fig. 9), and *Zfx* loss did not lead to decreased Smo levels or blunted Hh pathway activity in P14 cerebella of MB model mice (Fig. 17). These and other data from BCC and MB systems raise the possibility that the *Zfx*-dependent phenotypes are not explainable solely *via* regulation of *Smo*.

For this reason, we set out to find additional direct targets of *Zfx*, identified in both mouse and human ChIP-seq, with potential functional relevance in BCC and MB. To narrow down the list of direct gene targets to consider, we compared the overlap gene-list of Zfx binding targets from both mESC and DAOY cells (Fig. 22C) with genes in human MB cells whose mRNA expression levels decreased along with ZFX loss in human MB cells. We performed microarray-based gene expression analysis of DAOY cells at an early time point after transduction with lentiviral particles bearing shRNAs targeting *ZFX* for knockdown. We searched for genes whose RNA expression levels behaved similarly to that of ZFX (Fig. 24C), exhibiting strong reduction by qPCR due to shRNAs H2 and H3 and more moderate reduction with shRNA H4. A set of 163 genes whose expression level patterns matched that of *ZFX* in transduced DAOY cells has been identified (Fig.

29A). We then compared this gene-list with overlapping conserved direct targets of Zfx in mouse and human (Fig. 22C). Of these 163 genes identified by pattern-matching analysis of microarray data, 68 genes (42%) were bound by Zfx in DAOY cells, and 30 genes (18%) were direct binding targets in ChIP-seq from both DAOY and murine ESC (Fig. 29B).

Within this shortlist of 30 conserved direct targets of ZFX in mESC and DAOY (Fig. 30A&B), we chose to focus on two genes in particular, *DIS3L* and *UBE2J1*. *Dis3L* encodes a cytoplasmic RNA exonuclease with a possible role in mRNA degradation [149, 150]. *Ube2j1* encodes an E2 ubiquitin-conjugating enzyme that is thought to participate in the endoplasmic reticulum (ER)-associated degradation of misfolded proteins such as MHC class I [151]. The expression of *Dis3L* (formerly known as *AV340375*) strongly depends on Zfx in all examined murine cells including HSCs and ESCs (Fig. 30)[74] and activated B lymphocytes [76]. The expression of Ube2j1 is also Zfx-dependent in HSCs [74] and B lymphocytes [76], although not in ESCs (Fig. 30B)[74]. These data suggested *Dis3L* and *Ube2j1* as candidate genes with potential functional relevance downstream of Zfx in both mouse and human.

Knockdown of ZFX targets DIS3L *and* UBE2J1 *impairs human MB growth in vitro*

We next asked if *DIS3L* and *UBE2J1* were required for growth of human MB cells *in vitro*. Before addressing that question head-on, we first sought to confirm that *DIS3L* and *UBE2J1* were bound by ZFX directly in a relevant cellular context, and that expression of both genes was affected by *ZFX* loss.

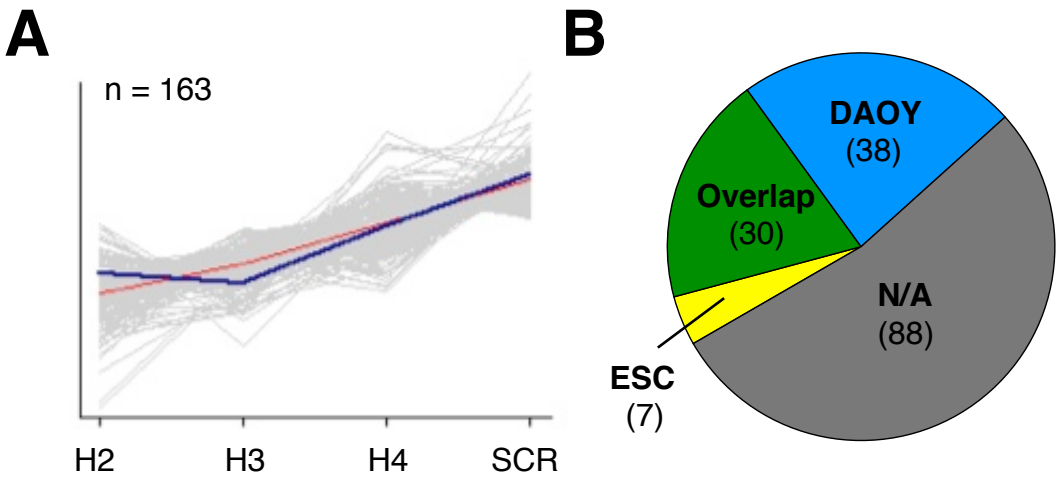

Figure 29. Identification of conserved Zfx targets by comparison of murine and human ZFX ChIP-Seq data from microarray data after ZFX knockdown in DAOY human MB

(A) Downregulated genes (n= 163) identified in pattern matching analysis of Affymetrix Gene ST 1.0 array data from DAOY cells after shRNA knockdown.

(B) Conserved ZFX transcriptional targets. Shown are numbers of pattern-matching genes from ZFX KD microarray in (A) that had enrichment peaks ≥1kb from TSS in ZFX ChIP-seq from DAOY cells, from murine embryonic stem cells (mESC), from both cell types (Overlap), or from neither cell type (N/A).

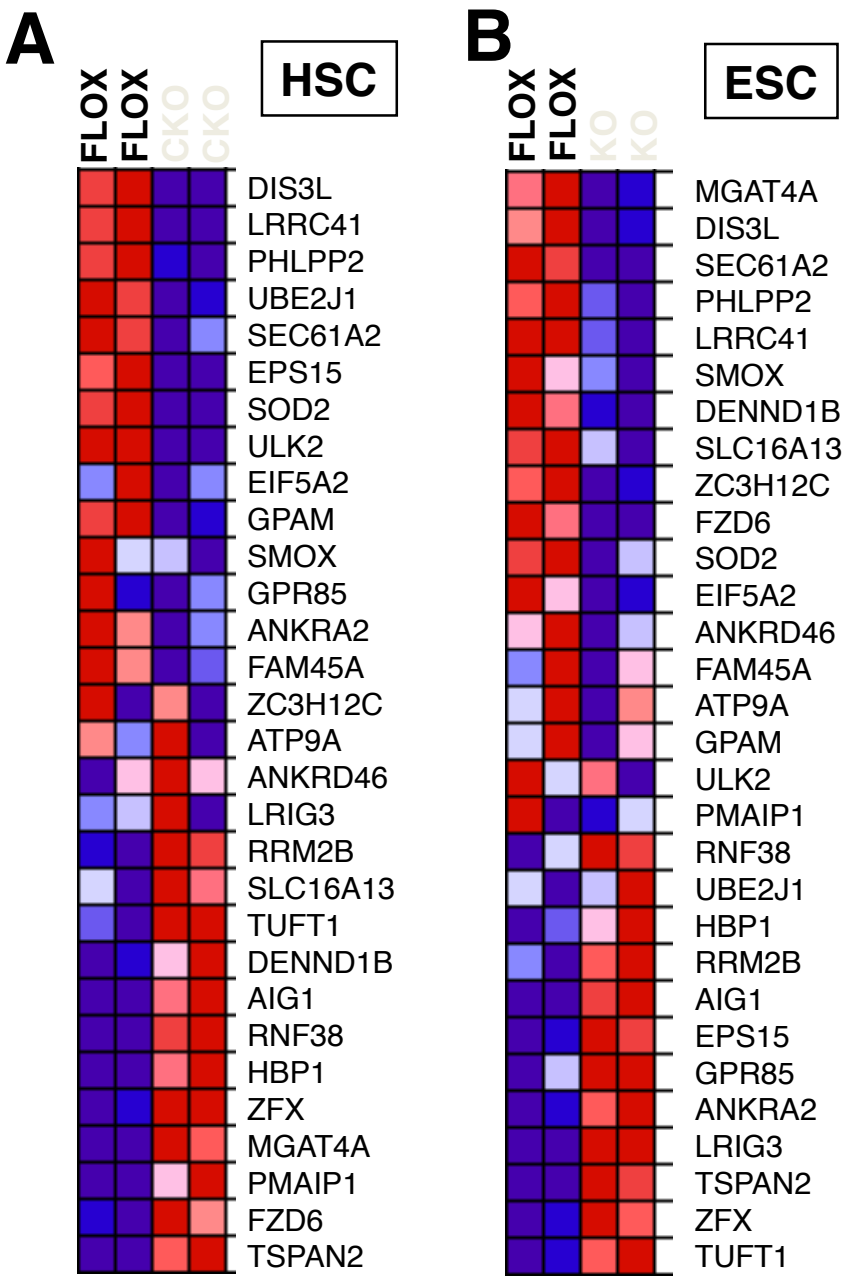

Figure 30. Expression of conserved Zfx targets in mouse HSC and ESC

(A&B) Heatmaps generated by gene set enrichment analysis (GSEA) software, comparing Overlap targets from ZFX KD microarray and ChIP-Seq targets ≥1kb from TSS in DAOY and murine ESC (Figure 27B; n=31) with previously published [74] microarray results from murine *Zfx*^{flox} and *Zfx*^{CKO} HSC (A) and *Zfx*^{flox} and *Zfx*^{KO} ESC (B).

Visualization of sequence-read enrichment peaks from ChIP-seq confirmed ZFX binding near the TSS of both *Dis3L* (Fig. 31A) and *Ube2j1* (Fig. 31B) in both murine ESC and human DAOY cells. We tested whether expression levels of the targets *Dis3L* and *Ube2j1* were affected in the context of BCC and MB following *Zfx* loss. *DIS3L* and UBE2J1 expression levels were both decreased after shRNA-mediated ZFX knockdown in DAOY cells (Fig. 31C). Moreover, both transcripts were reduced ~2-fold after tamoxifen-induced *Zfx* co-deletion in epidermis and hair follicles of treated dorsal skin from the *Ptch1*-dependent BCC model *in vivo* (Fig. 31D). Collectively with the ChIP-seq binding data in human DAOY cells, these data suggest Zfx can directly regulate *Dis3L* and *Ube2j1* expression in the contexts of BCC and MB models *in vivo* and *in vitro*.

To determine whether DIS3L or UBE2J1 themselves are required for growth of a human MB cell-line *in vitro*, we transduced DAOY cells with lentiviral vectors encoding several shRNAs targeting both genes for knockdown. Compared to untreated cells and a control shRNA targeting non-mammalian sequence (NonM), all tested shRNAs against DIS3L (4 shRNAs) or UBE2J1 (3 shRNAs) impaired the growth of DAOY cells (Fig. 32A). Successful knockdown *DIS3L* or *UBE2J1* by each in the battery 3-4 shRNAs targeting the respective genes was confirmed by qPCR (Fig. 32B). Thus, *DIS3L* and *UBE2J1* represent conserved direct binding targets of ZFX that are also required for optimal growth of DAOY human MB cells *in vitro*. These results suggest both genes as promising candidates for further research, to determine whether they are functionally required across BCC and MB tumors *in vivo*.

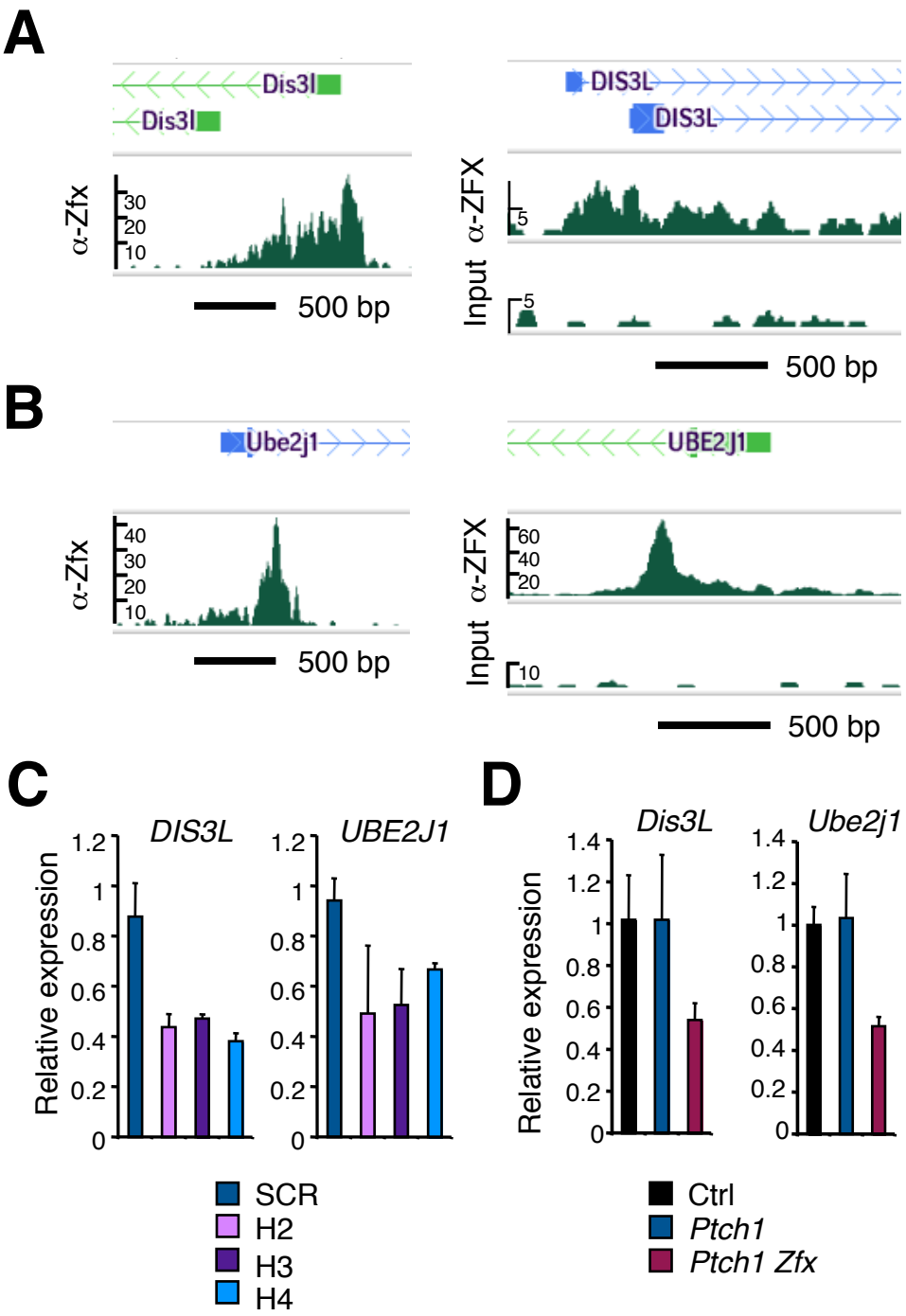
A
Dis3l
Dis3l
α-Zfx
30
20
10
500 bp
DIS3L
DIS3L
α-ZFX
5
Input
5
500 bp
B
Ube2j1
α-Zfx
40
30
20
10
500 bp
UBE2J1
α-ZFX
60
40
20
Input
10
500 bp
C
DIS3L
UBE2J1
Relative expression
1.2
1
0.8
0.6
0.4
0.2
0
SCR
H2
H3
H4
D
Dis3L
Ube2j1
Relative expression
1.4
1.2
1
0.8
0.6
0.4
0.2
0
Ctrl
Ptch1
Ptch1 Zfx

Figure 31. Zfx direct targets *Dis3L* and *Ube2j1* and regulates their expression in mouse BCC *in vivo* and human MB *in vitro*

(A) Zfx binding to *Dis3L* in murine and human ChIP-seq. Shown are sequencing-read enrichment peaks near TSS of *Dis3L* in anti-Zfx ChIP-seq from murine ESC [70] (left), and in anti-ZFX ChIP-seq and sheared nuclear lysate control (Input) from DAOY human MB cells (right).

(B) Zfx binding to *Ube2j1* in murine and human ChIP-seq. Shown are sequencing-read enrichment peaks near TSS of *Ube2j1* in anti-Zfx ChIP-seq from murine ESC [70] (left), and in anti-ZFX ChIP-seq and sheared nuclear lysate control (Input) from DAOY human MB cells (right).

(C) Expression of *DIS3L* and *UBE2J1* in DAOY cells after ZFX knockdown. Shown are *DIS3L* and *UBE2J1* expression levels by qPCR 4 days after transduction with lentivirus coding for ZFX-targeting (H2, H3, H4) or scrambled control (SCR) shRNA (mean ± SD of triplicate parallel cultures; representative of three independent experiments).

(D) Expression levels of *Dis3L* and *Ube2j1* in bulk epidermis and hair follicles from shaved dorsal skin 3 days after topical Tmx treatment in *Ptch1*, *Ptch1 Zfx*, and Cre^- (Ctrl) mice (as described in Fig. 4). Shown are normalized expression levels relative to Ctrl skin as determined by qPCR (mean ± SD of 2-4 mice; representative of four independent experiments).

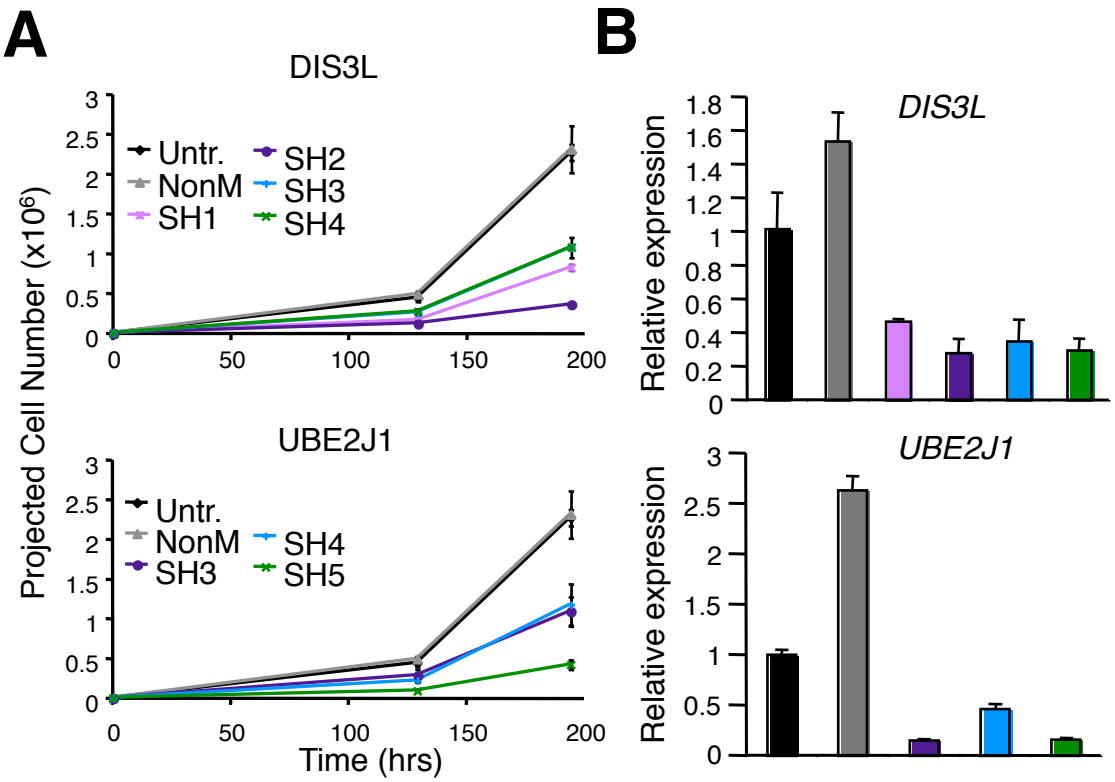
A
DIS3L
Projected Cell Number (x10^6)
Untr.
NonM
SH1
SH2
SH3
SH4
UBE2J1
Untr.
NonM
SH3
SH4
SH5
Time (hrs)
B
DIS3L
Relative expression
UBE2J1
Relative expression

Figure 32. Knockdown of DIS3L and UBE2J1 impairs growth of DAOY human MB cells *in vitro*

DAOY human MB cells were transduced *in vitro* with Sigma MISSION lentiviruses encoding shRNAs targeting DIS3L, UBE2J1, or a non-mammalian control gene (NonM).

(A) Growth curves for DAOY cells transduced with DIS3L- or UBE2J1-targeting shRNA lentivirus. Shown are projected cell numbers for untreated DAOY cells versus cells transduced with NonM control virus or 3-4 shRNA lentiviruses targeting DIS3L (SH1-SH4) or UBE2J1 (SH3-SH5) (mean $\pm$ SD of triplicate parallel cultures; beginning 2 days post- puromycin selection and 4 days post-transduction).

(B) Expression of *DIS3L* and *UBE2J1* in DAOY cells after shRNA knockdown. Shown are *DIS3L* (upper) and *UBE2J1* (lower) expression levels by qPCR in DAOY cells 5 days after transduction with Sigma MISSION lentiviruses coding for DIS3L- or UBE2J1-targeting shRNA, respectively, or for NonM control shRNA (mean ± SD of triplicate reactions; normalized to expression in untreated DAOY cells).

Discussion

In Chapters I and II, we demonstrated that the transcription factor *Zfx* is required for development of Hh-driven BCC and MB *in vivo*. In this Chapter, we delved deeper into the transcriptional targets of Zfx, to try to understand why it was required for development of these two quite different cancers. Using DAOY human MB cells, where we had already established a lentiviral shRNA system for knocking-down ZFX, we performed anti-ZFX ChIP-seq to identify genomic binding sites for ZFX in the context of human MB. We confirmed that ZFX binds very close (within 500 bp) to TSS of target genes (Fig. 22A), at sites enriched for the ZFX binding motif GGCCT (Fig. 22B, 23). ZFX binding targets in human DAOY also had a high degree of overlap with Zfx ChIP-seq targets from murine ESC [70], with over 3000 conserved ZFX direct binding targets >1 kb from TSS (Fig. 22C).

One target gene that was directly bound by Zfx in both mESC (Fig. 24A) and human DAOY ChIP-seq (Fig. 24B) was *Smo*. Identification of *Smo*, an essential component of the Hh pathway, as a direct binding target of ZFX suggested an attractively straightforward hypothesis explaining the requirement for *Zfx* in Hh-driven MB and BCC, namely: if Zfx regulates *Smo* expression in these tumors, then loss of Zfx means loss of Smo, and loss of Smo prevents Hh pathway activation and Hh-driven tumor progression. This is the same logic that spurred small molecule targeting of SMO with compounds like vismodegib (GDC-0449), which have indeed shown success in regressing Hh-dependent BCC and

MB in human patients [110, 134, 135 136]. Consistent with this explanation of BCC and MB phenotypes from Zfx loss centering around transcriptional regulation of *Smo*, we previously reported that *Zfx* co-deletion correlated with decreased *Smo* expression and blunted Hh target gene overexpression in skin from mice treated to induce *Ptch1* deletion and BCC formation (Fig. 25). Decreased *SMO* expression levels also resulted after ZFX knockdown in human DAOY MB cells *in vitro* (Fig. 24C). Additionally, Zfx-deficient ESC formed fewer MN in a Hh-dependent MN generation assay *in vitro* (Fig. 27). To summarize all the points in favor, genomic *Smo* is directly bound by Zfx in both mouse and human, and absence of Zfx tracks with decreased *Smo* expression in BCC *in vivo* and MB *in vitro*, in addition to impairing a known Hh-dependent differentiation assay *in vivo*.

Unfortunately for the simple hypothesis that Zfx is required in BCC and MB entirely because of transcriptional regulation of the Hh signal transducer *Smo*, observations contradicting this interpretation were made in BCC and MB models *in vivo*, as well as in DAOY cells *in vitro*. In Chapter I, we saw that *Zfx* loss severely impaired BCC development after induction of the activated SmoM2 allele in the skin (Fig. 9) but did not result in decreased *Smo* expression or blunted Hh pathway (Fig. 10). In Hh-driven MB in the brain, expression levels *Smo* or Hh target genes *Gli1* and *Mycn* were not reduced after *Zfx* co-deletion (Fig. 17). Furthermore, normal cerebellar development in *hGFAP-Cre*$^{+}$ *Zfx*$^{fox/Y}$ mice deleting only *Zfx* (Fig. 19) argued against any generalizable regulation of *Smo* throughout normal cerebellar development, since even partial disruption of

Hh pathway functionality causes defective growth and foliation in the developing cerebellum [23]. Successful Hh-dependent development of floor plate and motor neuron pools in spinal cords of *Zfx*^{CKO} embryos (Fig. 26) also argued against a requirement for *Zfx* in activation of the Hh pathway during normal embryogenesis. Finally, while ZFX knockdown correlates with decreased *SMO* expression in DAOY human MB cells, it is unclear that functional Hh signaling is active or required in DAOY cells, since treatment with either SMO chemical agonist or antagonist did not alter expression of the Hh target *GLI1* or affect DAOY cell growth in our hands (data not shown).

The results from the *SmoM2*-dependent BCC model *in vivo*, as well as from *Zfx*^{CKO} cerebella and spinal cords, do not conclusively exclude the possibility that Zfx-dependent transcriptional regulation of *Smo* is crucial in Hh-dependent BCC and MB. Deletion of *Zfx* does not disrupt normal Hh-dependent patterning of the cerebellum (Fig. 19) or floor plate and motor neuron pools in the embryonic spinal cord (Fig. 26). However, *Zfx* loss only generates a roughly 2-fold decrease in *Smo* expression in DAOY cells (Fig. 24) and epidermis from the murine BCC model (Fig. 25). *Smo*$^{+/-}$ embryos heterozygous for a null allele of *Smoothened* are phenotypically wild-type [44, 116], suggesting that decreases in Smo levels on the order of 2-fold do not block Hh-dependent processes during normal development. Moderate decreases in endogenous *Smo* levels could have significant effects in cases of hyperactivated Hh signaling such as Hh-dependent BCC and MB or *in vitro* Hh-dependent motor neuron generation, where levels of Smo could become

the rate-limiting agent. A comparable decrease in endogenous *Smo* expression due to *Zfx* loss could plausibly account for the prevention of SmoM2-dependent BCC after *Zfx* loss (Fig. 9), although changes in endogenous *Smo* expression could not be confirmed by qPCR due to confounding effects of *SmoM2* transgene overexpression (Fig. 10).

Nevertheless, given all of these potential contraindications pointing away from regulation of *Smo* as an explanation, we sought to investigate whether alternative downstream direct targets of Zfx might explain some of the phenotypes we observed in BCC and MB after Zfx loss. We endeavored to narrow the list of >3000 direct Zfx binding targets shared in mESC and DAOY ChIP-seq, by cross-referencing it against genes whose expression pattern mirrors ZFX knockdown in gene expression microarray from DAOY human MB cells, in order to identify additional conserved direct targets of Zfx to probe for functional significance in MB and BCC.

The overlapping list of conserved direct targets of ZFX derived from this comparison of ChIP-seq and microarray data was surprisingly short, encompassing only 30 genes in total (Fig. 29B, 30). These genes are mostly uncharacterized or only minimally characterized in the literature, with a few exceptions like FZD6, a Wnt signaling receptor characterized primarily for its role in patterning of hairs into whorls [152] but also implicated recently as a marker of a stem-cell-like fraction in neuroblastoma [153]. We elected to investigate two of the minimally characterized conserved target genes, *DIS3L* and *UBE2J1*, in greater

depth. Neither gene has been linked with cancers in humans, but mutations in the *DIS3L* homolog *DIS3L2* have been implicated in an overgrowth disorder (Perlman syndrome) and an associated kidney tumor (Wilms tumor) [154], showing that a Dis3L-like RNA exonuclease can play a critical role in the context of tumorigenesis. Notably, the functions so far ascribed to Dis3L (cytoplasmic RNA exonuclease possibly involved in mRNA degradation)[149, 150] and to Ube2J1 (E2 ubiquitin conjugating enzyme involved in misfolded protein degradation in ER)[151] suggest that they could interface with stress pathways (e.g.- proteotoxic stress), a hallmark of genes essential in cancers through "non-oncogene addiction" [140].

Genomic *Dis3L* and *Ube2j1* are both bound directly by Zfx in mESC and human DAOY cells, and transcript levels of both genes are decreased ~2-fold after *Zfx* loss in BCC *in vivo* and in human MB *in vitro* (Fig. 31). What's more, lentiviral shRNA-mediated KD targeting either DIS3L or UBE2J1 impaired growth of DAOY human MB cells *in vitro* (Fig. 32). Preliminarily, these results point towards a functional requirement for *DIS3L* and *UBE2J1* in a human MB *in vitro*, as well as suggest both genes as prime candidates to explain the non-oncogene addiction of Hh-driven BCC and MB to ZFX. However, care must be taken to ascertain the specificity of the effect in DAOY cells, as well as its applicability to Hh-dependent BCC and MB *in vivo*. Lentiviral shRNA-mediated KD is notoriously prone to non-specific toxicity in transduced cell-lines. To address this, rescue experiments in DAOY cells, involving co-delivery of DIS3L-targeting lentiviral shRNA and *DIS3L*-overexpressing retrovirus, are already underway to confirm

that DIS3L KD specifically causes growth impairment in human MB *in vitro*. Over the longer run, mice with null or conditionally targetable alleles of *Dis3L* or *Ube2j1*, or other promising genes off the shortlist of 30 conserved direct targets, could be used in concert with *Ptch1*-dependent BCC and MB models, to identify novel elements of a cell-intrinsic molecular machinery defined by *Zfx* and common across two distinct Hh-dependent cancers.

Materials & Methods

Animals

Mice with a conditional allele of *Ptch1* (*Ptch1*^{flox})[105] were bred with conditional *Zfx*^{flox} mice[74] to generate singly- and doubly-conditional *Ptch1*$^{flox/flox}$ and *Ptch1*$^{flox/flox}$ *Zfx*^{flox}/y mice. Tamoxifen (Tmx)-inducible *Rosa26-CreERT2* deleter mice (*R26-CreER*$^{+}$) were kindly provided by Dr. Thomas Ludwig, Columbia University[74]. They were bred with *Ptch1*^{flox} and *Ptch1*^{flox} *Zfx*^{flox} mice to generate the *R26*-CreER- *Ptch1*$^{flox/flox}$ *Zfx*$^{+}$/y (Ctrl), *R26*-CreER^{+} *Ptch1*$^{flox/flox}$ *Zfx*$^{+/y}$ (*Ptch1*), and *R26*-CreER^{+} *Ptch1*$^{flox/flox}$ *Zfx*^{flox}/y (*Ptch1 Zfx*) mice used in topical Tmx experiments. *hGFAP*-Cre mice[127] were obtained from the Jackson Laboratory and crossed with *Ptch1*^{flox} and *Ptch1*^{flox} *Zfx*^{flox} mice to generate *hGFAP*-Cre^{+} *Ptch1*$^{flox/flox}$ (*Ptch1*) and *hGFAP*-Cre^{+} *Ptch1*$^{flox/flox}$ *Zfx*^{flox}/y (*Ptch1 Zfx*) experimental animals, along with *hGFAP*-Cre^{-} or *hGFAP*-Cre^{+} *Ptch1*$^{flox/+}$ littermate controls (Ctrl). All animal studies were performed according to the investigator's protocol approved by the Institutional Animal Care and Use Committee of Columbia University.

Cell Culture

Zfx$^{flox\text{-}neo}$, *Zfx*^{null}, and *Zfx*^{TAG} murine ESCs and their culture conditions have been previously described[74]. ESCs were grown on gelatin-coated plates in complete DMEM with 5% - 15% Knockout SR (invitrogen) and recombinant leukemia inhibitory factor (LIF, Chemicon).

Murine ESCs were differentiated into motor neurons (MN) as described[148]. Briefly, ESCs were cultured on gelatin-coated plates in complete DMEM with 5% Knockout SR and LIF. Then, 1-2 x 10^6 ESC were plated in HEMA-coated 100 mm Petri dishes in differentiation medium (1:1 DMEM/F12: Neurobasal Medium with 10% Knockout SR, Invitrogen). Two days after plating in differentiation medium, embryoid bodies (EBs) were collected by gravity, rinsed with 1x DPBS (Gibco), and split into new Petri dishes containing differentiation medium supplemented with 1 μm retinoic acid (RA) and increasing concentrations of the synthetic *Smo* agonist $SAG_{1.3}$ (Calbiochem) or of recombinant, N-terminal murine SHH (R&D Biosystems). Three days later, treated EBs were collected by gravity and either resuspended in TriZol LS reagent (invitrogen) for RNA isolation or processed for cryosectioning and immunofluorescence.

DAOY cells were obtained from the ATCC and propagated in complete DMEM medium with 10% FBS, and replated by trypsinization.

RNA Isolation and qPCR

Total cellular RNA was isolated from samples in 0.5-1 mL TriZol LS reagent (Invitrogen). cDNA was synthesized from 1-2 μg RNA per sample using

SuperScript III reverse transcriptase (invitrogen). Quantitative real-time PCR (qPCR) assaying for SYBR Green incorporation were run on an Mx3000P instrument (Stratagene) using FastStart Universal SYBR Green Master mix containing Rox (Roche). Triplicate reactions were run for each sample, and all qPCR results were analyzed using the ΔΔCt method. The expression values for all genes were normalized to those for the housekeeping genes β-Actin (Actb) or GAPDH, and then expressed relative to the indicated control samples. The qPCR primers are listed below.

Species	Gene	Forward	Reverse
Mouse	Actb	ATCCTGACCCTGAAGTACC	TACGACCAGAGGCATACAG
	GAPDH	AAGGTCGGTGTGAACGGATTTG	CTCGCTCCTGGAAGATGGTGAT
	Zfx	GCAGTGCATGAACAGCAAGT	GCAAGGTGTTCAGGATGGTT
	Dis3L	AGGGGGAAGCCATGGAGAAG	GATTTGATGCCCGCTTCCAG
	Ube2j1	GACGCATAGTACTGCCACCA	ATGGCCCCCTCTCCTTTAGT
	Smo	CTCGGACTCGCAGGAGGAAG	TCAGGGAAGTGGTCCGGTGT
	Gli1	CATTGGGGAGGTTGCTCCAG	CCGAAGGTGCGTCTTGAGGT
	Mycn	GGAGAGGATACCTTGAGCGACTC	CGCCTTGTTGTTAGAGGAGGAAC
	Mnx1	AGGCGCAGTCGAACCTCTTG	TCCATTTCATTCGGCGGTTC
	Isl1	CAAGCGGTGCAAGGACAAGA	CAGGGCGGCTGGTAACTTTG
	Olig2	CACCTCCTCGTCCACGTCCT	GGCGATCTTGGAGAGCTTGC
	Tubb3	GGCCATTCTGGTGGACTTGG	GCCCTGCAGGCAGTCACAAT
Human	GAPDH	AAGGTGAAGGTCGGAGTCAACG	CCCACTTGATTTTGGAGGGATC
	Zfx	GCAGGATGATGACAAAGGCAAC	CAAGGATCAATTTCCGACTCTGTG
	Dis3L	CCAGGACAGGATGCCAATTGTT	CGTGGGCAGCTTTTAAATCAGG
	Ube2j1	GAAACTTGGCAGCCTTCGTG	ATGGCAGAGCCACATCCTTC
	Smo	GCTCATCGTGGGAGGCTACTTC	AGCATGGTCTCGTTGATCTTGC
	Gli1	CTCGGGCACCATCCATTTCTAC	GCCAGTCATTTCCACACCACTG

Tamoxifen Treatment of Dorsal Skin

Adult male mice of the designated genotypes were shaved across their dorsal skin at 7-8 weeks, temporally situating tamoxifen (Tmx) treatment within the second telogen of the hair cycle.[85] Animals were treated for five consecutive days topically with 100 μL per day of 10 mg/mL tamoxifen (Sigma) in acetone (i.e. – 1 mg tamoxifen q.d.). For gene expression analysis in bulk epidermis and hair follicles, Tmx-treated mice were sacrificed three days after final Tmx treatment. Tmx-treated dorsal skin was removed, and connective/adipose/vascular tissue was stripped from the dermis in cold PBS (Gibco). The remaining dermis and epidermis were floated in 0.25% trypsin - 1x EDTA (Gibco), with epidermis/hair follicles up, at 37°C, 7.5% CO_2 for 2 hours, and bulk hair follicles and epidermis were separated from dermis into DMEM with 10% FBS using sterile disposable scalpels. Bulk follicles/epidermis were minced, collected by centrifugation, and lysed in 2 mL TriZol LS reagent (Invitrogen). At 8-9 weeks after Tmx-treatment, mice were re-shaved if dorsal hair had regrown, and the Tmx-treated patch was removed, flattened, and fixed before processing for histology.

shRNA Constructs and Lentiviral Infection of DAOY Cells

Lentiviral constructs containing *Zfx*-targeting (H2, H3, H4) and non-specific (SCR) short hairpin RNAs (shRNAs) in the pLKO.1 backbone were purchased from Open Biosystems. To generate high-titer lentivirus, HEK293T cells were co-transfected with three plasmids encoding viral packaging proteins

(pCMVΔ8.9), envelope proteins (pVSVg) and the pLKO.1 shRNA sequences using the lipid-based transfection reagent Transit-293 (Mirus, LLC). After 48 hours incubation at 37°C, transfected cells were shifted to 32°C for 24 hours. Then viral supernatant was cleared using 0.45 micron filters and ultracentrifuged (50,000 x g, 2 hrs) to concentrate viral particles.

Triplicate cultures of $4x10^5$ DAOY cells were plated out overnight and then incubated with concentrated lentiviral supernatant and 7 μg/mL polybrene for 16-24 hrs, for a Mock, virus-less condition and for each lentiviral construct. Cells were allowed to rest for 2 days and then replated and grown henceforth in selective media containing 2 μg/mL puromycin (invitrogen). At 4 or 6 days post-infection (d.p.i.), plates were washed with 1x DPBS, and cells were collected in TriZol LS reagent for gene expression analysis or scraped, collected by centrifugation, and lysed in RIPA buffer for Western Blot.

Lentiviral shRNA knockdown of ZFX targets *DIS3L* and *UBE2J1* was conducted using pre-assembled lentiviral particles obtained from the MISSION shRNA library (Sigma-Aldrich). For each lentiviral shRNA construct (3-4 per gene, plus a control shRNA targeting non-mammalian sequence [NonM]), triplicate cultures of $1x10^4$ DAOY cells were transduced for 16-24 hours in 7 μg/mL polybrene, with lentiviral densities of 1 TU/cell (NonM) or 10 TU/cell (DIS3L- and UBE2J1-targeting constructs), based on manufacturer's provided titers. As above, cells were allowed to rest for 2 days and then replated and grown henceforth in selective media containing 2 μg/mL puromycin (invitrogen). Transduced cells, along with untreated cells grown without puromycin, were

followed for growth curves beginning 5 d.p.i., to ensure that any cell death from initial puromycin-selection was excluded. $3x10^4$ cells per shRNA condition were also pooled from triplicate cultures at 5 d.p.i. and collected in Trizol LS, for subsequent expression analysis by qRT-PCR. Sigma MISSION clone IDs for the DIS3L- and UBE2J1-targeting shRNA lentiviral particles used are provided below.

Lentivirus	Sigma MISSION ID	Sequence
DIS3L MH1	TRCN0000350506	CCGGGAACAAGGGCCACCACTTATTCTCG AGAATAAGTGGTGGCCCTTGTTCTTTTTG
DIS3L MH2	TRCN0000350507	CCGGGCATATCTGACGGAGTTATTTCTCG AGAAATAACTCCGTCAGATATGCTTTTTG
DIS3L MH3	TRCN0000315359	CCGGCTGGGTAGCTATTTCGCATATCTCG AGATATGCGAAATAGCTACCCAGTTTTTG
DIS3L MH4	TRCN0000315360	CCGGACGCAGCTGTTTGGTACTATCCTCG AGGATAGTACCAAACAGCTGCGTTTTTTG
UBE2J1 MH3	TRCN0000368973	CCGGTCCGGCTGTTAAACGTTTAATCTCG AGATTAAACGTTTAACAGCCGGATTTTTG
UBE2J1 MH4	TRCN0000320498	CCGGCCACCAAGCATTATTCTCCTACTCG AGTAGGAGAATAATGCTTGGTGGTTTTTG
UBE2J1 MH5	TRCN0000368905	CCGGGATGATATACCTACAACATTCCTCG AGGAATGTTGTAGGTATATCATCTTTTTG

Microarray and ChIP-seq

RNA for microarray analysis of DAOY human MB cells after ZFX knockdown was obtained 4 days after lentiviral transduction from one culture replicate for each of the ZFX-targeting shRNA constructs (H2, H3, H4) and non-targeting “scrambled” control (SCR). Labeled cDNA was analyzed on Affymetrix Human Gene 1.0 ST arrays. Pattern-matching genes whose downregulation in expression followed the expression profile of *Zfx* were identified using the

pattern-matching analytical tool in NIA Array,[132] applied only to microarray data for genes with extant Refseq annotations. Heatmaps comparing previously published microarray data from *Zfx*^{CKO} HSC and *Zfx*^{KO} mESC [74] with the Overlap shortlist of conserved ZFX direct targets (Fig. 27) were generated using Gene Set Enrichment Analysis software (GSEA 2.0.10).[155, 156]

Sonication-sheared chromatin from DAOY human MB cells was generated and isolated using Covaris *truChIP* High Cell Chromatin Shearing Kit with SDS Buffer and S2 Sonicator. ZFX ChIP was performed using rabbit polyclonal antibody[74] and Protein A Dynabeads (invitrogen), and unprobed sheared chromatin was used as a control (Input). Library construction and sequencing were performed by the Yale Center for Genome Analysis (New Haven, CT). For comparison with murine ESCs, previously reported Zfx ChIP-seq data were downloaded from the NCBI Sequence Read Archive (SRX000552).[70] Sequencing reads were aligned to the human genome (UCSC hg19) using the short read aligner, Bowtie (version 2.0.0).[157] Significant ZFX binding enrichment peaks were picked using MACS (1.4.0)[144] and were visualized using DNAnexus (Mt. View, CA). Peak distance to the nearest TSS was determined using PeakAnalyzer (version 1.4).[158] Unbiased motif analysis was performed on MACS-selected ChIP-seq peaks using the ChIPseeqer *FIRE* module of ChIPseeqer (2.0).[145]

Immunofluorescence

To analyze MN formation from ESCs *in vitro*, EBs were collected, washed, and then fixed overnight in 4% PFA. EBs were resuspended in PBS with 30% sucrose, embedded in OCT, and cryosectioned (16 μm sections).

To detect floor plate populations and motor neuron pools in developing spinal cord from *Zfx*^{CKO} embryos, E13.5/E14.5 *Sox2-Cre*$^{+}$ *Zfx*$^{flox/Y}$ embryos (and *Sox2-Cre*$^{-}$ littermates) were fixed overnight in 4% PFA and processed for croysectioning. Cryosections were stained with antibodies raised against the floor plate marker FOXA2 (Seven Hills Bioreagents) or the motor neuron marker HB9 (a gift from C. Henderson).

GENERAL DISCUSSION

Zfx is required for tumorigenesis in two distinct Hh-dependent cancers

The transcription factor *Zfx* has previously been shown to be essentially required for the self-renewal, but not differentiation, of multiple distinct stem cell types, murine and human ESC and murine adult HSC [74, 75]. The role of Zfx in the context of malignancy, however, remains unclear. We hypothesized that Zfx could also be required to facilitate aberrant self-renewal programs in certain cancers, particularly in tumors originating from stem/progenitor pools in their tissue-of-origin. To test this hypothesis, we generated Hh-driven BCC and MB *in vivo* using conditional deletion of the Hh inhibitory receptor *Ptch1* [11, 20], with or without concomitant deletion of *Zfx*. We found that *Zfx* co-deletion prevented Hh-dependent BCC formation and significantly delayed Hh-dependent MB formation in our tumor models *in vivo*.

Our results showing a partial or complete requirement for Zfx for MB and BCC progression contrast with, but do not necessarily contradict, the results from O'Donnell *et al*. (2012) identifying Zfx as a potential tumor suppressor in MYC-dependent liver cancer. Indeed, we found Zfx to be dispensable for PTEN-dependent glioblastoma development *in vivo*. The transcriptional program governed by Zfx may have different biological significance in different cancer cells, being dispensable for or even inhibitory to cancer growth in one context while being essential for growth in another. In our case, given the observed requirement for *Zfx* across Hh-dependent MB and BCC models *in vivo*, we

conclude that Zfx and its targets constitute a novel cell-intrinsic machinery both shared and required by at least two distinct Hh-dependent cancers.

Zfx regulation of Hh signal transducer Smo in BCC and MB

Zfx transcriptional regulation of the Hh signal transducer gene *Smo* is one possible explanation for these effects on Hh-driven cancers. We demonstrated that Zfx binds directly to *Smo* adjacent to its TSS in both mouse and human cell lines using ChIP-seq. Compellingly, we also found that the Zfx-dependent prevention of BCC formation in the skin correlated with decreased *Smo* levels and blunted Hh target genes normally overexpressed at early timepoints after induction of *Ptch1* deletion. A decrease in Smo levels and consequent block of downstream target overexpression is a plausible cause of prevention of Hh-dependent BCC. In mice that develop BCC due to overexpression of the Hh transcriptional activator Gli2, BCC are not maintained after the removal of Gli2 overexpression (and Hh pathway hyperactivation) [22]. Furthermore, the essential requirement for Smo for the Hh pathway activation driving BCC is the rationale behind developing small molecule inhibitors of Smo in order to treat this disease, inhibitors which have already shown promise in regressing tumors in human patients and been approved by the FDA for use in treating metastatic or locally advanced BCC [110, 136, 137] .

Zfx does not, however, seem to be generally required for all *Smo* expression during embryonic or post-natal development. Our laboratory

previously reported the observation that mice deleting *Zfx* throughout the embryo-proper are born grossly normal in appearance but die perinatally of causes unknown [74]. Here, we also showed Zfx^{CKO} embryos also successfully develop floor plate and motor neuron pools in their ventral spinal cord, patterning events known to depend on active Hh signaling [55, 116]. These results are incompatible with any premise that Zfx is necessary for all Smo expression during normal development generally, since $Shh^{-/-}$ or $Smo^{-/-}$ embryos develop massive skeletal and nervous system defects (e.g.- holoprosencephaly) [26], none of which were on display in perinatal Zfx^{CKO} pups. Furthermore, our data showed that *Zfx* deletion throughout the brain of *hGFAP-Cre*$^{+}$ $Zfx^{flox/Y}$ pups did not grossly impair cerebellar development, as one would expect if Zfx controlled *Smo* in the post-natal cerebellum, given the dependence of normal cerebellar foliation and size on Hh signaling [23, 24].

The striking decrease in *Smo* expression and blunting in *Gli1* and *Mycn* overexpression in the *Ptch1*-dependent BCC model was simply absent in our other *in vivo* models of Hh-driven BCC. Treated skin from the *SmoM2*-dependent BCC model and P14 cerebella from the *Ptch1*-driven MB model both showed no difference in Smo expression or Hh target gene overexpression after *Zfx* deletion. In the case of SmoM2-driven BCC, failure to detect changes in *Smo* expression levels does not necessarily mean that *Zfx* loss had no effect on endogenous *Smo* expression, since our qPCR for *Smo* could not distinguish between the endogenous mRNA and the SmoM2 transgenic mRNA. Since Smo dimerization

appears to be required during Hh pathway activation [48], endogenous Smo could have an essential role in SmoM2-driven BCC tumor progression as a dimerization partner with the transgenic activated SmoM2 allele. Thus, it remains a possibility that loss of *Zfx* impairs SmoM2-driven BCC *via* decreasing endogenous *Smo* expression.

The phenotype from *Zfx* loss was far weaker in general in Hh-driven MB than in the BCC models in the skin. Quantitative decrease in MB tumor size could be observed in P7 cerebella, and tumor progression was delayed enough by *Zfx* loss to enhance survival times for a fraction of the doubly-deleting mice. However, when looking at survival curves and P7 and P14 cerebellar sections, we are in fact observing fairly late events for this MB model. The *hGFAP-Cre* transgene driving *Ptch1* deletion turns on at E13.5, causes EGL expansion at least as early as E16.5, and kills mice *via* Hh-driven MB by ~4 weeks of age [11, 127]. Therefore, one possible explanation for the difference in phenotypes from *Zfx* loss observed in Hh-driven MB versus BCC is that *Smo* (or another relevant Zfx target) is only controlled by Zfx in the MB model over a temporally restricted window, early on after Cre-mediated excision begins. As the window closes, the cells would be acquiring the ability to discard the requirement for Zfx to express *Smo* or its other functionally relevant target, potentially *via* compensatory transcriptional activation from a redundant or alternative transcription factor. By the time MB are observed at P7 or P14, MB that lost *Zfx* would no longer be substantially different molecularly from those that had not, instead growing at the

same pace as the MB with wild-type Zfx. This hypothesis is supported by our microarray analysis of P14 MB cerebella, which revealed very few expression changes between *Ptch1* single-knockout and *Ptch1 Zfx* double knockout cerebella. Generating *Ptch1*-dependent MB using an inducible, GNP-specific Cre recombinase like *Math1-CreER* could test this explanation by inducing a more slowly progressing MB disease under temporal control *via* tamoxifen administration, allowing for easier observation of early events in incipient MB just after *Zfx* co-deletion.

Identification of conserved direct transcriptional targets of ZFX, DIS3L *and* UBE2J1, *and their functional requirement for growth of human MB cells* in vitro

Alternately, the differences in phenotype from Zfx loss between MB and BCC models could also be explainable if the effects in MB were mediated by different downstream Zfx targets besides *Smo*. We generated a shortlist of 30 conserved direct transcriptional targets of ZFX, by comparing ChIP-seq targets in murine ESC and DAOY human MB cells with genes whose expression decreased along with ZFX in DAOY human MB cells after lentiviral KD. From this list, we focused on two relatively uncharacterized targets, *DIS3L* and *UBE2J1,* whose expression also depends on Zfx in murine ESC and HSC [74]. The functions of *DIS3L* (cytoplasmic RNA exonuclease with a possible role in mRNA degradation) [149, 150] and *UBE2J1* (E2 ubiquitin-conjugating enzyme involved in ER-associated degradation of misfolded proteins) [151] suggest that disregulation of either gene could impact proteoxic or other stress pathways, a result

consistent with the non-oncogene addiction [140] to *Zfx* evident in Hh-driven BCC and MB *in vivo*. Also, the discovery that *DIS3L2*, a *DIS3L* homolog, is implicated in an overgrowth syndrome and Wilm's tumor lends credence to the consideration of an uncharacterized RNA exonuclease for a possible role in cancer [154].

Preliminary lentiviral shRNA knockdown experiments targeting DIS3L and UBE2J1 suggest that each is required for optimal growth of DAOY human MB cells *in vitro*, pending verification of the specificity of the RNAi-mediated growth defect with overexpression-based rescue experiments. Other targets from the 30 gene target list could also be tested in human MB cells *in vitro*. Even better, gene expression microarray data from treated skin in the BCC mice or cerebella in MB mice shortly after *Zfx* co-deletion, when compared with direct Zfx binding targets from mouse and human ChIP-seq, could generate superior shortlists likely enriched in targets relevant for Hh-dependent MB and BCC *in vivo*. Ideally, the most promising conserved direct targets of ZFX, after testing in *in vitro* cell lines by shRNA knockdown, could be eventually tested in mouse models of Hh-dependent BCC and MB, using knockout or conditional mice for the specific target genes, to conclusively identify the downstream targets of Zfx that comprise its required gene program in two very different Hh-dependent cancers.

Conclusion

We report that the transcription factor Zfx is required for the development of two highly disparate Hh-induced tumors, BCC and MB. Our results suggest

that this effect may be due at least in part to direct regulation by Zfx of the Hh pathway signal transducer Smo. An analysis of Zfx genomic targets in mouse and human also revealed a conserved set of Zfx target genes, some of which were required for growth of a human MB cell line *in vitro*. A more complete understanding of the relevant functional targets of Zfx in the context of MB and BCC could bear fruit with regard to molecular targeting of these malignancies. Trials have already shown promising results from molecular targeting of *Smo* in BCC and MB [110, 134, 135, 136, 137]. However, resistance mutations to small molecule therapies directed against *Smo* have already been documented [138], and treatment of Hh-driven MB with *Smo* inhibitors runs the risk of serious developmental side-effects, since most MB occur in young children where Hh signaling is required for ongoing normal development of their cerebellum, bones, and other tissues [7, 139]. Practically, treatment with Smo inhibitors like vismodegib (GDC-0449) also poses problems in adult patients. Phase II trial data with vismodegib in BCC patients revealed that delivery of Smo small molecule inhibitor resulted in non-life-threatening but highly unpleasant side effects such as alopecia and dysgeusia in the great majority of cases [136]. Future identification of the precise downstream targets with functional relevance in a Zfx-defined cell-intrinsic program shared by these two cancers offers the promise of yielding alternative druggable molecules for treatment of both BCC and the Hh-dependent subtype of MB - - treatments which could avoid these developmental pitfalls and adverse side effects.

Literature Cited

1 Visvader JE (2011). Cells of origin in cancer. *Nature* **469:** 314-322.

2 Barabé F, Kennedy JA, Hope KJ, Dick JE (2007). Modeling the Initiation and Progression of Human Acute Leukemia in Mice. *Science* **316:** 600-604.

3 Hope KJ, Jin L, Dick JE (2004). Acute myeloid leukemia originates from a hierarchy of leukemic stem cell classes that differ in self-renewal capacity. *Nat Immunol* **5:** 738-743.

4 Barker N, Ridgway RA, van Es JH, van de Wetering M, Begthel H, van den Born M *et al* (2009). Crypt stem cells as the cells-of-origin of intestinal cancer. *Nature* **457:** 608-611.

5 Sangiorgi E, Capecchi MR (2008). Bmi1 is expressed in vivo in intestinal stem cells. *Nat Genet* **40:** 915-920.

6 Zhu L, Gibson P, Currle DS, Tong Y, Richardson RJ, Bayazitov IT *et al* (2009). Prominin 1 marks intestinal stem cells that are susceptible to neoplastic transformation. *Nature* **457:** 603-607.

7 Ng JMY, Curran T (2011). The Hedgehog's tale: developing strategies for targeting cancer. *Nat Rev Cancer* **11:** 493-501.

8 Wang GY, Wang J, Mancianti M-L, Epstein Jr EH (2011). Basal Cell Carcinomas Arise from Hair Follicle Stem Cells in Ptch1+/- Mice. *Cancer Cell* **19:** 114-124.

9 Youssef KK, Van Keymeulen A, Lapouge G, Beck B, Michaux C, Achouri Y *et al* (2010). Identification of the cell lineage at the origin of basal cell carcinoma. *Nat Cell Biol* **12:** 299-305.

10 Schuller U, Heine VM, Mao J, Kho AT, Dillon AK, Han Y-G *et al* (2008). Acquisition of Granule Neuron Precursor Identity Is a Critical Determinant of Progenitor Cell Competence to Form Shh-Induced Medulloblastoma. *Cancer Cell* **14:** 123-134.

11 Yang Z-J, Ellis T, Markant SL, Read T-A, Kessler JD, Bourboulas M *et al* (2008). Medulloblastoma Can Be Initiated by Deletion of Patched in Lineage-Restricted Progenitors or Stem Cells. *Cancer Cell* **14:** 135-145.

12 Gibson P, Tong Y, Robinson G, Thompson MC, Currle DS, Eden C *et al* (2010). Subtypes of medulloblastoma have distinct developmental origins. *Nature* **468:** 1095-1099.

13 Clevers H (2006). Wnt/β-Catenin Signaling in Development and Disease. *Cell* **127:** 469-480.

14 Lobry C, Oh P, Aifantis I (2011). Oncogenic and tumor suppressor functions of Notch in cancer: it's NOTCH what you think. *The Journal of Experimental Medicine* **208:** 1931-1935.

15 Weng AP, Ferrando AA, Lee W, Morris JP, Silverman LB, Sanchez-Irizarry C *et al* (2004). Activating Mutations of NOTCH1 in Human T Cell Acute Lymphoblastic Leukemia. *Science* **306:** 269-271.

16 Koch U, Fiorini E, Benedito R, Besseyrias V, Schuster-Gossler K, Pierres M *et al* (2008). Delta-like 4 is the essential, nonredundant ligand for Notch1 during thymic T cell lineage commitment. *The Journal of Experimental Medicine* **205:** 2515-2523.

17 Radtke F, Wilson A, Stark G, Bauer M, van Meerwijk J, MacDonald HR *et al* (1999). Deficient T Cell Fate Specification in Mice with an Induced Inactivation of Notch1. *Immunity* **10:** 547-558.

18 Chiang C, Swan RZ, Grachtchouk M, Bolinger M, Litingtung Y, Robertson EK *et al* (1999). Essential Role for Sonic hedgehog during Hair Follicle Morphogenesis. *Developmental Biology* **205:** 1-9.

19 St-Jacques B, Dassule HR, Karavanova I, Botchkarev VA, Li J, Danielian PS *et al* (1998). Sonic hedgehog signaling is essential for hair development. *Current Biology* **8:** 1058-1069.

20 Adolphe C, Hetherington R, Ellis T, Wainwright B (2006). Patched1 Functions as a Gatekeeper by Promoting Cell Cycle Progression. *Cancer Research* **66:** 2081-2088.

21 Epstein EH (2008). Basal cell carcinomas: attack of the hedgehog. *Nat Rev Cancer* **8:** 743-754.

22 Hutchin ME, Kariapper MST, Grachtchouk M, Wang A, Wei L, Cummings D *et al* (2005). Sustained Hedgehog signaling is required for basal cell carcinoma proliferation and survival: conditional skin tumorigenesis recapitulates the hair growth cycle. *Genes & Development* **19:** 214-223.

23 Corrales JD, Blaess S, Mahoney EM, Joyner AL (2006). The level of sonic hedgehog signaling regulates the complexity of cerebellar foliation. *Development* **133:** 1811-1821.

24 Dahmane N, Ruiz-i-Altaba A (1999). Sonic hedgehog regulates the growth and patterning of the cerebellum. *Development* **126:** 3089-3100.

25 Ingham PW, Nakano Y, Seger C (2011). Mechanisms and functions of Hedgehog signalling across the metazoa. *Nat Rev Genet* **12:** 393-406.

26 Varjosalo M, Taipale J (2008). Hedgehog: functions and mechanisms. *Genes & Development* **22:** 2454-2472.

27 Nusslein-Volhard C, Wieschaus E (1980). Mutations affecting segment number and polarity in Drosophila. *Nature* **287:** 795-801.

28 Lee JJ, Ekker SC, von Kessler DP, Porter JA, Sun BI, Beachy PA (1994). Autoproteolysis in hedgehog protein biogenesis. *Science (New York, NY)* **266:** 1528-1537.

29 Chamoun Z, Mann RK, Nellen D, von Kessler DP, Bellotto M, Beachy PA *et al* (2001). Skinny Hedgehog, an Acyltransferase Required for Palmitoylation and Activity of the Hedgehog Signal. *Science* **293:** 2080-2084.

30 Chen M-H, Li Y-J, Kawakami T, Xu S-M, Chuang P-T (2004). Palmitoylation is required for the production of a soluble multimeric Hedgehog protein complex and long-range signaling in vertebrates. *Genes & Development* **18:** 641-659.

31 Beachy PA, Cooper MK, Young KE, von Kessler DP, Park WJ, Hall TM *et al* (1997). Multiple roles of cholesterol in hedgehog protein biogenesis and signaling. *Cold Spring Harb Symp Quant Biol* **62:** 191-204.

32 Peters C, Wolf A, Wagner M, Kuhlmann J, Waldmann H (2004). The cholesterol membrane anchor of the Hedgehog protein confers stable membrane association to lipid-modified proteins. *Proceedings of the National Academy of Sciences of the United States of America* **101:** 8531-8536.

33 Burke R, Nellen D, Bellotto M, Hafen E, Senti K-A, Dickson BJ *et al* (1999). Dispatched, a Novel Sterol-Sensing Domain Protein Dedicated to the Release of Cholesterol-Modified Hedgehog from Signaling Cells. *Cell* **99:** 803-815.

34 Caspary T, García-García MaJ, Huangfu D, Eggenschwiler JT, Wyler MR, Rakeman AS *et al* (2002). Mouse Dispatched homolog1 Is Required for Long-Range, but Not Juxtacrine, Hh Signaling. *Current Biology* **12:** 1628-1632.

35 Kawakami T, Kawcak TN, Li Y-J, Zhang W, Hu Y, Chuang P-T (2002). Mouse dispatched mutants fail to distribute hedgehog proteins and are defective in hedgehog signaling. *Development* **129:** 5753-5765.

36 Lewis PM, Dunn MP, McMahon JA, Logan M, Martin JF, St-Jacques B *et al* (2001). Cholesterol Modification of Sonic Hedgehog Is Required for Long-Range Signaling Activity and Effective Modulation of Signaling by Ptc1. *Cell* **105:** 599-612.

37 Beachy PA, Hymowitz SG, Lazarus RA, Leahy DJ, Siebold C (2010). Interactions between Hedgehog proteins and their binding partners come into view. *Genes & Development* **24:** 2001-2012.

38 Tenzen T, Allen BL, Cole F, Kang J-S, Krauss RS, McMahon AP (2006). The Cell Surface Membrane Proteins Cdo and Boc Are Components and Targets of the Hedgehog Signaling Pathway and Feedback Network in Mice. *Developmental Cell* **10:** 647-656.

39 Ayers KL, Thérond PP (2010). Evaluating Smoothened as a G-protein-coupled receptor for Hedgehog signalling. *Trends in Cell Biology* **20:** 287-298.

40 Alcedo J, Ayzenzon M, Von Ohlen T, Noll M, Hooper JE (1996). The Drosophila smoothened Gene Encodes a Seven-Pass Membrane Protein, a Putative Receptor for the Hedgehog Signal. *Cell* **86:** 221-232.

41 Chen W, Burgess S, Hopkins N (2001). Analysis of the zebrafish smoothened mutant reveals conserved and divergent functions of hedgehog activity. *Development* **128:** 2385-2396.

42 van den Heuvel M, Ingham PW (1996). smoothened encodes a receptor-like serpentine protein required for hedgehog signalling. *Nature* **382:** 547-551.

43 Varga ZM, Amores A, Lewis KE, Yan Y-L, Postlethwait JH, Eisen JS *et al* (2001). Zebrafish smoothened functions in ventral neural tube specification and axon tract formation. *Development* **128:** 3497-3509.

44 Zhang XM, Ramalho-Santos M, McMahon AP (2001). Smoothened Mutants Reveal Redundant Roles for Shh and Ihh Signaling Including Regulation of L/R Asymmetry by the Mouse Node. *Cell* **105:** 781-792.

45 Taipale J, Cooper MK, Maiti T, Beachy PA (2002). Patched acts catalytically to suppress the activity of Smoothened. *Nature* **418:** 892-896.

46 Goetz SC, Anderson KV (2010). The primary cilium: a signalling centre during vertebrate development. *Nat Rev Genet* **11:** 331-344.

47 Rohatgi R, Milenkovic L, Scott MP (2007). Patched1 Regulates Hedgehog Signaling at the Primary Cilium. *Science* **317:** 372-376.

48 Zhao Y, Tong C, Jiang J (2007). Hedgehog regulates smoothened activity by inducing a conformational switch. *Nature* **450:** 252-258.

49 Sasaki H, Nishizaki Y, Hui C, Nakafuku M, Kondoh H (1999). Regulation of Gli2 and Gli3 activities by an amino-terminal repression domain: implication of Gli2 and Gli3 as primary mediators of Shh signaling. *Development* **126:** 3915-3924.

50 Humke EW, Dorn KV, Milenkovic L, Scott MP, Rohatgi R (2010). The output of Hedgehog signaling is controlled by the dynamic association between Suppressor of Fused and the Gli proteins. *Genes & Development* **24:** 670-682.

51 Haycraft CJ, Banizs B, Aydin-Son Y, Zhang Q, Michaud EJ, Yoder BK (2005). Gli2 and Gli3 Localize to Cilia and Require the Intraflagellar Transport Protein Polaris for Processing and Function. *PLoS Genet* **1:** e53.

52 Tukachinsky H, Lopez LV, Salic A (2010). A mechanism for vertebrate Hedgehog signaling: recruitment to cilia and dissociation of SuFu–Gli protein complexes. *The Journal of Cell Biology* **191:** 415-428.

53 Kenney AM, Cole MD, Rowitch DH (2003). Nmyc upregulation by sonic hedgehog signaling promotes proliferation in developing cerebellar granule neuron precursors. *Development* **130:** 15-28.

54 Kenney AM, Rowitch DH (2000). Sonic hedgehog Promotes G1 Cyclin Expression and Sustained Cell Cycle Progression in Mammalian Neuronal Precursors. *Molecular and Cellular Biology* **20:** 9055-9067.

55 Bai CB, Stephen D, Joyner AL (2004). All Mouse Ventral Spinal Cord Patterning by Hedgehog Is Gli Dependent and Involves an Activator Function of Gli3. *Developmental Cell* **6:** 103-115.

56 Yauch RL, Gould SE, Scales SJ, Tang T, Tian H, Ahn CP *et al* (2008). A paracrine requirement for hedgehog signalling in cancer. *Nature* **455:** 406-410.

57 Yuan Z, Goetz JA, Singh S, Ogden SK, Petty WJ, Black CC *et al* (2006). Frequent requirement of hedgehog signaling in non-small cell lung carcinoma. *Oncogene* **26:** 1046-1055.

58 Watkins DN, Berman DM, Burkholder SG, Wang B, Beachy PA, Baylin SB (2003). Hedgehog signalling within airway epithelial progenitors and in small-cell lung cancer. *Nature* **422:** 313-317.

59 Clement V, Sanchez P, de Tribolet N, Radovanovic I, Ruiz i Altaba A (2007). HEDGEHOG-GLI1 Signaling Regulates Human Glioma Growth, Cancer Stem Cell Self-Renewal, and Tumorigenicity. *Current Biology* **17:** 165-172.

60 Stecca B, Mas C, Clement V, Zbinden M, Correa R, Piguet V *et al* (2007). Melanomas require HEDGEHOG-GLI signaling regulated by interactions between GLI1 and the RAS-MEK/AKT pathways. *Proceedings of the National Academy of Sciences* **104:** 5895-5900.

61 Karhadkar SS, Steven Bova G, Abdallah N, Dhara S, Gardner D, Maitra A *et al* (2004). Hedgehog signalling in prostate regeneration, neoplasia and metastasis. *Nature* **431:** 707-712.

62 Thayer SP, di Magliano MP, Heiser PW, Nielsen CM, Roberts DJ, Lauwers GY *et al* (2003). Hedgehog is an early and late mediator of pancreatic cancer tumorigenesis. *Nature* **425:** 851-856.

63 Olive KP, Jacobetz MA, Davidson CJ, Gopinathan A, McIntyre D, Honess D *et al* (2009). Inhibition of Hedgehog Signaling Enhances Delivery of Chemotherapy in a Mouse Model of Pancreatic Cancer. *Science* **324:** 1457-1461.

64 Gailani MR (1992). Developmental defects in Gorlin syndrome related to a putative tumor suppressor gene on chromosome 9. *Cell* **69:** 111-117.

65 Hahn H, Wicking C, Zaphiropoulos PG, Gailani MR, Shanley S, Chidambaram A *et al* (1996). Mutations of the Human Homolog of Drosophila patched in the Nevoid Basal Cell Carcinoma Syndrome. *Cell* **85:** 841-851.

66 Johnson RL, Rothman AL, Xie J, Goodrich LV, Bare JW, Bonifas JM *et al* (1996). Human Homolog of patched, a Candidate Gene for the Basal Cell Nevus Syndrome. *Science* **272:** 1668-1671.

67 Northcott PA, Jones DTW, Kool M, Robinson GW, Gilbertson RJ, Cho Y-J *et al* (2012). Medulloblastomics: the end of the beginning. *Nat Rev Cancer* **12:** 818-834.

68 Northcott PA, Korshunov A, Witt H, Hielscher T, Eberhart CG, Mack S *et al* (2011). Medulloblastoma Comprises Four Distinct Molecular Variants. *Journal of Clinical Oncology* **29:** 1408-1414.

69 Schneider-Gadicke A, Beer-Romero P, Brown LG, Mardon G, Luoh S-W, Page DC (1989). Putative transcription activator with alternative isoforms encoded by human ZFX gene. *Nature* **342:** 708-711.

70 Chen X, Xu H, Yuan P, Fang F, Huss M, Vega VB *et al* (2008). Integration of External Signaling Pathways with the Core Transcriptional Network in Embryonic Stem Cells. *Cell* **133:** 1106-1117.

71 L'Haridon M, Paul P, Xerri J-G, Dastot H, Dolliger C, Schmid M *et al* (1996). Transcriptional Regulation of the MHC Class I HLA-A11 Promoter by the Zinc Finger Protein ZFX. *Nucleic Acids Research* **24:** 1928-1935.

72 Taylor-Harris P, Swift S, Ashworth A (1995). Zfy1 encodes a nuclear sequence-specific DNA binding protein. *FEBS Letters* **360:** 315-319.

73 Koopman P, Ashworth A, Lovell-Badge R (1991). The ZFY gene family in humans and mice. *Trends in Genetics* **7:** 132-136.

74 Galan-Caridad JM, Harel S, Arenzana TL, Hou ZE, Doetsch FK, Mirny LA *et al* (2007). Zfx Controls the Self-Renewal of Embryonic and Hematopoietic Stem Cells. *Cell* **129:** 345-357.

75 Harel S, Tu EY, Weisberg S, Esquilin M, Chambers SM, Liu B *et al* (2012). ZFX Controls the Self-Renewal of Human Embryonic Stem Cells. *PLoS ONE* **7:** e42302.

76 Arenzana TL, Smith-Raska MR, Reizis B (2009). Transcription factor Zfx controls BCR-induced proliferation and survival of B lymphocytes. *Blood* **113:** 5857-5867.

77 Fang J, Yu Z, Lian M, Ma H, Tai J, Zhang L *et al* (2012). Knockdown of zinc finger protein, X-linked (ZFX) inhibits cell proliferation and induces apoptosis in human laryngeal squamous cell carcinoma. *Molecular and Cellular Biochemistry* **360:** 301-307.

78 Jiang H, Zhang L, Liu J, Chen Z, Na R, Ding G *et al* (2012). Knockdown of zinc finger protein X-linked inhibits prostate cancer cell proliferation and induces apoptosis by activating caspase-3 and caspase-9. *Cancer Gene Ther* **19:** 684-689.

79 Zhou Y, Su Z, Huang Y, Sun T, Chen S, Wu T *et al* (2011). The Zfx gene is expressed in human gliomas and is important in the proliferation and apoptosis of the human malignant glioma cell line U251. *Journal of Experimental & Clinical Cancer Research* **30:** 114.

80 O'Donnell KA, Keng VW, York B, Reineke EL, Seo D, Fan D *et al* (2012). A Sleeping Beauty mutagenesis screen reveals a tumor suppressor role for Ncoa2/Src-2 in liver cancer. *Proceedings of the National Academy of Sciences* **109:** E1377-E1386.

81 Hardy MH (1992). The secret life of the hair follicle. *Trends in Genetics* **8:** 55-61.

82 Paus R, Muller-Rover S, van der Veen C, Maurer M, Eichmuller S, Ling G *et al* (1999). A Comprehensive Guide for the Recognition and Classification of Distinct Stages of Hair Follicle Morphogenesis **113:** 523-532.

83 Schneider MR, Schmidt-Ullrich R, Paus R (2009). The Hair Follicle as a Dynamic Miniorgan. *Current Biology* **19:** R132-R142.

84 Alonso L, Fuchs E (2006). The hair cycle. *Journal of Cell Science* **119:** 391-393.

85 Muller-Rover S, Handjiski B, van der Veen C, Eichmuller S, Foitzik K, McKay IA *et al* (2001). A Comprehensive Guide for the Accurate

Classification of Murine Hair Follicles in Distinct Hair Cycle Stages. *Journal of Investigative Dermatology* **117:** 3-15.

86 Blanpain C, Fuchs E (2009). Epidermal homeostasis: a balancing act of stem cells in the skin. *Nat Rev Mol Cell Biol* **10:** 207-217.

87 Cotsarelis G, Sun T-T, Lavker RM (1990). Label-retaining cells reside in the bulge area of pilosebaceous unit: Implications for follicular stem cells, hair cycle, and skin carcinogenesis. *Cell* **61:** 1329-1337.

88 Oshima H, Rochat A, Kedzia C, Kobayashi K, Barrandon Y (2001). Morphogenesis and Renewal of Hair Follicles from Adult Multipotent Stem Cells. *Cell* **104:** 233-245.

89 Taylor G, Lehrer MS, Jensen PJ, Sun T-T, Lavker RM (2000). Involvement of Follicular Stem Cells in Forming Not Only the Follicle but Also the Epidermis. *Cell* **102:** 451-461.

90 Jaks V, Barker N, Kasper M, van Es JH, Snippert HJ, Clevers H *et al* (2008). Lgr5 marks cycling, yet long-lived, hair follicle stem cells. *Nat Genet* **40:** 1291-1299.

91 Liu Y, Lyle S, Yang Z, Cotsarelis G (2003). Keratin 15 Promoter Targets Putative Epithelial Stem Cells in the Hair Follicle Bulge **121:** 963-968.

92 Morris RJ, Potten CS (1999). Highly Persistent Label-Retaining Cells in the Hair Follicles of Mice and Their Fate Following Induction of Anagen **112:** 470-475.

93 Trempus CS, Morris RJ, Bortner CD, Cotsarelis G, Faircloth RS, Reece JM *et al* (2003). Enrichment for Living Murine Keratinocytes from the Hair Follicle Bulge with the Cell Surface Marker CD34. *J Investig Dermatol* **120:** 501-511.

94 Ito M, Liu Y, Yang Z, Nguyen J, Liang F, Morris RJ *et al* (2005). Stem cells in the hair follicle bulge contribute to wound repair but not to homeostasis of the epidermis. *Nat Med* **11:** 1351-1354.

95 Morris RJ, Liu Y, Marles L, Yang Z, Trempus C, Li S *et al* (2004). Capturing and profiling adult hair follicle stem cells. *Nat Biotech* **22:** 411-417.

96 Tumbar T, Guasch G, Greco V, Blanpain C, Lowry WE, Rendl M *et al* (2004). Defining the Epithelial Stem Cell Niche in Skin. *Science* **303:** 359-363.

97 Wang LC, Liu Z-Y, Gambardella L, Delacour A, Shapiro R, Yang J *et al* (2000). Conditional Disruption of Hedgehog Signaling Pathway Defines its Critical Role in Hair Development and Regeneration. *J Investig Dermatol* **114:** 901-908.

98 Sato N, Leopold PL, Crystal RG (1999). Induction of the hair growth phase in postnatal mice by localized transient expression of Sonic hedgehog. *The Journal of Clinical Investigation* **104:** 855-864.

99 Oro AE, Higgins K (2003). Hair cycle regulation of Hedgehog signal reception. *Developmental Biology* **255:** 238-248.

100 Brownell I, Guevara E, Bai CB, Loomis Cynthia A, Joyner Alexandra L (2011). Nerve-Derived Sonic Hedgehog Defines a Niche for Hair Follicle Stem Cells Capable of Becoming Epidermal Stem Cells. *Cell Stem Cell* **8:** 552-565.

101 Rubin AI, Chen EH, Ratner D (2005). Basal-Cell Carcinoma. *New England Journal of Medicine* **353:** 2262-2269.

102 Aszterbaum M, Epstein J, Oro A, Douglas V, LeBoit PE, Scott MP *et al* (1999). Ultraviolet and ionizing radiation enhance the growth of BCCs and trichoblastomas in patched heterozygous knockout mice. *Nat Med* **5:** 1285-1291.

103 Mancuso M, Pazzaglia S, Tanori M, Hahn H, Merola P, Rebessi S *et al* (2004). Basal Cell Carcinoma and Its Development: Insights from Radiation-Induced Tumors in Ptch1-Deficient Mice. *Cancer Research* **64:** 934-941.

104 Mao J, Ligon KL, Rakhlin EY, Thayer SP, Bronson RT, Rowitch D *et al* (2006). A Novel Somatic Mouse Model to Survey Tumorigenic Potential Applied to the Hedgehog Pathway. *Cancer Research* **66:** 10171-10178.

105 Ellis T, Smyth I, Riley E, Graham S, Elliot K, Narang M *et al* (2003). Patched 1 conditional null allele in mice. *genesis* **36:** 158-161.

106 Vidal VPI, Ortonne N, Schedl A (2008). SOX9 expression is a general marker of basal cell carcinoma and adnexal-related neoplasms. *Journal of Cutaneous Pathology* **35:** 373-379.

107 Xie J, Murone M, Luoh S-M, Ryan A, Gu Q, Zhang C *et al* (1998). Activating Smoothened mutations in sporadic basal-cell carcinoma. *Nature* **391:** 90-92.

108 Kasper M, Jaks V, Hohl D, Toftg, xE, rd R (2012). Basal cell carcinoma — molecular biology and potential new therapies. *The Journal of Clinical Investigation* **122:** 455-463.

109 Kwasniak LA, Garcia-Zuazaga J (2011). Basal cell carcinoma: evidence-based medicine and review of treatment modalities. *International Journal of Dermatology* **50:** 645-658.

110 Von Hoff DD, LoRusso PM, Rudin CM, Reddy JC, Yauch RL, Tibes R *et al* (2009). Inhibition of the Hedgehog Pathway in Advanced Basal-Cell Carcinoma. *New England Journal of Medicine* **361:** 1164-1172.

111 Jeong J, Mao J, Tenzen T, Kottmann AH, McMahon AP (2004). Hedgehog signaling in the neural crest cells regulates the patterning and growth of facial primordia. *Genes & Development* **18:** 937-951.

112 Ahn S, Joyner AL (2004). Dynamic Changes in the Response of Cells to Positive Hedgehog Signaling during Mouse Limb Patterning. *Cell* **118:** 505-516.

113 Chang DT, Lopez A, von Kessler DP, Chiang C, Simandl BK, Zhao R *et al* (1994). Products, genetic linkage and limb patterning activity of a murine hedgehog gene. *Development* **120:** 3339-3353.

114 Riddle RD, Johnson RL, Laufer E, Tabin C (1993). Sonic hedgehog mediates the polarizing activity of the ZPA. *Cell* **75:** 1401-1416.

115 Dessaud E, McMahon AP, Briscoe J (2008). Pattern formation in the vertebrate neural tube: a sonic hedgehog morphogen-regulated transcriptional network. *Development* **135:** 2489-2503.

116 Wijgerde M, McMahon JA, Rule M, McMahon AP (2002). A direct requirement for Hedgehog signaling for normal specification of all ventral progenitor domains in the presumptive mammalian spinal cord. *Genes & Development* **16:** 2849-2864.

117 Hatten ME, Roussel MF (2011). Development and cancer of the cerebellum. *Trends in Neurosciences* **34:** 134-142.

118 Gilbertson RJ, Ellison DW (2008). The Origins of Medulloblastoma Subtypes. *Annual Review of Pathology: Mechanisms of Disease* **3:** 341-365.

119 Lewis PM, Gritli-Linde A, Smeyne R, Kottmann A, McMahon AP (2004). Sonic hedgehog signaling is required for expansion of granule neuron precursors and patterning of the mouse cerebellum. *Developmental Biology* **270:** 393-410.

120 Cho Y-J, Tsherniak A, Tamayo P, Santagata S, Ligon A, Greulich H *et al* (2011). Integrative Genomic Analysis of Medulloblastoma Identifies a Molecular Subgroup That Drives Poor Clinical Outcome. *Journal of Clinical Oncology* **29:** 1424-1430.

121 Kool M, Koster J, Bunt J, Hasselt NE, Lakeman A, van Sluis P *et al* (2008). Integrated Genomics Identifies Five Medulloblastoma Subtypes with Distinct Genetic Profiles, Pathway Signatures and Clinicopathological Features. *PLoS ONE* **3:** e3088.

122 Northcott PA, Korshunov A, Pfister SM, Taylor MD (2012). The clinical implications of medulloblastoma subgroups. *Nat Rev Neurol* **8:** 340-351.

123 Thompson MC, Fuller C, Hogg TL, Dalton J, Finkelstein D, Lau CC *et al* (2006). Genomics Identifies Medulloblastoma Subgroups That Are Enriched for Specific Genetic Alterations. *Journal of Clinical Oncology* **24:** 1924-1931.

124 Pei Y, Moore Colin E, Wang J, Tewari Alok K, Eroshkin A, Cho Y-J *et al* (2012). An Animal Model of MYC-Driven Medulloblastoma. *Cancer Cell* **21:** 155-167.

125 Goodrich LV, Milenkovic L, Higgins KM, Scott MP (1997). Altered Neural Cell Fates and Medulloblastoma in Mouse patched Mutants. *Science* **277:** 1109-1113.

126 Oliver TG, Read TA, Kessler JD, Mehmeti A, Wells JF, Huynh TTT *et al* (2005). Loss of patched and disruption of granule cell development in a pre-neoplastic stage of medulloblastoma. *Development* **132:** 2425-2439.

127 Zhuo L, Theis M, Alvarez-Maya I, Brenner M, Willecke K, Messing A (2001). hGFAP-cre transgenic mice for manipulation of glial and neuronal function in vivo. *genesis* **31:** 85-94.

128 Lei L, Sonabend AM, Guarnieri P, Soderquist C, Ludwig T, Rosenfeld S *et al* (2011). Glioblastoma Models Reveal the Connection between Adult Glial Progenitors and the Proneural Phenotype. *PLoS ONE* **6:** e20041.

129 Jacobsen PF, Jenkyn DJ, Papadimitriou JM (1985). Establishment of a Human Medulloblastoma Cell Line and Its Heterotransplantation into Nude Mice. *Journal of Neuropathology & Experimental Neurology* **44:** 472-485.

130 Wetmore C, Eberhart DE, Curran T (2001). Loss of p53 but not ARF Accelerates Medulloblastoma in Mice Heterozygous for patched. *Cancer Research* **61:** 513-516.

131 Trotman LC, Niki M, Dotan ZA, Koutcher JA, Di Cristofano A, Xiao A *et al* (2003). Pten Dose Dictates Cancer Progression in the Prostate. *PLoS Biol* **1:** e59.

132 Sharov AA, Dudekula DB, Ko MSH (2005). A web-based tool for principal component and significance analysis of microarray data. *Bioinformatics* **21:** 2548-2549.

133 Yang ZJ (2008). Medulloblastoma can be initiated by deletion of Patched in lineage-restricted progenitors or stem cells. *Cancer Cell* **14:** 135-145.

134 LoRusso PM, Rudin CM, Reddy JC, Tibes R, Weiss GJ, Borad MJ *et al* (2011). Phase I Trial of Hedgehog Pathway Inhibitor Vismodegib (GDC-0449) in Patients with Refractory, Locally Advanced or Metastatic Solid Tumors. *Clinical Cancer Research* **17:** 2502-2511.

135 Rudin CM, Hann CL, Laterra J, Yauch RL, Callahan CA, Fu L *et al* (2009). Treatment of Medulloblastoma with Hedgehog Pathway Inhibitor GDC-0449. *New England Journal of Medicine* **361:** 1173-1178.

136 Sekulic A, Migden MR, Oro AE, Dirix L, Lewis KD, Hainsworth JD *et al* (2012). Efficacy and Safety of Vismodegib in Advanced Basal-Cell Carcinoma. *New England Journal of Medicine* **366:** 2171-2179.

137 Axelson M, Liu K, Jiang X, He K, Wang J, Zhao H *et al* (2013). U.S. Food and Drug Administration Approval: Vismodegib for Recurrent, Locally Advanced, or Metastatic Basal Cell Carcinoma. *Clinical Cancer Research* **19:** 2289-2293.

138 Yauch RL, Dijkgraaf GJP, Alicke B, Januario T, Ahn CP, Holcomb T *et al* (2009). Smoothened Mutation Confers Resistance to a Hedgehog Pathway Inhibitor in Medulloblastoma. *Science* **326:** 572-574.

139 Kimura H, Ng JMY, Curran T (2008). Transient Inhibition of the Hedgehog Pathway in Young Mice Causes Permanent Defects in Bone Structure. *Cancer Cell* **13:** 249-260.

140 Luo J, Solimini NL, Elledge SJ (2009). Principles of Cancer Therapy: Oncogene and Non-oncogene Addiction. *Cell* **136:** 823-837.

141 Richardson PG, Mitsiades C, Hideshima T, Anderson KC (2006). Bortezomib: Proteasome Inhibition as an Effective Anticancer Therapy. *Annual Review of Medicine* **57:** 33-47.

142 Bryant HE, Schultz N, Thomas HD, Parker KM, Flower D, Lopez E *et al* (2005). Specific killing of BRCA2-deficient tumours with inhibitors of poly(ADP-ribose) polymerase. *Nature* **434:** 913-917.

143 Farmer H, McCabe N, Lord CJ, Tutt ANJ, Johnson DA, Richardson TB *et al* (2005). Targeting the DNA repair defect in BRCA mutant cells as a therapeutic strategy. *Nature* **434:** 917-921.

144 Zhang Y, Liu T, Meyer C, Eeckhoute J, Johnson D, Bernstein B *et al* (2008). Model-based Analysis of ChIP-Seq (MACS). *Genome Biology* **9:** R137.

145 Giannopoulou E, Elemento O (2011). An integrated ChIP-seq analysis platform with customizable workflows. *BMC Bioinformatics* **12:** 277.

146 Fasano CA, Chambers SM, Lee G, Tomishima MJ, Studer L (2010). Efficient Derivation of Functional Floor Plate Tissue from Human Embryonic Stem Cells. *Cell Stem Cell* **6:** 336-347.

147 Sasaki H, Hogan BLM (1994). HNF-3β as a regulator of floor plate development. *Cell* **76:** 103-115.

148 Wichterle H, Lieberam I, Porter JA, Jessell TM (2002). Directed Differentiation of Embryonic Stem Cells into Motor Neurons. *Cell* **110:** 385-397.

149 Staals RHJ, Bronkhorst AW, Schilders G, Slomovic S, Schuster G, Heck AJR *et al* (2010). Dis3-like 1: a novel exoribonuclease associated with the human exosome. *EMBO J* **29:** 2358-2367.

150 Tomecki R, Kristiansen MS, Lykke-Andersen S, Chlebowski A, Larsen KM, Szczesny RJ *et al* (2010). The human core exosome interacts with

differentially localized processive RNases: hDIS3 and hDIS3L. *EMBO J* **29:** 2342-2357.

151 Burr ML, Cano F, Svobodova S, Boyle LH, Boname JM, Lehner PJ (2011). HRD1 and UBE2J1 target misfolded MHC class I heavy chains for endoplasmic reticulum-associated degradation. *Proceedings of the National Academy of Sciences* **108:** 2034-2039.

152 Wang Y, Chang H, Nathans J (2010). When whorls collide: the development of hair patterns in frizzled 6 mutant mice. *Development* **137:** 4091-4099.

153 Cantilena S, Pastorino F, Chayka O, Pezzolo A, Pistoia V, Ponzoni M *et al* (2011). *Frizzled receptor 6 marks rare, highly tumourigenic stem-like cells in mouse and human neuroblastomas*, vol. 2.

154 Astuti D, Morris MR, Cooper WN, Staals RHJ, Wake NC, Fews GA *et al* (2012). Germline mutations in DIS3L2 cause the Perlman syndrome of overgrowth and Wilms tumor susceptibility. *Nat Genet* **44:** 277-284.

155 Mootha VK, Lindgren CM, Eriksson K-F, Subramanian A, Sihag S, Lehar J *et al* (2003). PGC-1[alpha]-responsive genes involved in oxidative phosphorylation are coordinately downregulated in human diabetes. *Nat Genet* **34:** 267-273.

156 Subramanian A, Tamayo P, Mootha VK, Mukherjee S, Ebert BL, Gillette MA *et al* (2005). Gene set enrichment analysis: A knowledge-based approach for interpreting genome-wide expression profiles. *Proceedings of the National Academy of Sciences of the United States of America* **102:** 15545-15550.

157 Langmead B, Trapnell C, Pop M, Salzberg S (2009). Ultrafast and memory-efficient alignment of short DNA sequences to the human genome. *Genome Biology* **10:** R25.

158 Salmon-Divon M, Dvinge H, Tammoja K, Bertone P (2010). PeakAnalyzer: Genome-wide annotation of chromatin binding and modification loci. *BMC Bioinformatics* **11:** 415.